

Report No. NCEER-96-0003

**Ductility of Rectangular Reinforced Concrete  
Bridge Columns with Moderate Confinement**

by

Nadim Wehbe<sup>1</sup>  
M. Saïd Saïidi<sup>2</sup>  
David Sanders<sup>3</sup>  
Bruce Douglas<sup>4</sup>

January 19, 1996  
NCEER Task Number 112-D-5.1(d)  
FHWA Contract Number DTFH61-92-C-0012

A Report for

National Center for Earthquake Engineering Research  
State University of New York at Buffalo  
Red Jacket Quadrangle, Buffalo, NY 14261

---

<sup>1</sup>Graduate Research Assistant, Department of Civil Engineering/258, University of Nevada, Reno. Reno, NV 89557-0152

<sup>2</sup>Professor, Department of Civil Engineering/258, University of Nevada, Reno. Reno, NV 89557-0152

<sup>3</sup>Assistant Professor, Department of Civil Engineering/258, University of Nevada, Reno. Reno, NV 89557-0152

<sup>4</sup>Professor, Department of Civil Engineering/258, University of Nevada, Reno. Reno, NV 89557-0152

## ABSTRACT

This study is part of a project to develop detailing guidelines for reinforced concrete bridge columns and walls in areas of moderate seismicity. The research examined the ductility and behavior of rectangular reinforced concrete bridge columns with moderate confinement. The research comprised experimental and analytical investigation of the response of such columns when subjected to lateral loading.

Four half-scaled rectangular bridge columns were built and tested. The geometrical dimensions and the amount of longitudinal reinforcement were kept the same for all specimens. Each specimen was tested under constant axial load while subjected to lateral load reversals with increasing drift levels. The lateral loading was quasi-static and uniaxial in the column strong direction.

Two parameters were varied: the transverse steel reinforcement amount and the axial load level. Based on the amount of lateral steel, the specimens were divided into two groups. The transverse reinforcement ratios,  $A_s/(s \cdot h)$ , in the long direction for the two groups corresponded to 42 percent and 54 percent of the minimum lateral reinforcement required by AASHTO for seismic detailing. The applied axial loads were approximately  $0.1 f_c' A_g$  and  $0.25 f_c' A_g$ . The specimens exhibited moderate displacement ductilities ranging between 4 and 7.

In the analytical study, several existing models pertaining to the concrete stress-strain relationship and the plastic hinge length were utilized and compared. For unconfined concrete, the Kent and Park model was used. On the other hand, the modified Kent and Park model and the model by Mander et al. (as modified by Paulay and Priestley) were utilized to represent the constitutive relationship of confined concrete. The equivalent plastic hinge length was calculated using two different models, the Baker's model and the model by Paulay and Priestley. The analytical study revealed that for rectangular bridge columns with relatively low axial loads and moderate confinement, it is possible to predict with reasonable accuracy the response of the columns to lateral cyclic loading.

## TABLE OF CONTENTS

SECTION	TITLE	PAGE
<b>1</b>	<b>INTRODUCTION</b>	<b>1</b>
1.1	Bridge Design Philosophy in Seismic Zones	1
1.2	Current Seismic Provisions	1
1.2.1	American Concrete Institute (ACI)	1
1.2.2	American Association of State Highway and Transportation Officials (AASHTO)	2
1.2.3	California Department of Transportation (CALTRANS)	2
1.2.4	Paulay and Priestley	3
1.2.5	New Zealand Code	3
1.2.6	Commission of the European Communities	3
1.2.7	Example Bridge Column	5
1.3	Review of Previous Works	6
1.4	Objective and Scope	7
<b>2</b>	<b>DUCTILITY OF REINFORCED CONCRETE COLUMNS</b>	<b>9</b>
2.1	Introductory Remarks	9
2.2	Concrete Stress-Strain Models	9
2.2.1	Modified Kent and Park	9
2.2.2	Mander, et al. as Modified by Paulay and Priestley	10
2.3	Verification and Comparison of Concrete Models	11
<b>3</b>	<b>EXPERIMENTAL STUDIES</b>	<b>15</b>
3.1	Introduction	15
3.2	Design of Test Specimens	15
3.2.1	Column Cross Section	15
3.2.2	Column Height	15
3.2.3	Transverse Reinforcement	17
3.2.4	Footing Design	19
3.3	Construction of Test Specimens	20
3.4	Material Properties	23
3.5	Instrumentation	26
3.6	Test Setup	28
3.7	Experimental Procedure and Results	30
3.7.1	General Remarks	30
3.7.2	Specimen A1	32
3.7.3	Specimen A2	36
3.7.4	Specimen B1	42
3.7.5	Specimen B2	50
3.8	Summary and Observations	56

## TABLE OF CONTENTS (*Cont'd*)

SECTION	TITLE	PAGE
4	ANALYTICAL STUDY	59
4.1	Introduction	59
4.2	Theoretical Analysis	59
4.2.1	Lateral Deflection	59
4.2.2	Moment-Curvature Analysis	63
4.2.3	Plastic Hinge Length	66
4.2.4	Calculated Deflections	67
4.3	Remarks and Observations	70
5	SUMMARY AND CONCLUSIONS	73
5.1	Summary	73
5.1.1	Experimental Study	73
5.1.2	Analytical Study	74
5.2	Conclusions	75
5.3	Recommendations	75
6	REFERENCES	77
Appendix A	BOND SLIP ROTATION	81

## LIST OF TABLES

TABLE	TITLE	PAGE
1-1	Specimen Data of Previous Research	8
2-1	Calculated and Measured Ductilities of Square Columns	12
3-1	Lateral Steel Ratios inside Potential Plastic Hinge Regions of Test Specimens	17
3-2	Estimated Shear Demand and Shear Capacity of the Test Specimens	20
3-3	Measured Concrete Properties	23
3-4	Measured Steel Properties	23
3-5	Measured Displacements and Ductilities	32
3-6	Measured Lateral Loads, Yield Curvatures, and Plastic Hinge Lengths	56
4-1	Calculated Curvature	66
4-2	Calculated Equivalent Plastic Hinge Lengths	68
4-3	Calculated Ultimate Plastic Displacement, $\Delta_p$	68
4-4	Calculated Beam Shear Deflections	69
4-5	Calculated Displacements and Ductilities-Modified Kent and Park Model	69
4-6	Calculated Displacements and Ductilities-Mander et al. Model	70
4-7	Measured and Calculated Displacements at Yield	71
4-7	Comparison of Measured and Calculated Displacements at Ultimate	71

## LIST OF FIGURES

FIGURE	TITLE	PAGE
1-1	Cross Section of the Example Column	5
1-2	Confinement Steel Requirements for Different Design Methods	6
1-3	Available Test Data for Cyclic Response of Square Columns	7
3-1	Column Details for Specimens in Group I	16
3-2	Column Details for Specimens in Group II	16
3-3	Footing Details of the Test Specimens	21
3-4	Reinforcement Cage of a Test Specimen	22
3-5	Measured Stress-Strain Relationship of $\phi$ 6 mm (#2) Steel Bars	24
3-6	Measured Stress-Strain Relationship of $\phi$ 10 mm (#3) Steel Bars	24
3-7	Measured Stress-Strain Relationship of $\phi$ 19 mm (#6) Steel Bars	25
3-8	Averaged Measured Properties of Steel Bars	25
3-9	Strain Gaging of Longitudinal Bars	26
3-10	Strain Gaging of Transverse Steel	27
3-11	LVDT Setup for the Test Specimens	28
3-12	Test Setup	29
3-13	Idealized Moment-Curvature Relationship	31
3-14	Experimental Determination of Effective Yield Displacement	31
3-15	Lateral Load History for Specimen A1	33
3-16	Measured Lateral Load-Deflection Hysteresis Loops for Specimen A1	33
3-17	Specimen A1 at $\mu_{\Delta} = +1$ (1st Excursion)	34
3-18	Specimen A1 at $\mu_{\Delta} = +4$ (1st Excursion)	35
3-19	Specimen A1 at $\mu_{\Delta} = +6$ (1st Excursion)	35
3-20	Plastic Hinge in Specimen A1 at the End of the Test	36
3-21	Measured Lateral Load-Strain Hysteresis in Specimen A1 Longitudinal Bar	37
3-22	Measured Lateral Load-Strain in Specimen A1 Lateral Steel at SG 19	37
3-23	Measured Lateral Load-Strain in Specimen A1 Lateral Steel at SG 22	38
3-24	Measured Curvature Envelop along the Plastic Hinge of Specimen A1	38
3-25	Lateral Load History for Specimen A2	39
3-26	Measured Lateral Load-Deflection Hysteresis Loops for Specimen A2	40
3-27	Specimen A2 at $\mu_{\Delta} = +1$ (2nd Excursion)	40
3-28	Specimen A2 at $\mu_{\Delta} = -2$ (2nd Excursion)	41
3-29	Specimen A2 at $\mu_{\Delta} = -4$ (1st Excursion)	41
3-30	Plastic Hinge in Specimen A2 at the End of the Test	42
3-31	Measured Lateral Load-Strain Hysteresis in Specimen A2 Longitudinal Bar	43
3-32	Measured Lateral Load-Strain in Specimen A2 Lateral Steel at SG 18	43
3-33	Measured Lateral Load-Strain in Specimen A2 Lateral Steel at SG 19	44
3-34	Measured Curvature Envelop along the Plastic Hinge of Specimen A2	44
3-35	Lateral Load History for Specimen B1	45

## LIST OF FIGURES (*Cont'd*)

FIGURE	TITLE	PAGE
3-36	Measured Lateral Load-Deflection Hysteresis Loops for Specimen B1	46
3-37	Specimen B1 at $\mu_{\Delta} = -4$ (1st Excursion)	46
3-38	Specimen B1 at $\mu_{\Delta} = -6$ (1st Excursion)	47
3-39	Specimen B1 at $\mu_{\Delta} = +8$	47
3-40	Plastic Hinge in Specimen B1 at the End of the Test	48
3-41	Measured Lateral Load-Strain Hysteresis in Specimen B1 Longitudinal Bar	48
3-42	Measured Lateral Load-Strain in Specimen B1 Lateral Steel at SG 20	49
3-43	Measured Lateral Load-Strain in Specimen B1 Lateral Steel at SG 22	49
3-44	Measured Curvature Envelop along the Plastic Hinge of Specimen B1	50
3-45	Lateral Load History for Specimen B2	51
3-46	Measured Lateral Load-Deflection Hysteresis Loops for Specimen B2	52
3-47	Specimen B2 at $\mu_{\Delta} = -1$ (1st Excursion)	52
3-48	Specimen B2 at $\mu_{\Delta} = +3$ (1st Excursion)	53
3-49	Specimen B2 at $\mu_{\Delta} = +4$ (1st Excursion)	53
3-50	Plastic Hinge in Specimen B2 at the End of the Test	54
3-51	Measured Lateral Load-Strain Hysteresis in Specimen B2 Longitudinal Bar	54
3-52	Measured Lateral Load-Strain in Specimen B2 Lateral Steel at SG 19	55
3-53	Measured Lateral Load-Strain in Specimen B2 lateral Steel at SG 22	55
3-54	Measured Curvature Envelop along the Plastic Hinge of Specimen B2	56
4-1	Flexural Deflection of a Cantilever Column	60
4-2	Bending Moment and Curvature at Yield of Fixed End	61
4-3	Idealized Curvature at the Equivalent Plastic Hinge	61
4-4	Idealized Stress-Strain Curve of Main Steel	64
4-5	Unconfined Concrete Models	64
4-6	Confined Concrete Models for Specimens A1 and A2	65
4-7	Confined Concrete Models for Specimens B1 and B2	65

## SECTION 1 INTRODUCTION

### 1.1 Bridge Design Philosophy in Seismic Zones

Structures in earthquake-prone areas should be designed to withstand strong earthquakes without collapse. For the majority of structures, it is often more economical to dissipate the large seismic energy through inelastic deformations. This can be accomplished by plastic hinging at predetermined locations of a structure.

Bridge structures should remain functional after large earthquakes. This requires that bridge superstructures do not undergo plastic deformations and that bridges maintain their gravity loads carrying capacities. Thus, inelastic deformations in bridges should be accommodated through the formation of plastic hinges in the columns.

In the case of reinforced concrete bridge columns, it is necessary to allow for relatively large ductilities without sudden shear failure or significant strength degradation. It is well established that high ductilities could be achieved in reinforced concrete members by furnishing adequate lateral confinement steel. When properly detailed, lateral steel would provide higher ductilities, prevent premature buckling of main reinforcement, and avert shear failure.

### 1.2 Current Seismic Provisions

Different methods are available for the design of confinement reinforcement. A summary of the methods for the plastic hinge region of rectangular columns is presented in this section. Note that the required steel areas need to be satisfied for each orthogonal principal direction of the column section.

#### 1.2.1 American Concrete Institute (ACI)

The American Concrete Institute (2) provisions consider a structural member to be a column if the axial load index,  $P_u / (f'_c A_g)$ , exceeds 0.1. Parameters  $P_u$ ,  $f'_c$ , and  $A_g$  are the factored axial load, concrete compressive strength, and the gross cross sectional area of the member, respectively. Bridge columns typically meet this requirement. The minimum total cross sectional area of rectangular hoops and cross ties is the greater of

$$A_{sh} = 0.3 s h_c \frac{f'_c}{f_y} \left[ \left( \frac{A_g}{A_{ch}} \right) - 1 \right] \quad (1-1)$$

and

$$A_{sh} = 0.09 s h_c \frac{f'_c}{f_{yh}} \quad (1-2)$$

where

- $s$  = spacing of transverse reinforcement along the axis of the member.
- $h_c$  = cross-sectional dimension of column core measured center-to-center of confining reinforcement.
- $A_g$  = gross area of section.
- $A_{ch}$  = cross-section area of a structural member measured out-to-out of transverse reinforcement.
- $f_{yh}$  = specified yield strength of transverse reinforcement.

The general purpose of the requirements is to improve ductility of concrete. The above equations intend to provide the same degree of confinement as that in spiral columns. In the ACI equation for spiral reinforcement, the lateral confining pressure provided by the spiral on the core concrete is based on axially loaded columns. The spiral is proportioned so that the compressive strength lost by the spalling of the cover concrete is equal to the additional compressive strength provided by the core concrete due to the lateral pressure exerted by the spiral when it is stressed to yield. Considering that ACI provisions are generally for building design, the applicability of the requirements to bridge columns is not addressed in the code. The spacing of lateral reinforcement is limited to the smaller of 100 millimeters (4 inches) or one-quarter of the minimum member dimension.

### 1.2.2 American Association of State Highway and Transportation Officials (AASHTO)

The current provisions of AASHTO (1) are adopted from those of ACI. The lateral steel area is based on Equation 1-1, but Equation 1-2 has a coefficient of 0.12 instead of 0.09. The maximum spacing limits in AASHTO are the same as those in ACI.

### 1.2.3 California Department of Transportation (CALTRANS)

The CALTRANS (5) provisions specify Equation 1-1 as one of two expressions for the minimum area of transverse reinforcement. The other equation is:

$$A_{sh} = 0.12 s_t h_c \frac{f'_c}{f_y} \left( 0.5 + 1.25 \frac{P_e}{f'_c A_g} \right) \quad (1-3)$$

where

- $s_t$  = spacing of transverse reinforcement along the axis of the member.
- $P_e$  = axial load

Equation 1-3 acknowledges that tests have shown that confinement requirement should be a function of the magnitude of axial force. This equation is adopted from the New Zealand Code. A minimum spacing of 50 mm (2 in.) is specified for the transverse steel. The maximum spacing limit is the smallest of one-fifth of the column section dimension, 200 mm (8 in.), and six times the longitudinal bar diameter. The last limit is to prevent buckling of the column bars. These limits apply regardless

of whether the lateral reinforcement is controlled by shear or confinement.

#### 1.2.4 Paulay and Priestley

Based on research work on bridge columns conducted at the University of Canterbury, New Zealand, Zahn et al. and Watson et al. (24, 23) derived an equation relating the amount of confinement steel in columns to the applied axial load and the required curvature ductility. Paulay and Priestley (15) simplified the equation as follows

$$A_{sh} = k s h_c \frac{f'_c}{f_y} \frac{A_g}{A_c} \left( \frac{P}{f'_c A_g} - 0.08 \right) \quad (1-4)$$

where  $k = 0.35$  for a required curvature ductility  $\mu_\phi = 20$  and  $k = 0.25$  when  $\mu_\phi = 10$ . Other values may be found by interpolation or extrapolation.

In addition to the axial load, this equation depends on the expected curvature ductility demand. The flexibility provided by including the ductility demand makes the expression useful for not only bridge columns which experience large drifts but also those which are in areas of moderate seismicity where the ductility demand may be lower. For low values of the axial load index,  $P_u / (f'_c A_g)$ , the confinement requirements become relatively small and shear will control the design. The maximum spacing of the confinement bars is limited to the smallest of one-third of the minimum column dimension, six times the longitudinal bar diameter, and 180 mm (7 in.).

#### 1.2.5 New Zealand Code

The New Zealand code (22) specifies the larger of steel area from two expressions both of which are functions of the axial load. The total area of transverse bars in each direction is the larger of

$$A_{sh} = 0.3 s h_c \left( \frac{A_g}{A_c} - 1 \right) \frac{f'_c}{f_{yh}} \left( 0.5 + \frac{1.25 P_c}{\phi f'_c A_g} \right) \quad (1-5)$$

and the steel area from Equation 1-3. These equations are similar to the AASHTO requirement except that they are modified by the factor which reflects the effect of axial load. The vertical spacing of the transverse steel is limited to the smallest of six longitudinal bar diameter, one-fifth of the minimum dimension of the column section, and 200 mm (8 in.).

#### 1.2.6 Commission of the European Communities

A draft document for the seismic design of bridges was prepared in March 1994 by the Commission of the European Communities (6). In this document, bridge piers with an axial load index of 0.08 are required to be detailed to provide concrete confinement in the plastic hinge region. A mechanical reinforcement ratio is defined for each direction of the column as follows:

$$\omega_{wd} = \rho_w \frac{f_{yd}}{f_{cd}} \quad (1-6)$$

where

- $\rho_w$  = transverse reinforcement ratio
- =  $A_{sw}/s.b$
- $A_{sw}$  = total area of hoops or ties in the one direction of confinement
- $b$  = dimension of the concrete core perpendicular to the direction of confinement under consideration, measured to the outside of the perimeter hoop
- $f_{yd}$  = design strength of longitudinal reinforcement
- $f_{cd}$  = concrete compressive design strength related to the specified compressive strength,  $f_c'$

The reinforcement ratio is determined from

$$\omega_{wd} = 1.30 (0.15 + 0.01 \mu_c) \frac{A_c}{A_{cc}} (\eta_k - 0.08) \geq 0.08 \quad (1-7)$$

where

- $\mu_c$  = required curvature ductility
- $A_c$  = gross concrete area of the section
- $A_{cc}$  = confined (core) concrete area of the section
- $\eta_k$  = normalized axial load
- =  $N_c / (A_c f_{ck})$
- $N_c$  = axial load
- $f_{ck}$  = characteristic concrete strength

The minimum amount of transverse ties is specified as

$$\frac{A_t}{s} = \frac{\sum A_s f_{ys}}{1.6 f_{yt}} \quad (mm^2/m) \quad (1-8)$$

where

- $A_t$  = area of one leg tie,  $mm^2$
- $s$  = distance between tie legs,  $mm^2$
- $\sum A_s$  = sum of the areas of the longitudinal bars restrained by the tie,  $mm^2$
- $f_{yt}$  = yield strength of tie
- $f_{ys}$  = yield strength of the longitudinal reinforcement

The vertical spacing of the transverse steel is limited to the smaller of six longitudinal bar diameter and one-fifth of the minimum dimension of the column core section.

### 1.2.7 Example Bridge Column

To compare the confinement steel designed based on different guidelines, a representative rectangular bridge column was designed. The cross section of the column excluding the transverse reinforcement is shown in Figure 1-1. The longitudinal steel ratio in this column is approximately 2.2 percent. The concrete compressive strength was assumed at 27.6 MPa (4,000 psi) and the steel yield stress was assumed at 414 MPa (60,000 psi). The confinement steel ratio was determined as a function of the axial load ratio using different guidelines. The ACI and AASHTO minimum transverse steel requirements for gravity loads only were also included in the analysis.

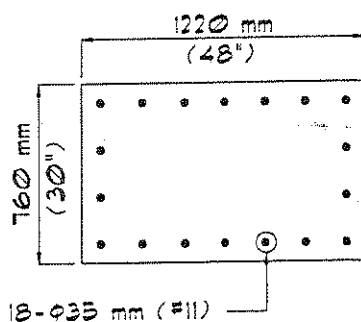


Figure 1-1 Cross Section of the Example Column

Figure 1-2 shows the results. The confinement steel ratios based on Paulay and Priestley's method are for an assumed column height of 6.1 m (20') and for displacement ductilities,  $\mu_\Delta$ , ranging from 2 to 8. Notice that the value of the multiplier  $k$  in Equation 1-4 depends on the curvature ductility. To present the plot of Equation 1-4 in terms of displacement ductility, a plastic hinge length of 610 mm (24") was assumed for the example column. The plastic hinge length is equivalent to one half the section depth as recommended by Paulay and Priestley (15). For low values of axial load, shear and not confinement would control the amount of lateral reinforcement. Future provisions for some of bridge columns which are located in areas of moderate seismicity could perhaps require reinforcement ratios which may be in between the gravity load design and the seismic design requirements. Note that the ACI and AASHTO requirements are independent of the level of axial load, whereas CALTRANS results depend on the axial load level although to a lesser degree than the results based on Paulay and Priestley.

For the example column, it can be seen in Figure 1-2 that the lateral reinforcement ratio required by AASHTO for seismic design is 33 percent more than that required by ACI. Moreover, for an axial load index of less than 0.4 which is typical in bridge columns, AASHTO seismic specifications require more transverse steel than that required by CALTRANS. The difference between AASHTO and CALTRANS requirements decreases as the axial load index approaches 0.4. At relatively low axial loads, the equation given by Paulay and Priestley results in a reinforcement ratio that is considerably less than those required by the codes. For instance, at an axial load index of 0.2 and a displacement ductility of 8, the calculated lateral steel ratio for the example column according to the equation by Paulay and Priestley is 33 percent less than the minimum ratio required by either

ACI or CALTRANS and 50 percent less than the minimum ratio required by AASHTO.

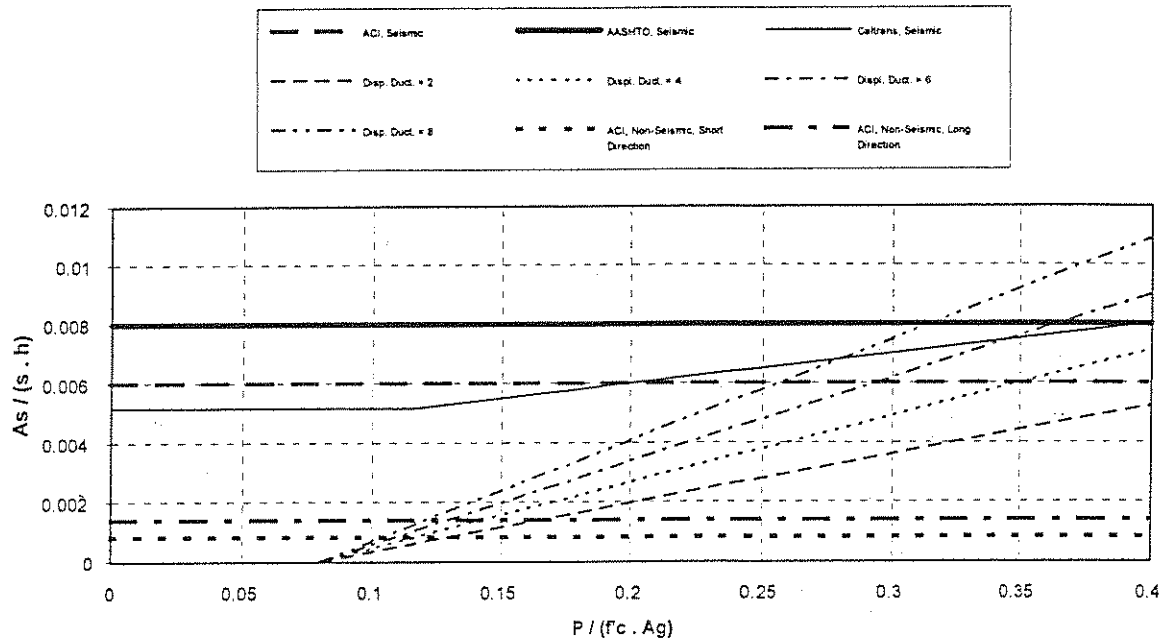


Figure 1-2 Confinement Steel Requirements for Different Design Methods

### 1.3 Review of Previous Works

Because of the apparent similarity of the confinement provided by square ties to that of the rectangular ties and due to a lack of experimental data on the earthquake response of rectangular columns, a review of previous cyclic load tests of square columns with rectilinear ties and cross ties was conducted (3, 12, 13, 16, 19, 21). Figure 1-3 shows a summary of the peak displacement ductilities in terms of the axial load index,  $P_v / (f_c' A_g)$ , where  $P_v$ ,  $f_c'$ , and  $A_g$  are the applied axial load, concrete compressive strength, and the gross cross sectional area of the member. The numbers in the figure refers to the names of the first authors of the publications from which the data were obtained. The ductilities are the maximum values attained by specimen failure or by terminating the test. Table 1-1 presents the main data from each reference. It can be seen that the material properties are generally in the range of the values used in bridge columns, and the dimensions may be thought of as being one-fourth to one-half scaled representation of prototype bridge columns. The longitudinal steel ratios in the specimens tested by Ozcebe and Sheikh are somewhat larger than what is usually used in bridge columns.

The axial load ratio for bridge columns is typically less than 0.3. It can be noted in Figure 1-3 that for moderate ductility demand of the order of 2 to 4, and for columns with a relatively small axial load ratios, very little data are available on specimens with rectilinear transverse steel. This is particularly true in light of the fact that the data points marked by "4" are for columns with a

longitudinal steel ratio which is higher than that of bridge columns.

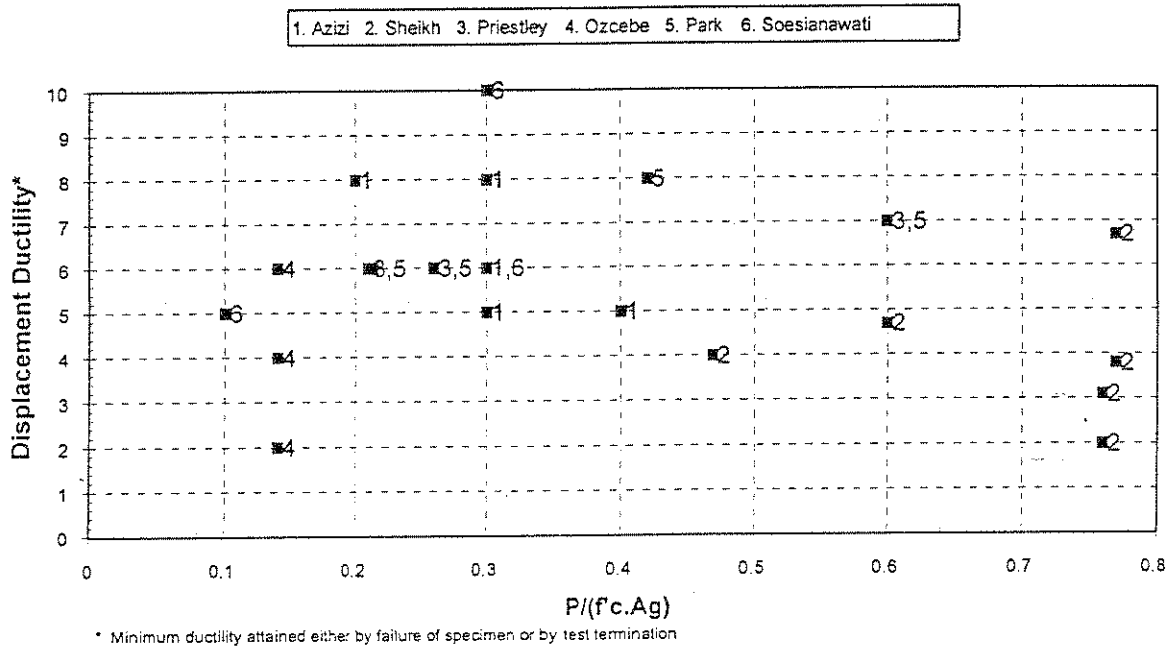


Figure 1-3 Available Test Data for Cyclic Response of Square Columns

#### 1.4 Objective and Scope

The objective of this study was to investigate the ductility of reinforced concrete bridge columns and develop detailing guidelines for areas of moderate seismicity. Because it was observed that the amount of test data on circular and square columns may be sufficient, the focus of the research is on rectangular columns. To investigate moderate ductilities of rectangular bridge columns, limited lateral reinforcement below the minimum required by current codes for seismic design was studied experimentally and analytically.

Four half-scaled rectangular bridge columns were built and tested. The geometrical dimensions and the amount of longitudinal reinforcement were kept the same for all specimens. Based on the amount of lateral confinement, the specimens were divided into two groups, Group I (Specimens A1 and A2) and Group II (Specimens B1 and B2). The lateral confinement for the specimens in Group I and Group II corresponded to about 40 percent and 60 percent, respectively, of the current AASHTO seismic requirement. The column specimens were tested under constant vertical axial loads representing the dead load of the superstructure. Columns A1 and B1 were each subjected to an axial load of  $0.1 f'_c A_g$ . For columns A2 and B2, the axial load was increased to  $0.25 f'_c A_g$ . The specimens were subjected to cyclic lateral loads with increasing drift levels. Bending was about the strong axis of the columns.

Table 1-1 Specimen Data of Previous Research

Specimen	Lateral Steel Ratio $\rho_l, \%$	Lateral Steel Yield Strength $f_{yh}, \text{MPa}$ (Ksi)	Longitudinal Steel Ratio $\rho_l, \%$	Axial Load % of $f_c' A_g$	Displacement Ductility $\mu_A$
Azizi	2.35	414 (60)	1.95	20	8
	1.29	414 (60)	1.95	30	5
Priestley	1.5	297 (43)	1.79	26	6
	3.5	297 (43)	1.79	60	7
Ozcebe	1.69	470 (63.5)	3.32	15	2
	1.95	425 (61.6)	3.32	15	>6.5
Park	2.3	316 (45.8)	1.79	21	>6
	2	297 (43.1)	1.79	42	8
Soesianawati	0.84	364 (53)	1.51	10	10
	0.9	364 (53)	1.51	30	≤6

## SECTION 2 DUCTILITY OF REINFORCED CONCRETE COLUMNS

### 2.1 Introductory Remarks

Ductility of a structural member can be described as the ability of that member to deform beyond the elastic limit without significant strength degradation. Ductility is usually defined as the ratio of ultimate deformation to yield deformation. Thus, curvature ductility  $\mu_\phi$  of a section is the ratio  $\phi_u/\phi_y$  where  $\phi_u$  and  $\phi_y$  are the ultimate and yield curvatures, respectively. Similarly, displacement ductility,  $\mu_\Delta$ , is the ratio of the displacement at ultimate to the displacement at yield,  $\Delta_u/\Delta_y$ .

As mentioned earlier, ductility of bridge columns is essential in seismic design of bridges. The formation of plastic hinges in bridge columns allows for the dissipation of seismic energy through inelastic deformation and prompts the bridge system to "attract" smaller lateral loads under earthquake motion.

The ability of reinforced concrete columns to deform beyond the elastic limit and the ultimate deformation that can be reached depend mainly on the level of confinement of the core concrete. The confinement provided by lateral hoops and cross ties delays the spalling of the core concrete and allows concrete to attain higher strains.

### 2.2 Concrete Stress-Strain Models

To calculate the failure displacement, a representative constitutive model for concrete is needed. The primary features of the stress-strain relationship for concrete are the peak stress and the failure strain. Other parameters such as the shape of the stress-strain relationship do not generally affect the outcome (15). The peak stress and the failure strain are both sensitive to the amount and distribution of the confinement steel. Many models have been developed for the constitutive relationship of confined concrete, the majority of which are based on compression loading of test specimens (9, 11, 18, 20).

Based on a review of different models and their applicability to rectangular hoops, two confinement relationships, the modified Kent and Park (9) and the other by Mander et al. (11), were selected for this study. Compared to the test data on square columns described in previous sections, these models appear to provide the upper and lower bound estimates of displacement ductilities. These models are briefly described herein.

#### 2.2.1 Modified Kent and Park (9)

In this model, strength and ductility of core concrete are enhanced by the confinement provided by transverse hoops. The model consists of an ascending parabolic branch and a descending straight branch. The concrete strength,  $Kf'_c$ , is reached at a strain of  $0.002K$ .  $K$  is defined in Equation 2-2. The stress-strain relationship is

(i) For  $\epsilon_c \leq 0.002K$ :

$$f_c = Kf'_c \left[ \frac{2\epsilon_c}{0.002K} - \left( \frac{\epsilon_c}{0.002K} \right)^2 \right] \quad (2-1)$$

$$K = 1 + \frac{\rho_s f_{yh}}{f'_c} \quad (2-2)$$

(ii) For  $\epsilon_c > 0.002K$ :

$$f_c = Kf'_c \left[ 1 - Z_m(\epsilon_c - 0.002K) \right] \geq 0.2Kf'_c \quad (2-3)$$

$$Z_m = \frac{0.5}{\frac{3 + 0.26f'_c}{145f'_c - 1000} + \frac{3}{4} \rho_s \sqrt{\frac{h''}{s_h} - 0.002K}} \quad (\text{MPa}) \quad (2-4)$$

where:

- $\epsilon_c$  = strain of confined concrete
- $f_c$  = stress of confined concrete
- $f'_c$  = unconfined concrete compressive strength
- $f_{yh}$  = yield stress of the confining steel
- $\rho_s$  = lateral steel volumetric ratio measured to outside of hoops
- $h''$  = width of confined core measured to outside of hoops
- $s_h$  = center to center spacing of hoop sets

### 2.2.2 Mander et al. (11) as Modified by Paulay and Priestley (15)

In this model, the strength of confined concrete,  $f_{cc}'$ , is related to the confining pressure,  $f_l'$ , provided by the lateral reinforcement. For circular sections, or square sections of equal confining steel in both directions, the confined concrete strength is

$$f_{cc}' = f'_c \left( -1.254 + 2.254 \sqrt{1 + \frac{7.94f_l'}{f'_c} - \frac{2f_l'}{f'_c}} \right) \quad (2-5)$$

where:

- $f'_c$  = unconfined concrete compressive strength

For a rectangular section with unequal lateral steel ratios along the depth and the width of the cross section ( $x$  and  $y$  directions), the confining pressures  $f_{lx}'$  and  $f_{ly}'$ , in the  $x$  and  $y$  directions, respectively, can be found as follows

$$f_{lx}' = K_{cx} \rho_x f_{yh} \quad (2-6)$$

$$f'_{ly} = K_{ey} \rho_y f_{yh} \quad (2-7)$$

where

- $K_{ex}$  = confinement effectiveness coefficient in the x direction
- $K_{ey}$  = confinement effectiveness coefficient in the y direction
- $\rho_x$  = volumetric ratio of lateral steel in the x direction
- $\rho_y$  = volumetric ratio of lateral steel in the y direction
- $f_{yh}$  = yield stress of lateral steel

Once the confining pressures in both directions are found, the confined concrete strength can be found from a set of curves. Those curves were based on multiaxial failure criterion and were verified by comparing the solution to triaxial tests results.

The strain,  $\epsilon_{cc}$ , at maximum stress is given by

$$\epsilon_{cc} = 0.002 \left[ 1 + 5 \left( \frac{f'_{cc}}{f'_c} - 1 \right) \right] \quad (2-8)$$

To find the ultimate strain of concrete at failure, Mander et al. applied a strain energy approach. In this method, the longitudinal compressive concrete strain at failure corresponds to the first fracture in the hoops. In addition to the monotonic stress-strain model, Mander et al. also presented a stress-strain relationship for confined concrete under cyclic loading including the effect of strain rate on the stress-strain curves. A detailed description of the model is presented in Reference 11.

Paulay and Priestley (15) adopted a modified version of the Mander et al. model to represent the stress-strain behavior of confined concrete under monotonic loading. In the modified model, the stress-strain curve, confined strength, and strain at confined strength are kept the same as in the original model. However, the modified model prescribes a lower conservative ultimate concrete compression strain as follows

$$\epsilon_{cu} = 0.004 + \frac{1.4 \rho_x f_{yh} \epsilon_{sm}}{f'_{cc}} \quad (2-9)$$

where

- $\epsilon_{sm}$  = steel strain at maximum tensile stress

Moreover, Paulay and Priestley suggested a confinement coefficient  $k_c$  of 0.95 for circular columns, 0.75 for rectangular columns, and 0.60 for rectangular walls.

### 2.3 Verification and Comparison of Concrete Models

The displacement ductility of the selected square test specimens that were presented in Section 1.3 was calculated based on the confined concrete models described in the previous sections. Those columns were selected for the analysis because of their relatively low axial load index which would

be representative of axial load index in bridge columns. Measured concrete and steel properties were used when they were reported. Otherwise, the specified values were used. The "yield" displacement was calculated by including the rigid body rotation of the columns due to bond slip. The bond strength was assumed to be  $20 \sqrt{f'_c}/d_b$  (MPa) (10). The plastic hinge length was assumed to be that recommended by Paulay and Priestley (15) as follows

$$l_p = 0.08l + 0.022d_b f_y \quad (\text{MPa}) \quad (2-10)$$

where

- $l_p$  = plastic hinge length
- $l$  = length from maximum bending moment to inflection point
- $d_b$  = diameter of longitudinal bar
- $f_y$  = yield stress of longitudinal reinforcement

Equation 2-10 is based on tests of reinforced concrete columns, and it implicitly accounts for the effect of bond slip.

Comparison of calculated and measured ductilities for the selected tests are presented in Table 2-1. A ">" in the measured column indicates that the specimen did not necessarily fail at that ductility level. The "<" for the last specimen indicates that the ductility of 6 was accomplished only for one cycle followed by a drastic strength degradation.

**Table 2-1 Calculated and Measured Ductilities of Square Columns**

Specimen	$\mu_A^{(1)}$	$\mu_A^{(2)}$	$\mu_A^{(3)}$
Azizi	6.6	13.7	8
	3.7	5.6	5
Priestley	5.9	10.4	6
	4.1	11.6	7
Ozcebe	8.6	12.6	2
	8.7	15.7	>6.5
Park	3.2	9.5	>6
	2.5	7.3	8
Soesianawati	5.6	9.6	10
	2.5	4.0	≤6

<sup>(1)</sup> Mander et al. as modified by Paulay and Priestley

<sup>(2)</sup> Modified Kent and Park

<sup>(3)</sup> Measured

The first specimen shown for Ozcebe was reinforced only with perimeter tie bars which is not representative of the current practice. Concrete constitutive models implicitly assume that the lateral bars are distributed within the section. As expected, the measured ductility capacity of this specimen was very low. A comparison of the measured and calculated ductilities shows that the measured values were generally within the limits predicted by Mander et al., as modified by Paulay and Priestley, and the modified Kent and Park. The modified Kent and Park model led to upper bound estimates of ductilities. The results suggest that the Mander's model, as modified by Paulay and Priestley, would provide a reasonable and a lower bound estimate of the displacement ductilities.

## SECTION 3 EXPERIMENTAL STUDIES

### 3.1 Introduction

Four half-scale rectangular bridge columns were designed, constructed, and tested in the course of this research. Two parameters were varied in this study: the transverse steel reinforcement amount and the axial load level. Each specimen was tested under constant axial load while subjected to lateral load reversals in the strong direction of the column.

The specimens were designed to attain moderate ductility capacities before significant reduction in strength. To accomplish this, reduced amounts of confining steel below that required by the codes (1, 5) for bridge seismic design were selected. Based on the maximum lateral loads expected to be reached during the tests, the selected amounts of transverse steel were checked to ensure that the shear capacity of each specimen exceeded the corresponding shear demand to prevent shear failure. Other details pertaining to lateral and vertical spacing of ties, minimum size of tie bars, and extension of standard hooks were maintained according to code requirements.

### 3.2 Design of Test Specimens

The column specimens were designed to represent half-scale models of the prototype rectangular column discussed in Section 1.2.5 of this report. The columns were supported by rectangular footings which would transfer the applied loads to the strong floor of the testing laboratory. Rocking of the footing under lateral loads was prevented by tie-downs holding the footing to the floor. Each column was assumed fixed at the bottom end where it connected to the footing and hinged at the top end where the lateral load was to be applied. The loading point represented the column inflection point. Figures 3-1 and 3-2 present the final design of the test specimens in Group I and Group II, respectively. Following are the steps taken in designing the test specimens.

#### 3.2.1 Column Cross Section

All four specimens had the same cross sectional dimensions and identical longitudinal reinforcement. Each test column was 380 millimeters (15 inches) wide by 610 mm (24 in.) deep and was reinforced with 18-  $\phi$ 19 mm (#6) bars, resulting in longitudinal reinforcement ratio,  $\rho_l$ , of 2.2%. The specified concrete compressive strength and steel yield stress were 27.6 MPa (4,000 psi) and 414 MPa (60,000 psi), respectively.

#### 3.2.2 Column Height

To determine the height of the column specimens, two main factors were considered: the prototype height and the constraints of the testing facility. A height of 2050 mm (6.7 ft) was selected for the column specimen. The loading assembly at the top of the specimen increased the moment arm by 305 mm (12 in.), thus making the height from the horizontal loading point to the top of the footing

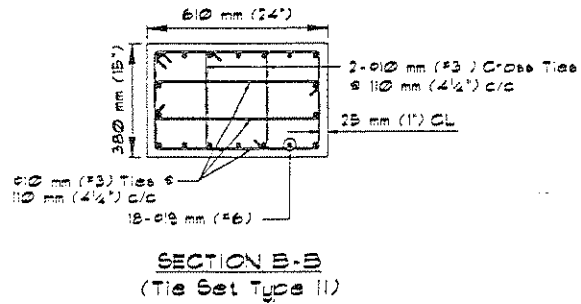
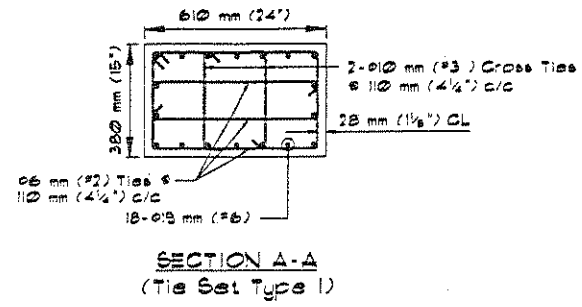
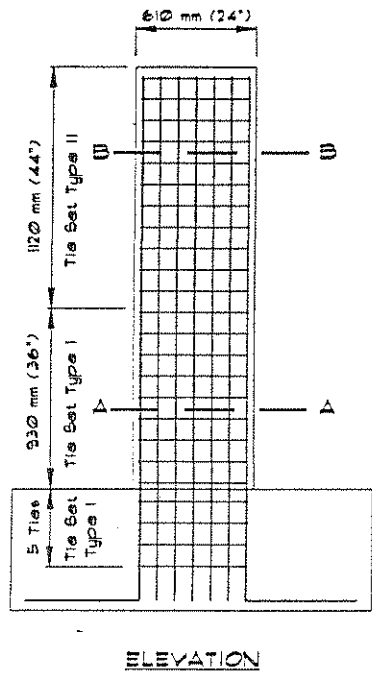


Figure 3-1 Column Details for Specimens in Group I

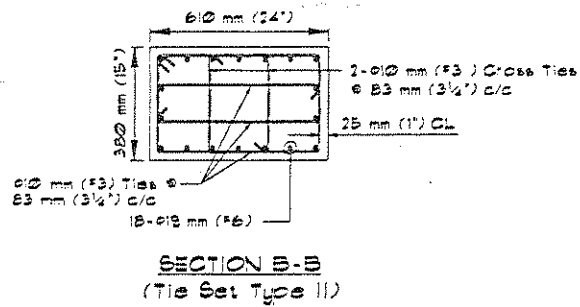
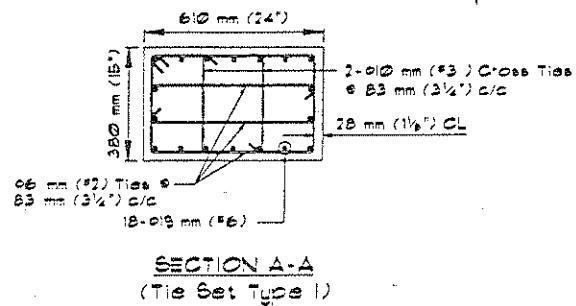
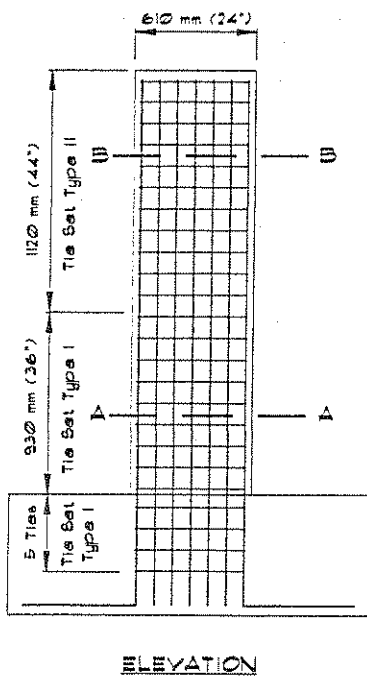


Figure 3-2 Column Details for Specimens in Group II

2355 mm (7.7 ft). For bridge columns bending in single curvature under lateral loads, this height would correspond to a prototype column height of approximately 4700 mm (15 ft). For columns which bend in double curvature, the corresponding full-scale column height would be approximately 9400 mm (30 ft).

### 3.2.3 Transverse Reinforcement

To design transverse reinforcement in the potential plastic hinge zone, the minimum amount required by AASHTO was first calculated according to Section 1.2.2 of this report. Based on Equations 1-1 and 1-2 with a modified coefficient of 0.12, it was found that the minimum required lateral steel ratio  $A_{sh}/(s \cdot h_c)$ , would be 0.008. For a transverse steel ratio of 0.004 (one-half of AASHTO requirement) and an axial load index of 0.25, Equation 1-4 given by Paulay and Priestley would predict a moderate displacement ductility of about 4 as can be seen in Figure 1-2. Based on this analysis, it was decided to furnish the test specimens with lateral confinement ratios in the vicinity of one-half of the minimum AASHTO requirement.

To prevent premature buckling of longitudinal bars, an upper limit on hoop set spacing,  $s$ , was set at six times the longitudinal bar diameter ( $6d_b$ ) resulting in a limit of 114 mm (4.5 in.). Each tie set in the potential plastic hinge zone of the test specimens consisted of 1-  $\phi$  6 mm (#2) perimeter hoop, 2-  $\phi$  6 mm (#2) cross ties in the long direction, and 2-  $\phi$  10 mm (#3) cross ties in the short direction (Figures 3-1 and 3-2). Such arrangement allowed for the engagement of all longitudinal bars along the short side of the column, and every other longitudinal bar along the long side of the column. The perimeter tie free ends were  $135^\circ$  bends whereas the cross tie had  $135^\circ$  bend on one end and  $90^\circ$  bend on the other. In all cases the bend extension was equivalent to ten times the bar diameter. A scaled down concrete cover of 28 mm ( $1\frac{1}{8}$  in.) was employed. For the specimens in Group I (Specimens A1 and A2) the tie set spacing was set at 110 mm (4.25 in.) corresponding to a transverse reinforcement ratio in the long direction of 0.0033 or 42 percent of the minimum confinement steel required by AASHTO. In Group II (Specimens B1 and B2) the spacing of the tie sets was reduced to 83 mm (3.25 in.) resulting in a transverse reinforcement ratio in the long direction of 0.0043 or 54 percent of the minimum AASHTO requirement. In the short direction, the lateral steel reinforcement ratios were 0.0034 and 0.0044 for specimens in Group I and Group II, respectively. These ratios correspond to 42 percent and 55 percent of the minimum requirement by AASHTO. The lateral steel ratios for the test specimens inside the potential plastic hinge regions are presented in Table 3-1.

Table 3-1 Lateral Steel Ratios inside Potential Plastic Hinge Regions of Test Specimens

Specimen	Lateral Steel Ratio $A_{sh}/(s \cdot h_c)$	
	Long Direction	Short Direction
Group I (Specimens A1 & A2)	0.0033	0.0043
Group II (Specimens B1 & B2)	0.0034	0.0044

Based on the described transverse steel arrangements, the shear capacities inside the plastic hinge region of the test specimens were calculated and compared with the shear demands. The nominal shear capacity,  $V_n$ , was found from the following equation (1):

$$V_n = V_c + V_s \quad (3-1)$$

where

- $V_c$  = concrete nominal shear capacity  
 $V_s$  = steel nominal shear capacity

$V_s$  is given by

$$V_s = \frac{A_v f_y d}{s} \quad (3-2)$$

where

- $A_v$  = area of shear reinforcement  
 $f_y$  = yield strength of shear reinforcement  
 $d$  = distance from extreme compression fiber to centroid of tension reinforcement  
 $s$  = spacing of shear reinforcement in direction parallel to main reinforcement

When plastic hinging occurs, the nominal shear capacity of concrete is reduced due to the formation of flexural-shear cracks and is in inverse proportion to the ductility level. Consequently, the code equations (1) to calculate  $V_c$  for non-seismic loads are not applicable. A method used by CALTRANS (25) relates  $V_c$  to the level of confinement, ductility ratio, and the applied axial load as follows

$$V_c = 0.083 (F_1)(F_2) \sqrt{f'_c} A_e \leq 0.332 \sqrt{f'_c} A_e \quad (MPa) \quad (3-3)$$

$$V_c = (F_1)(F_2) \sqrt{f'_c} A_e \leq 4 \sqrt{f'_c} A_e \quad (psi) \quad (3-4)$$

where

- $F_1$  : factor that is proportional to the level of confinement and inversely proportional to the ductility ratio. It ranges between 0.3 and 1.0  
 $F_2$  : factor that depends on the applied compressive axial stress. It ranges between 1.0 for zero axial stress and 1.5 for a compressive stress of 6.9 MPa (1000 psi)  
 $A_e$  = effective concrete area which is equal to 80% of the gross cross sectional area of the column

Priestley et al. (17) presented a different model to calculate the shear capacity. According to this model, the shear resistance is provided by three components as follows

$$V_n = V_c + V_t + V_p \quad (3-5)$$

where

- $V_c$  = shear force carried by concrete  
 $V_t$  = shear force carried by truss action (lateral reinforcement)

$V_p$  = lateral component of compression strut in the column due to the applied compressive axial load

Priestley's method is adopted in the Seismic Retrofitting Manual for Highway Bridges (7) with a simplified term for  $V_p$ . In Reference 7, the shear capacity components for rectangular columns are obtained as follows

$$V_c = v_c A_e \quad (3-6)$$

$$V_s = \frac{A_v f_y d}{s} \cot \theta \quad (3-7)$$

$$V_p = 0.2 P \quad (3-8)$$

$A_v$ ,  $f_y$ ,  $d$ ,  $s$ , and  $A_e$  are the same as defined in Equations 3-2 and 3-3.  $\theta$  is the angle between the column axis and the diagonal concrete compression strut ( $\theta$  is considered  $45^\circ$  in ACI-318).  $v_c$  is depends on the attained ductility of a cross section and is obtained as follows

- (i) For non-ductile regions and for plastic hinge regions where the displacement ductility of the column  $\mu_\Delta \leq 2$ :

$$v_c = 0.29 \sqrt{f'_c} \text{ (MPa)} = 3.5 \sqrt{f'_c} \text{ (psi)} \quad (3-9)$$

- (ii) For plastic hinge regions where the displacement ductility of the column  $\mu_\Delta \geq 4$ :

$$v_c = 0.1 \sqrt{f'_c} \text{ (MPa)} = 1.2 \sqrt{f'_c} \text{ (psi)} \quad (3-10)$$

- (iii) For displacement ductilities between 2 and 4, a linear interpolation is used.

To estimate the shear demand, the ideal moment capacity of each specimen was first calculated. The nominal moment capacity is defined as the moment capacity of a concrete member without taking into consideration the over strength due to confinement (14). Considering that the specimens were moderately confined, the over strength factor was assumed to be 20%. Having the over strength moment capacity and the moment arm, the shear demand was calculated and compared to the shear capacity. It was found that the specimens would be safe in shear. Table 3-2 presents the estimated shear demand and shear capacity inside the plastic hinge region for all four specimens.

### 3.2.4 Footing Design

The reinforced concrete footings were designed such that no flexural yielding and/or shear failure would occur under the estimated extreme loading conditions. For ease of construction and setup, a uniform footing design was adopted for all four specimens. The specified concrete compressive strength and the steel yield stress were 27.6 MPa (4,000 psi) and 414 MPa (60,000 psi), respectively. Each footing was 2.44 meters (8 feet) long by 1.83 m (6 ft) wide by 0.71 m (2.33 ft) deep.

**Table 3-2 Estimated\* Shear Demand and Shear Capacity of the Test Specimens**

Specimen	Shear Capacity (CALTRANS) kN (Kips)			Shear Capacity (FHWA Retrofit Manual) kN (Kips)				Shear Demand kN (Kips)
	$V_s$	$V_c$	$V_n$	$V_s^{**}$	$V_c$	$V_p$	$V_n$	$V$
A1	246 (55.3)	100 (22.5)	346 (77.8)	246 (55.3)	151 (21.9)	199 (28.8)	596 (106.0)	323 (72.6)
A2	246 (55.3)	125 (28.1)	371 (83.4)	246 (55.3)	151 (21.9)	497 (72.0)	894 (149.2)	368 (82.7)
B1	322 (72.3)	100 (22.5)	422 (94.8)	322 (72.3)	151 (21.9)	199 (28.8)	672 (123.0)	323 (72.6)
B2	322 (72.3)	125 (28.1)	447 (100.4)	322 (72.3)	151 (21.9)	497 (72.0)	970 (166.2)	368 (82.7)

\* Based on specified material properties

\*\* Based on  $\theta = 45^\circ$

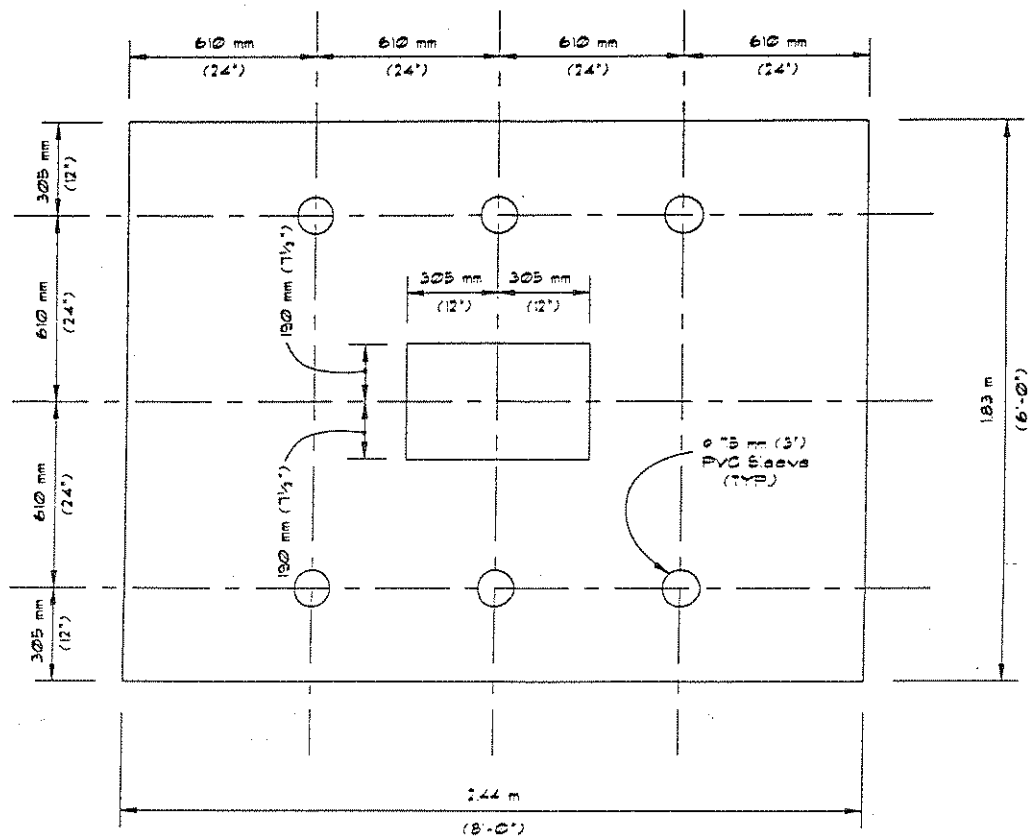
Since rocking was prevented by means of tie-downs, the footing was designed for positive and negative bending moments in both directions. Flexural reinforcement consisted of identical top and bottom steel mats. Each mat comprised 8-  $\phi$  25 mm (#8) bars in the long direction and 10-  $\phi$  25 mm (#8) bars in the short direction. The bar ends consisted of a 90° bent plus a 405 mm (16 in.) extension. The concrete cover was 75 mm (3 in.) on all sides. Shear reinforcement was not provided in the footings because it was found that the nominal shear capacity of the footing concrete exceeded the shear demand. A typical footing is shown in Figure 3-3.

### 3.3 Construction of Test Specimens

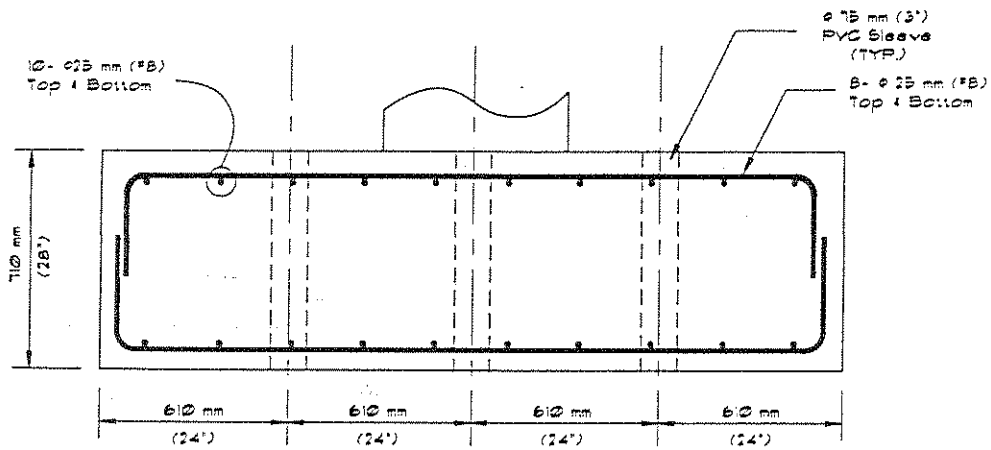
The specimens were built in pairs at the laboratory. The footings were constructed on a flat plywood platform to provide a smooth bottom surface and to protect the concrete floor of the laboratory.

The footing form was erected then a layer of form release oil was applied to the plywood surfaces that would be in contact with concrete. The pre-assembled bottom mat of the footing reinforcing steel cage was lifted and placed inside the mould. To facilitate the placement of column ties inside the footing, the column main reinforcement was installed before placing the footing top steel mat. Although the footing depth was ample to develop the column main bars, all embedded column bar ends inside the footings were provided with 90° bends and 250 mm (10 in.) extensions for added anchorage and ease of construction. Prior to pouring concrete, six-  $\phi$  75 mm (3 in.) by 740 mm (28 in.) long plastic sleeves were placed vertically inside the footing mould to allow for the passage of tie-down and axial load Dywidag™ bars later during the test.

The concrete was ready mixed and was supplied by a local batch plant. Concrete slump was always measured prior to pouring. Slump measures are reported in Section 3.4 of this report. The footing



PLAN



SECTION

Figure 3-3 Footing Details of the Test Specimens

concrete was poured and vibrated in 350 mm (13 in.) lifts then the surface of the footing was troweled to a smooth finish. Nine 150 mm (6 in.) diameter by 300 mm (12 in.) concrete cylinders were sampled for every footing. The footings were moisture cured for seven days.

The column steel cage was completed by tying the transverse steel around the main bars extending from the footing then the column forms were fitted in place. Figure 3-4 presents a completed steel cage prior to pouring of footing concrete. To facilitate the installation of LVDT's (linear variable differential transformers) along the potential plastic hinge length, five pairs of  $\phi$  6 mm (0.25 in.) by 710 mm (28 in.) long galvanized threaded rods were placed horizontally through the mould. The rods were positioned parallel to the long side of the column at predetermined height intervals and they extended about 50 mm (2 in.) outside the column face at both ends. Plastic cones were fitted at both ends of each rod to form cavities in the cover concrete around the rods. This was needed to prevent deviations in the LVDT readings during spalling of the column cover concrete. Four  $\phi$  35 mm (1 3/8 in.) A325 anchor bolts were placed vertically at the top of the column mould to allow for the hook up of the loading mechanism. For added anchorage, the bolts were fully threaded and were fitted with 100 mm x 75 mm x 6 mm (4 in. x 3 in x 0.5 in.) anchor plates at the embedded ends. Each bolt had a 530 mm (21 in) embedded length and 100 mm (4 in.) extension above the top of the column. The column concrete was placed and vibrated in 460 mm (18 in.) lifts, then moisture cured for seven days. Similar to the footings, nine concrete test cylinders were taken for each column.

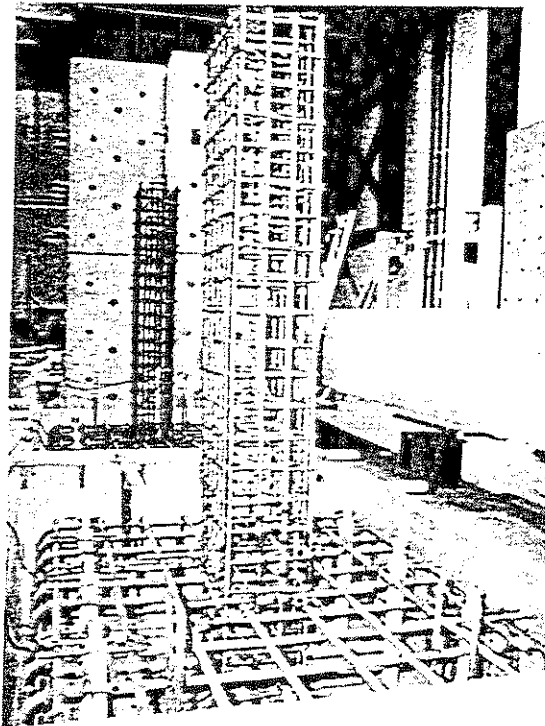


Figure 3-4 Reinforcement Cage of a Test Specimen

### 3.4 Material Properties

In order to evaluate the column test results, material tests were carried out to determine the actual material properties of concrete and steel.

The concrete compressive strength was obtained from compression tests of the concrete cylinders. For each batch, sets of three cylinders were tested at seven days, twenty eight days, and on the day of testing of the column specimen. Concrete slump and compressive strength results are presented in Table 3-3.

Table 3-3 Measured\* Concrete Properties

Specimen	Concrete Location	Concrete Slump mm (in.)	Concrete Strength, $f'_c$ MPa (Ksi)
A1	Footing	38 (1.5)	31.7 (4.60)
A2	Column	50 (2)	27.2 (3.95)
B1	Footing	50 (2)	29.7 (4.30)
B2	Column	50 (2)	28.1 (4.08)

\* Average values on the day of testing

Tensile tests of the reinforcing steel were carried out for bar sizes  $\phi$  6 mm (#2),  $\phi$  10 mm (#3), and  $\phi$  19 mm (#6). For each bar size, three specimens were tested. Figures 3-5 to 3-7 present the measured stress-strain relationships for bar sizes  $\phi$  6 mm,  $\phi$  10 mm, and  $\phi$  19 mm, respectively. The average measured stress-strain values of the three bar sizes are shown on the same plot in Figure 3-8 and the average measured steel properties are also summarized in Table 3-4.

Table 3-4 Measured Steel Properties

Bar Size	@ Yield		@ Ultimate	
	$\epsilon_y$	$f_y$ , MPa (Ksi)	$\epsilon_u$	$f_u$ , MPa (Ksi)
$\phi$ 6 mm (#2)	0.0023	455 (66)	0.160	676 (98)
$\phi$ 10 mm (#3)	0.0021	428 (62)	0.121	738 (107)
$\phi$ 19 mm (#6)	0.0022	448 (65)	0.110	731 (106)

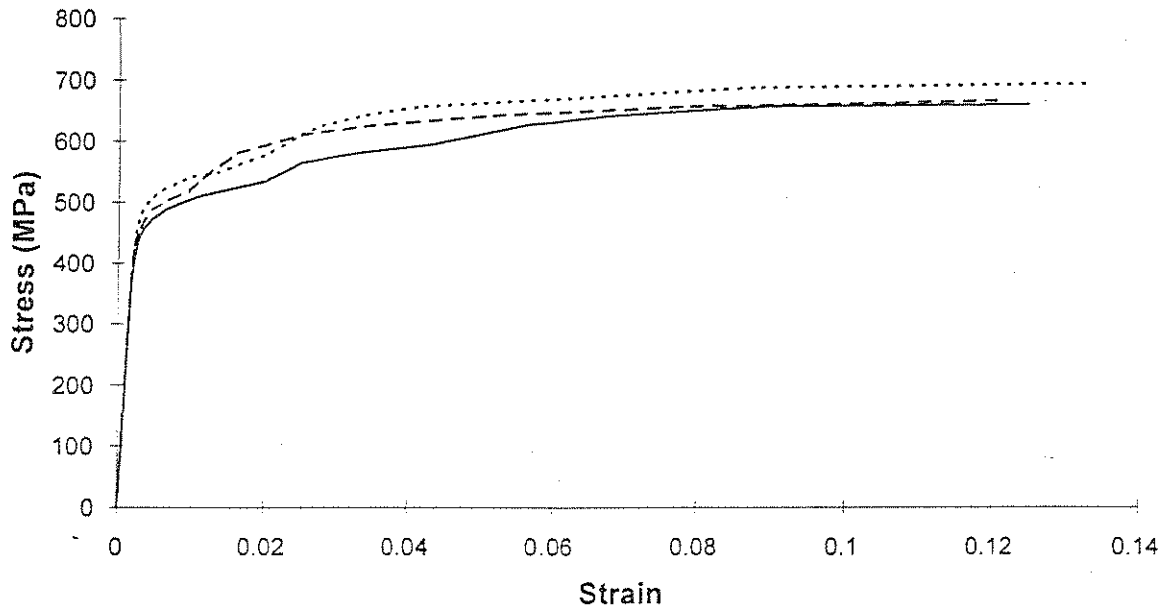


Figure 3-5 Measured Stress-Strain Relationship of  $\phi$  6 mm (#2) Steel Bars

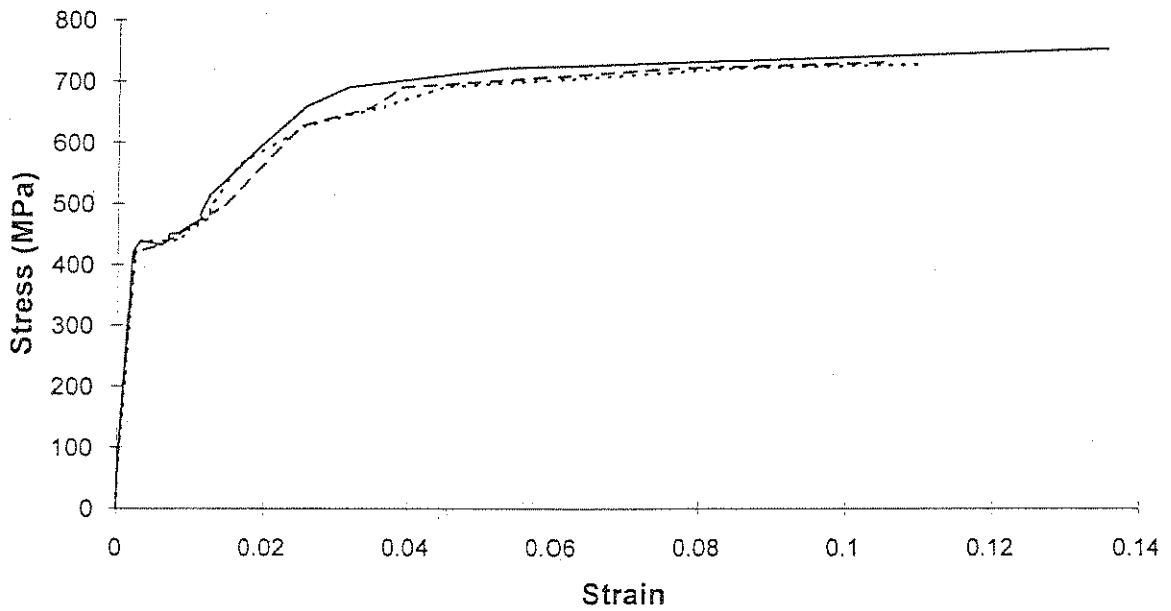


Figure 3-6 Measured Stress-Strain Relationship of  $\phi$  10 mm (#3) Steel Bars

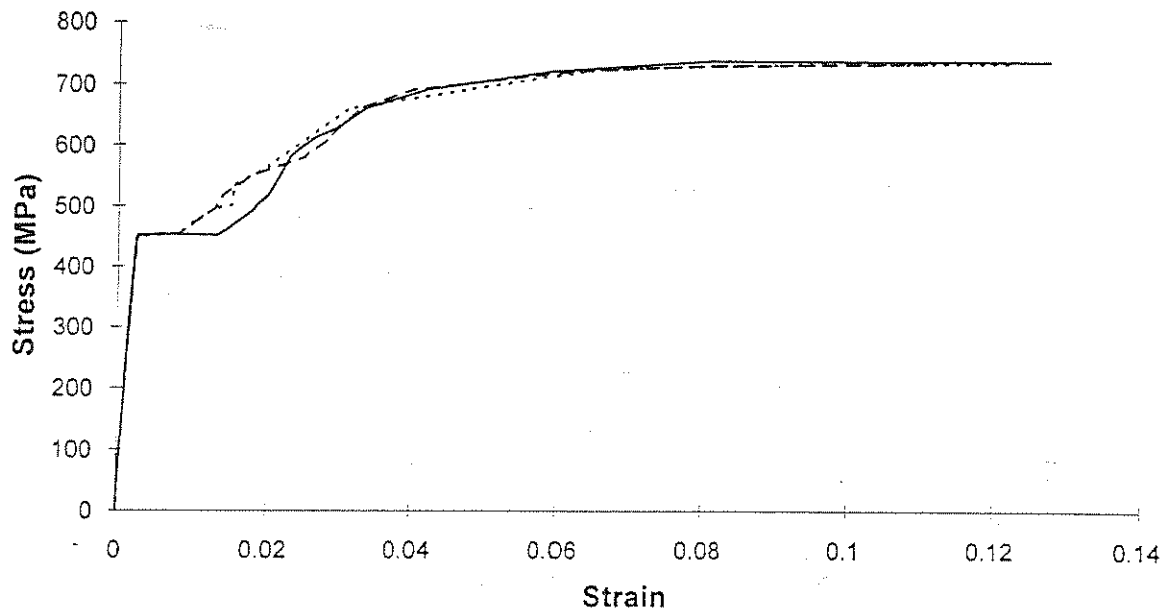


Figure 3-7 Measured Stress-Strain Relationship of  $\phi$  19 mm (#6) Steel Bars

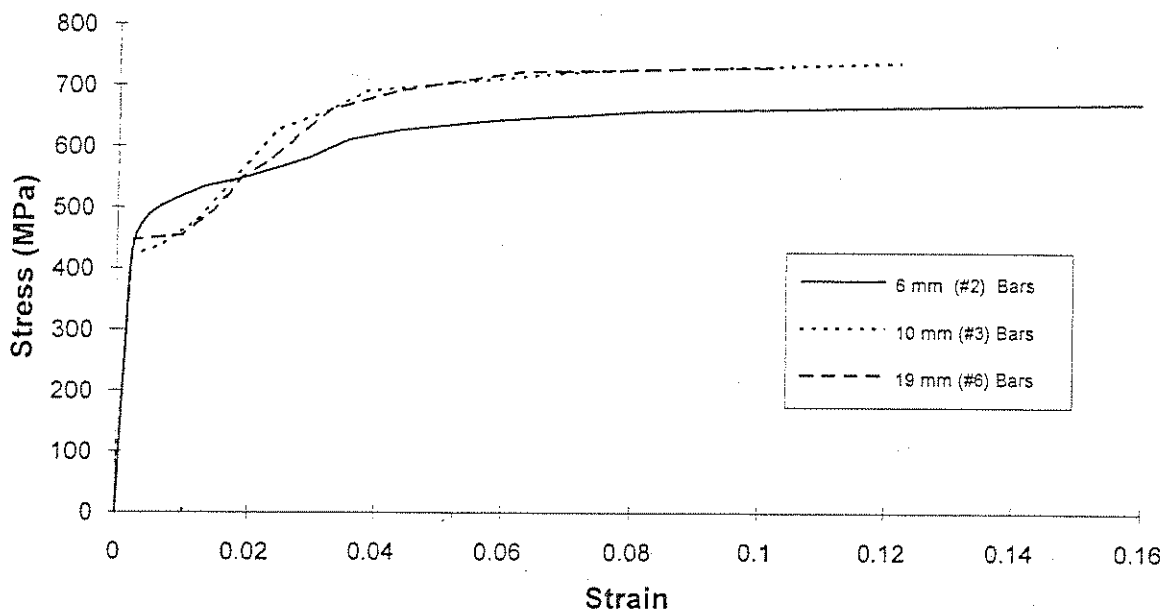


Figure 3-8 Averaged Measured Properties of Steel Bars

### 3.5 Instrumentation

The specimens were instrumented with an array of strain gages, LVDT's, and load cells. The instrumentation arrangement was nearly identical in the four specimens. In all, twenty eight strain gages, eleven LVDT's, and three load cells were used to collect data from each test.

In each column specimen, eight longitudinal bars and three tie sets were instrumented with strain gages. Longitudinal bars with strain gages were placed in the first and the last two steel layers as shown in Figure 3-9. Each instrumented longitudinal bar was fitted with two strain gages, one at the interface of the column and the footing, and the other at mid-distance between the first and the second tie sets from the bottom of the column.

To study the effectiveness of the confining steel, the first three tie sets from the bottom of the column were fitted with strain gages. For each tie set, four gauges were attached as follows: one gage at each short side of the perimeter tie, one gage at one long side of the perimeter tie, and one gage at one of the long cross ties. The strain gage arrangement in the transverse steel is shown in Figure 3-10.

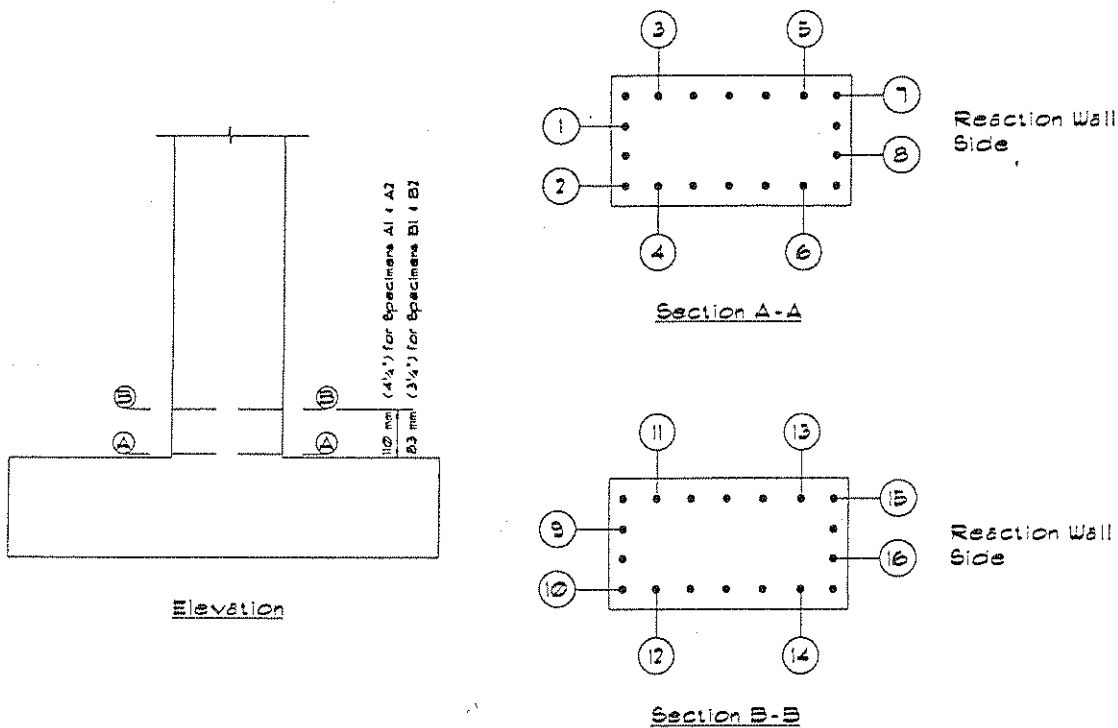


Figure 3-9 Strain Gaging of Longitudinal Bars

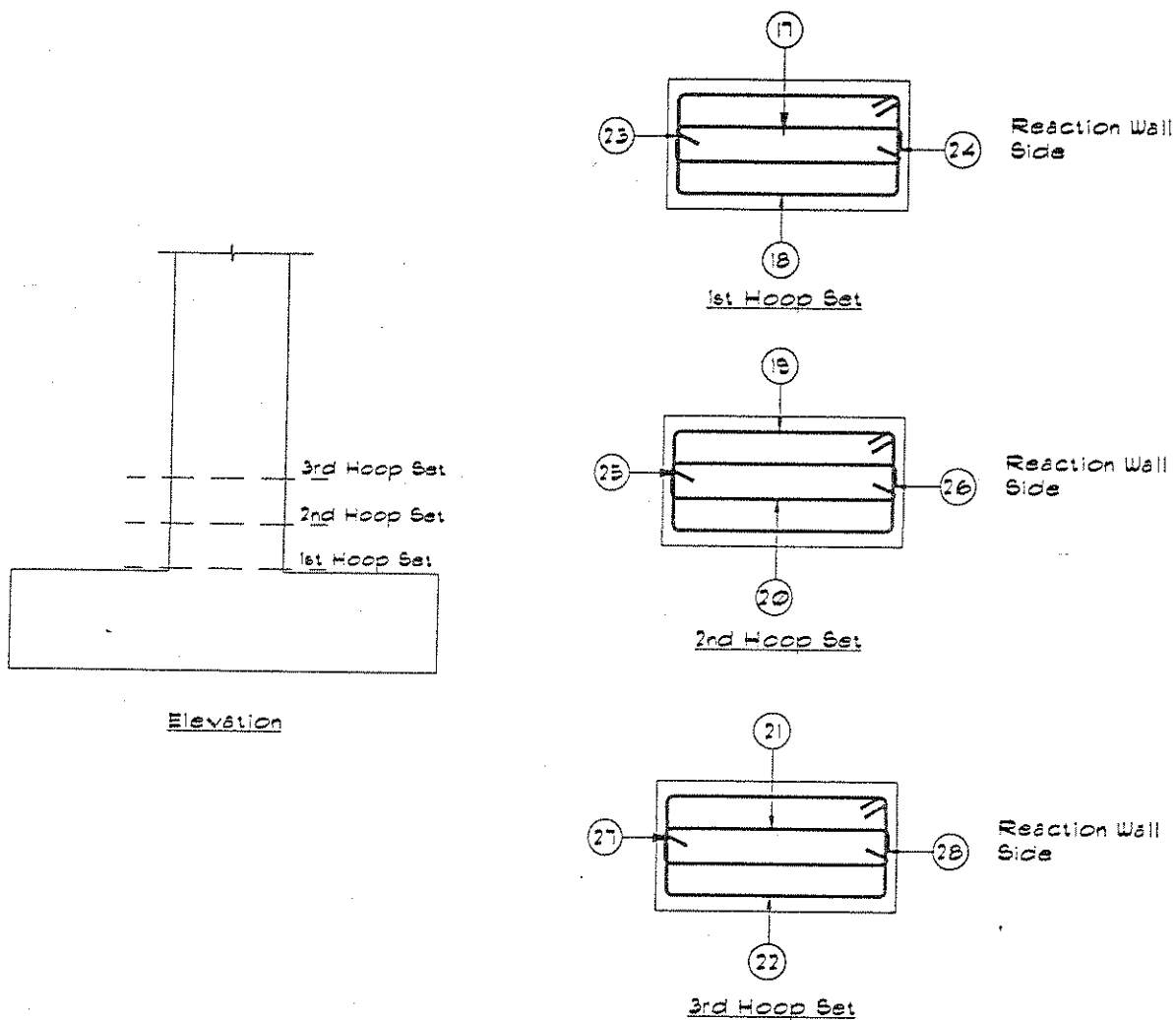


Figure 3-10 Strain Gaging of Transverse Steel

To measure strain in the concrete and section curvature along the potential plastic hinge zone, five pairs of LVDT's were fitted within a height of 685 mm (27 in.) from the bottom of the column. This height was divided into five intervals representing five gage lengths as shown in Figure 3-11. In each interval, two LVDT's were placed, one at each side of the column. Based on the gauge length, different range LVDT's were selected. The bottom 76 mm (3 in.) and 100 mm (4 in.) gauge lengths were fitted with  $\pm 13$  mm ( $\pm 0.5$  in.) and  $\pm 25$  mm ( $\pm 1$  in.) range LVDT's, respectively. The top three gauge lengths were all fitted with  $\pm 50$  mm ( $\pm 2$  in.) range LVDT's.

The lateral deflection of the column was measured along the centerline of the hydraulic actuator applying the lateral load. This was accomplished through the actuator LVDT.

To measure the axial load applied by the two Dywidag<sup>TM</sup> prestressing bars, a load cell was installed under the top anchor mechanism of each bar. The lateral load applied at the top of the column was measured by means of the actuator load cell.

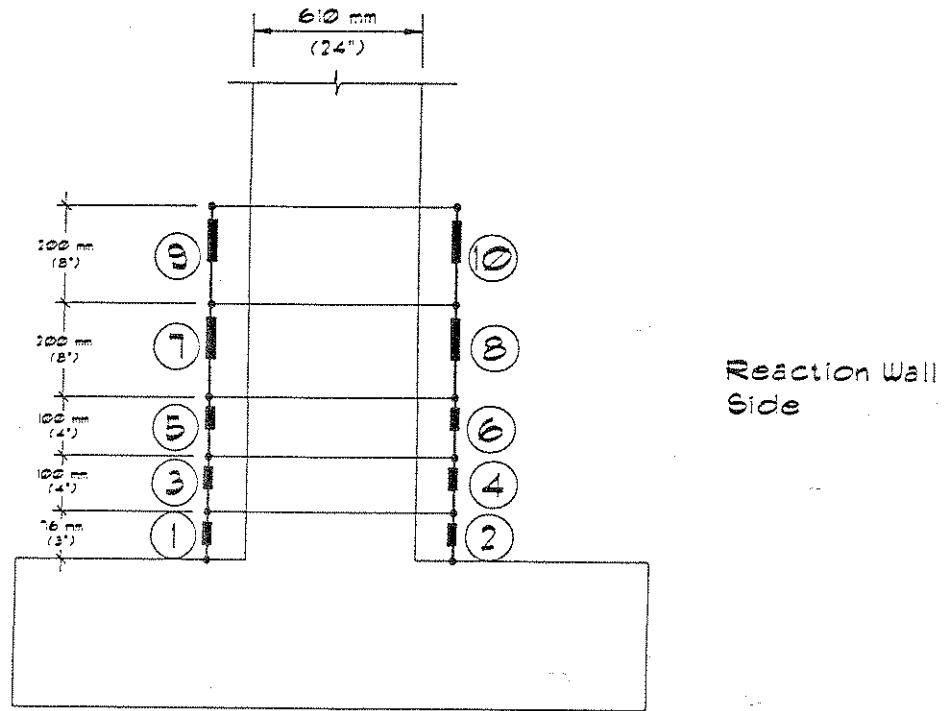


Figure 3-11 LVDT Setup for the Test Specimens

Data from strain gages, LVDT's and load cells were collected and recorded by means of a Megadac Model 5033A data acquisition system. The system was set to scan and record instrument readings at a rate of one reading per second. Data recording could be stopped and resumed at any instant during the test.

### 3.6 Test Setup

The test specimen was lifted and set at the test location. To level the specimen and to provide full contact between the footing and the floor of the testing laboratory, the bottom of the footing was set about 13 mm (0.5 in.) above the floor, then a mix of gypsum cement was poured to fill the gap between the bottom of the footing and the floor. The test setup is shown in Figure 3-12.

The transfer of axial and lateral loads to the specimen was accomplished through a steel I-beam that was placed across the top of the column as shown in Figure 3-12. The flange width, flange thickness and web thickness of the steel beam were 305 mm (12 in.), 50 mm (2 in.) and 25 mm (1 in.), respectively. The beam length was 1520 mm (5 ft) and the overall depth was 610 mm (24 in.). Four  $\phi$  38 mm (1.5 in.) holes were drilled in the bottom flange of the beam to allow for the passage of the column anchor bolts. To prevent stress concentrations and cracking of the concrete at the top of the column, a 610 mm (24 in.) by 380 mm (15 in.) by 16 mm ( $\frac{5}{8}$  in.) steel plate was placed between the steel beam and the top of the column. The cross beam was then placed in position and secured to

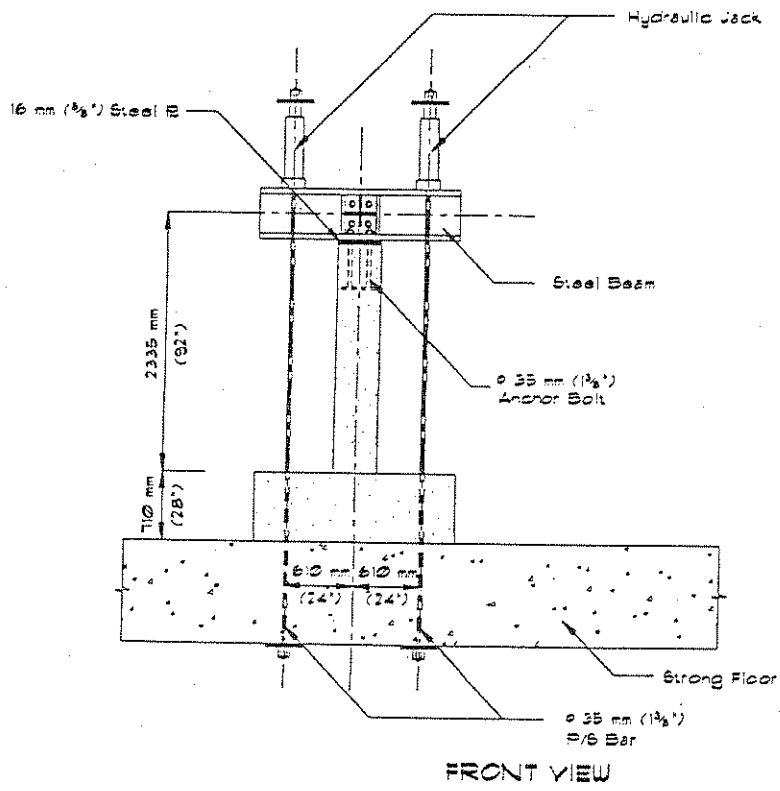
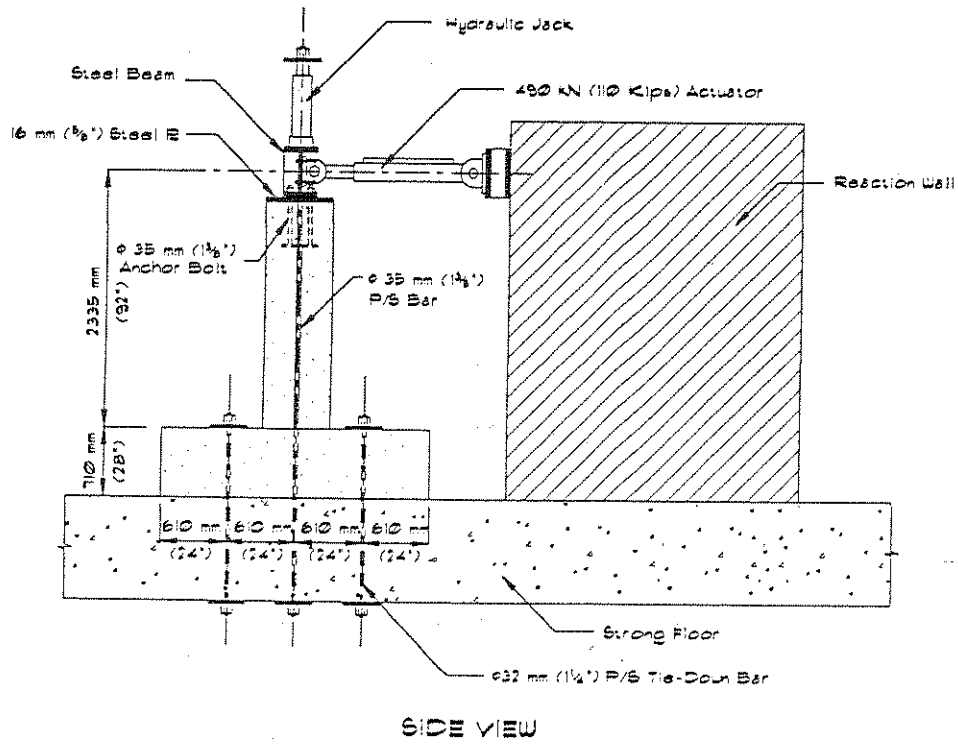


Figure 3-12 Test Setup

the top of the column by means of four  $\phi$  35 mm (1 $\frac{3}{8}$  in.) nuts.

To prevent rocking of the footing under the applied overturning moments during the test, four  $\phi$  32 mm (1.25 in.) Dywidag™ bars were used to tie down the footing to the strong floor. The prestressing bars were passed through the sleeves in the footing and the strong floor. Each bar was stressed to an initial jacking force of 134 kN (30 Kips) then was anchored at the top of the footing and the bottom of the floor slab.

Lateral load was applied by means of a 490 kN (110 Kip) MTS hydraulic actuator. The actuator base was first connected to the reaction wall by means of a connector steel plate then the actuator head was extended and connected to the web of the cross beam on top of the column. In its initial position, the actuator was level and had a potential maximum stroke of  $\pm 280$  mm ( $\pm 11$  in.).

Two  $\phi$  35 mm (1.375 in.) Dywidag™ bars were used to apply the axial load. The initial prestressing force was applied by means of one hydraulic jack per each bar. The jacks were placed at the top of the steel cross beam, then the prestressing bars were extended vertically and anchored at the top of the jacks and the bottom of the strong floor. The jacks were identical and were connected in parallel to the same pressurizing pump. To minimize axial load fluctuation caused by variation in the prestressing bars length under different drift levels, a 70 MPa (10,000 psi) pressure accumulator was hooked to the hydraulic system between the pump and the jacks. At the beginning of each test, the desired axial load was applied prior to lateral loading.

### 3.7 Experimental Procedure and Results

#### 3.7.1 General Remarks

Unlike reinforced concrete members with only two layers of steel placed at opposite ends, a concrete section with main reinforcement distributed throughout the depth of the section does not normally exhibit a well defined yield point, but rather a yield region that depends mainly on the amount and the distribution of the main reinforcement. To facilitate the analysis of such cases, it is customary to determine an effective yield point of the member as shown in Figure 3-13. For reinforced concrete columns, it is normally acceptable to assume that the calculated ultimate moment capacity of the unconfined section is the effective yield moment of the confined section (15).

Experimentally, one way to determine the effective yield displacement ( $\Delta_y$ ) corresponding to the effective yield load ( $M_y$  or  $F_y$ ) is found as follows. First, the specimen is loaded in one direction up to 75 percent of the effective yield load then the load is reversed until it reaches 75 percent of the yield load in the other direction. The corresponding displacements are measured and the average of the maximum displacements in both direction is considered as  $0.75\Delta_y$ , as shown in Figure 3-14. The effective yield displacement can then be found by extrapolation. This procedure was followed in this study.

Readings of LVDT's located at the bottom of the column were employed to measure curvatures

along the potential plastic hinge zone. To find the average strain at each LVDT location, the measured displacement was divided by the corresponding gage length. This strain was considered to be the strain at the middle of the gauge length. Knowing the distance between the LVDT's placed at opposite sides, it was possible to measure curvatures at column sections along the mid-height of the gage lengths.

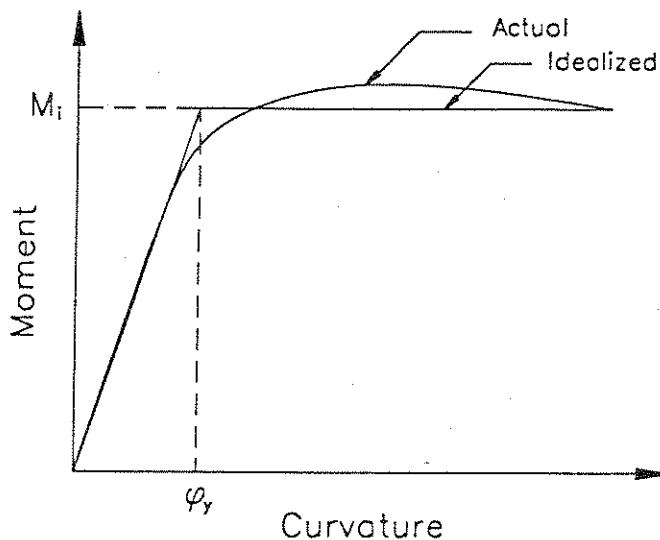


Figure 3-13 Idealized Moment-Curvature Relationship

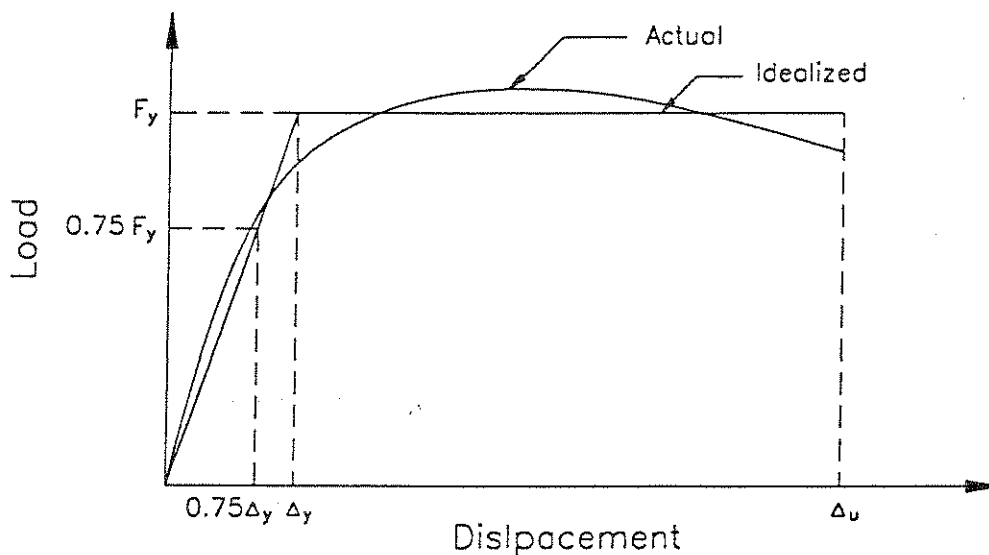


Figure 3-14 Experimental Determination of Effective Yield Displacement

On the day of testing, the desired axial load was first applied then the specimen was subjected to unidirectional lateral cyclic loading in the strong direction of the column. The lateral load was monotonic, load controlled up to  $\pm 75$  percent the effective yield moment ( $\pm 0.75 M_y$ ) at the bottom of the column, and displacement controlled afterward. Each specimen was first subjected to one full cycle at post-cracking moment ( $M_{cr}$ ), one full cycle at  $0.75 M_y$ , two full cycles at a displacement ductility  $\mu_\Delta$  of  $\pm 1$ , and two full cycles at a displacement ductility  $\mu_\Delta$  of  $\pm 2$ . Afterward, in general, specimens with lower axial load (A1 and B1) were then cycled at displacement ductility increments of 2 whereas those with higher axial loads (A2 and B2) were cycled at displacement ductility increments of 1, until failure. At each ductility level, the specimen was taken through at least two full excursions. Failure of the specimen was considered to occur when the lateral load carrying capacity was reduced by at least 25% of the maximum measured section capacity. This failure criterion was set to ensure that the test specimen does not lose stability at high drift and reduced strength. Test results are summarized in Table 3-5.

Table 3-5 Measured Displacements and Ductilities

Specimen	Measured			
	$\Delta_y$ mm (in)	$\Delta_u$ mm (in.)	$\mu_\Delta$	Drift Ratio %
A1	23 (0.92)	122 (4.82)	5.2	5.2
A2	20 (0.79)	102 (4.02)	5.1	4.4
B1	23 (0.92)	161 (6.33)	6.9	6.9
B2	21 (0.82)	130 (5.10)	6.2	5.5

### 3.7.2 Specimen A1

Specimen A1 was first subjected to an initial axial load of 615 kN (138 Kips) corresponding to an axial load index of 0.1. Under high lateral displacements the axial load increased but was still very close to the target value of  $0.1 f'_c A_g$ . In general the axial load fluctuated during the test between a minimum of 592 kN (133 Kips) and a maximum of 641 kN (144 Kips). Based on the measured material properties and an axial load of 641 kN (144 Kips), the effective yield moment of Specimen A1 was calculated as 643 kN-m (5690 Kip-in) corresponding to a lateral load of 275 kN (61.8 Kips).

The lateral cyclic load history, shown in Figure 3-15, was applied according to the procedure described in Section 3.7.1. At a lateral load of approximately 89 kN (20 Kips), two flexural cracks were visible at 125 mm (5 in.) and 230 mm (9 in.) from the bottom of the column. Prior to first bar yield, one post-crack cycle was completed to establish the effective yield displacement,  $\Delta_y$ . The average measured  $\Delta_y$  was 23 mm (0.92 in.). The hysteretic load-displacement response of Specimen A1 is shown in Figure 3-16.

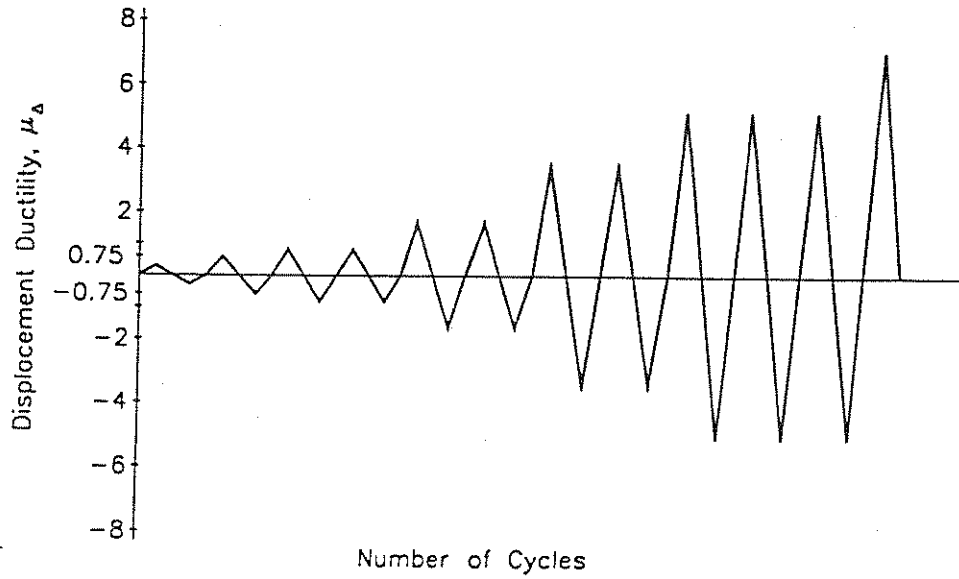


Figure 3-15 Lateral Load History for Specimen A1

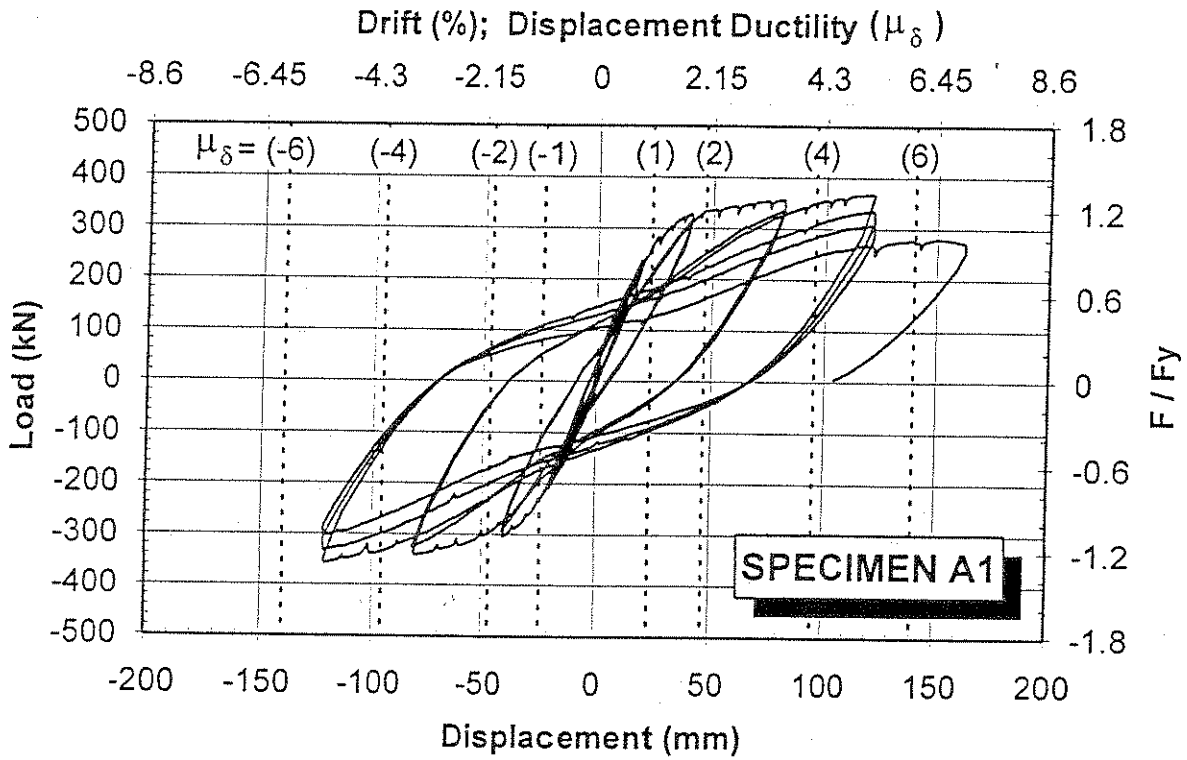


Figure 3-16 Measured Lateral Load-Deflection Hysteresis Loops for Specimen A1

At a displacement ductility  $\mu_{\Delta}$  of approximately  $\pm 1$ , the specimen did not show signs of strength decay or significant stiffness degradation. During the second excursion of  $\mu_{\Delta} = +2$ , slight stiffness degradation was apparent with minor decay in strength. When the specimen was taken to a second cycle of  $\mu_{\Delta} = -2$ , the cover concrete started to spall on the compression side. As the specimen was pushed to higher ductility levels, the cover concrete at the bottom of the column spalled at an increasing rate, exposing the first and second main steel layers on both sides of the column. Flexural-shear cracks were also developing along the column height. The peak measured lateral load was 361 kN (81 Kips). This peak load occurred at the end of the first excursion of  $\mu_{\Delta} = +5.2$ , corresponding to a ram displacement of 122 mm (4.82 in.). During the second excursion of  $\mu_{\Delta} = +5.2$ , the compression longitudinal bars began to buckle and the 90° hook of the second tie set from the bottom of the column started to open, accompanied by significant reduction in the column stiffness. As the specimen was cycled to a third excursion of  $\mu_{\Delta} = \pm 5.2$ , the core concrete suffered more degradation and the 135° hooks on the second and third tie sets began to open. When the specimen was pushed to a displacement of +163 mm (6.41 in.), corresponding to  $\mu_{\Delta} = +7$ , the longitudinal bars on the compression side completely buckled and the lateral load capacity was reduced to 267 kN (60 Kips). This load corresponded to 74 percent of the measured peak load and 97 percent of the effective lateral yield load. At this point the specimen was considered to have failed. Figures 3-17 through 3-20 show Specimen A1 during several stages of the test.

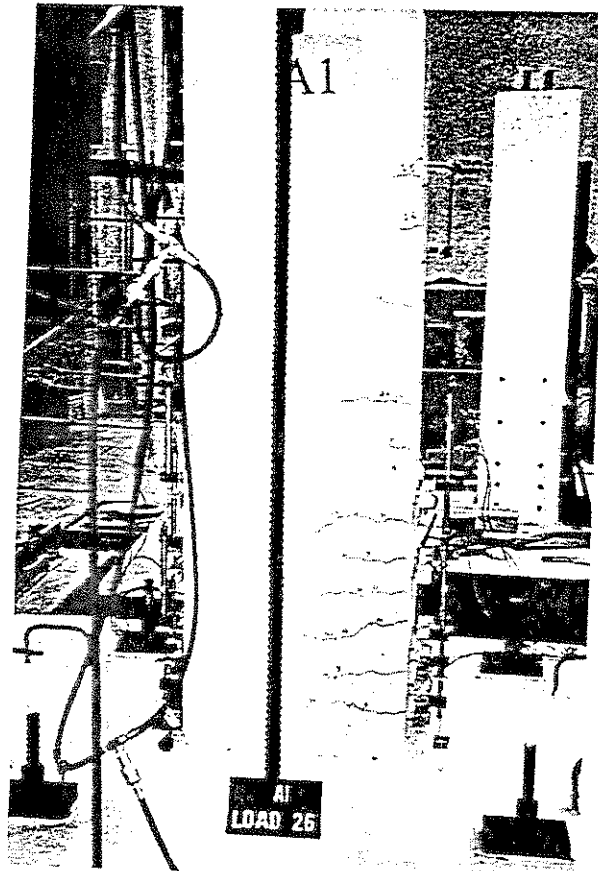


Figure 3-17 Specimen A1 at  $\mu_{\Delta} = +1$  (1st Excursion)

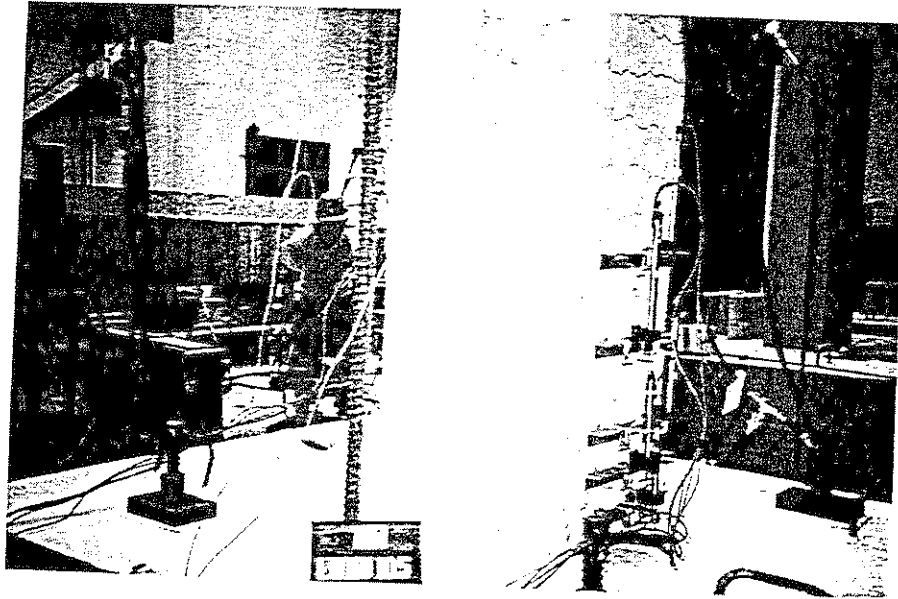


Figure 3-18 Specimen A1 at  $\mu_{\Delta} = +4$  (1st Excursion)

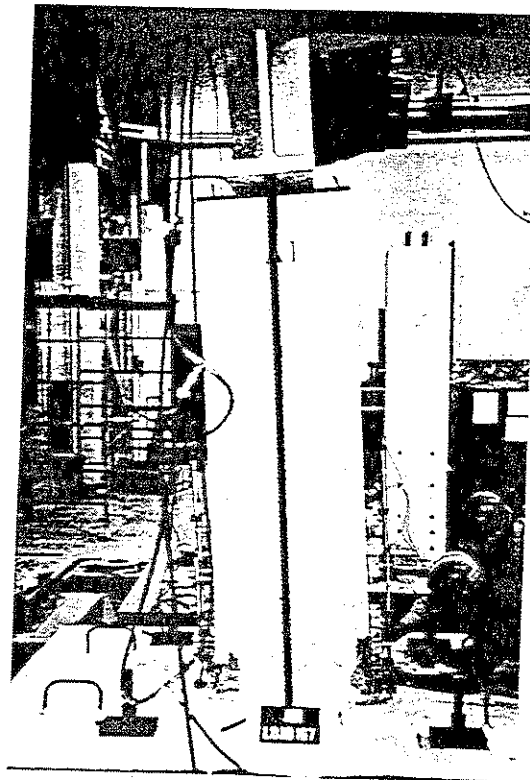
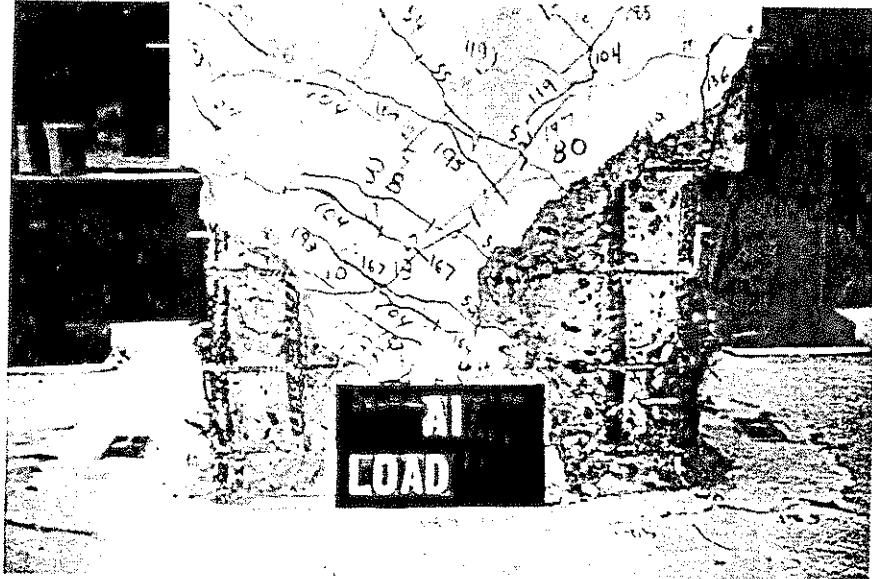


Figure 3-19 Specimen A1 at  $\mu_{\Delta} = +6$  (1st Excursion)



**Figure 3-20 Plastic Hinge in Specimen A1 at the End of the Test**

A review of the strain gage data revealed that yielding occurred in longitudinal steel at an early stage of the test before reaching the calculated effective section yield. Figure 3-21 presents the measured load-strain relationship of a first layer longitudinal bar at the column-footing interface (Gage No. 1 in Figure 3-9). On the other hand, some of the transverse steel yielded towards the end of the test and some attained high strains but did not yield. Figure 3-22 and Figure 3-23 show the measured load-strain of lateral steel at the second and third tie set levels, respectively (Gages No. 19 and 22 in Figure 3-10).

The measured curvature envelop along the potential plastic hinge is presented in Figure 3-24. The intersection of the curvature line at yield with the curvature envelop represents the upper limit of the plastic hinge. Consequently, the measured plastic hinge length was found to be 445 mm (17.5 in.).

### **3.7.3 Specimen A2**

For Specimen A2, the initial applied axial load was 1505 kN (338 Kips) corresponding to an actual load index of 0.24. During the test, the axial load varied between a minimum of 1479 kN (332 Kips) and a maximum of 1581 kN (355 Kips). For the purpose of determining the effective yield displacement, the effective yield moment was computed prior to the test and was found to be 732 kN-m (6480 Kip-in). This moment corresponded to a lateral load of 314 kN (70.4 Kips) at the ram level.

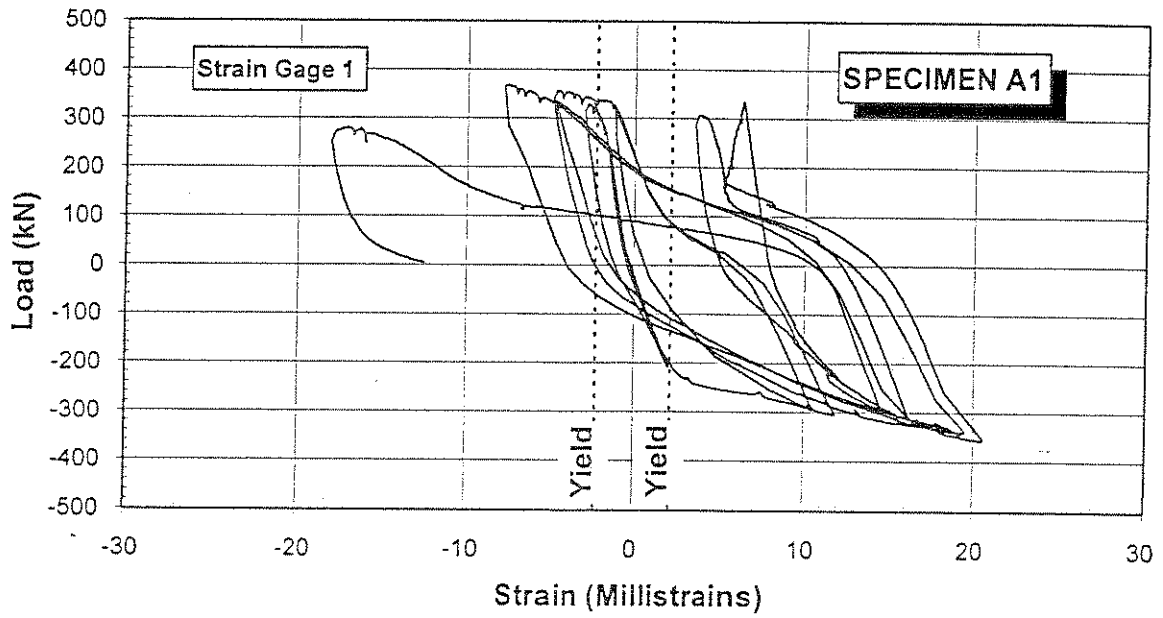


Figure 3-21 Measured Lateral Load-Strain Hysteresis in Specimen A1 Longitudinal Bar

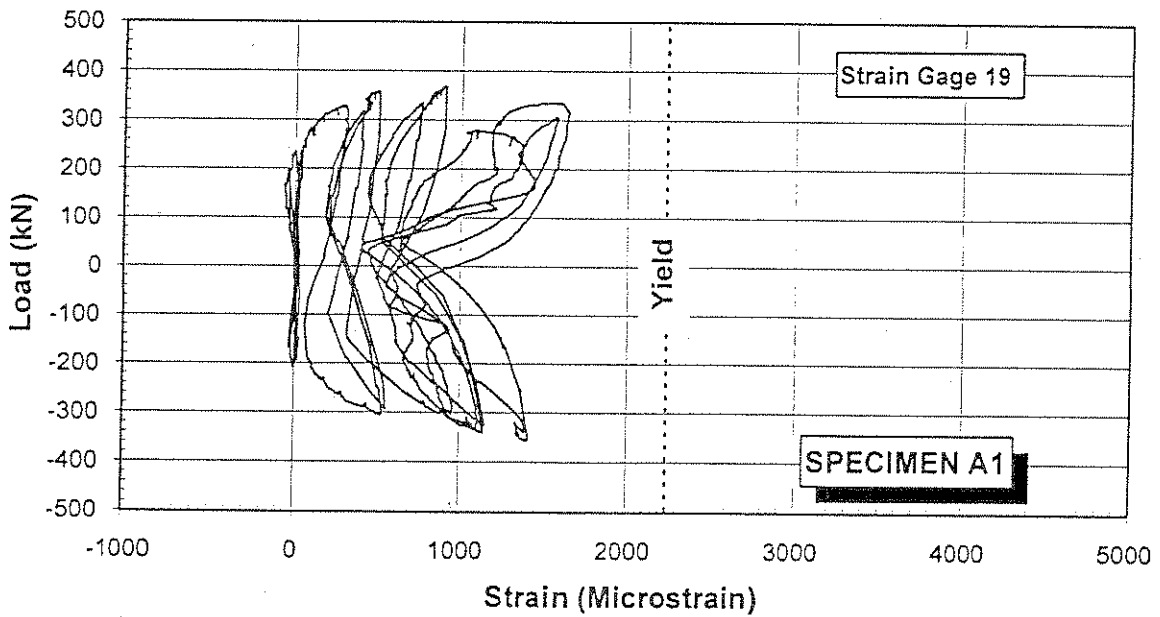


Figure 3-22 Measured Lateral Load-Strain in Specimen A1 Lateral Steel at SG 19

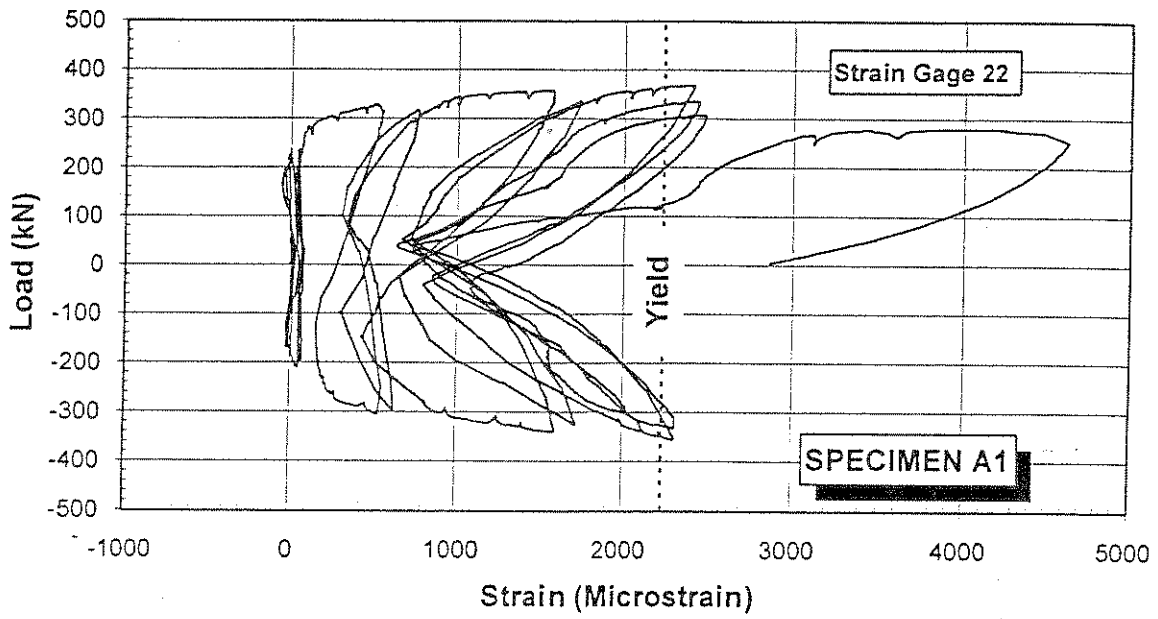


Figure 3-23 Measured Lateral Load-Strain in Specimen A1 Lateral Steel at SG 22

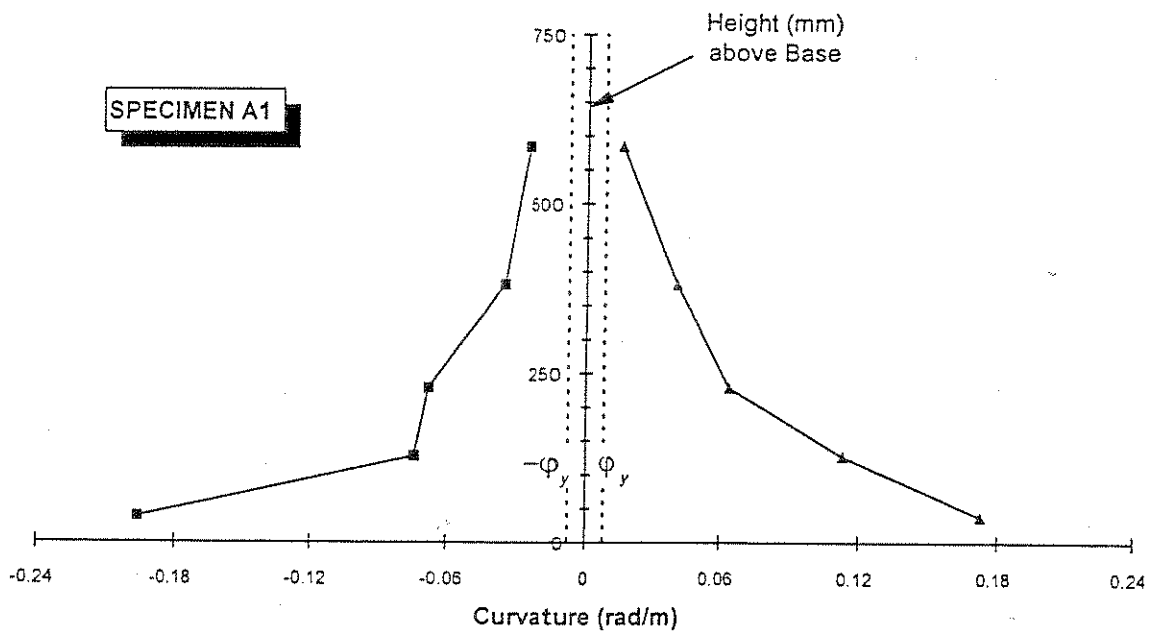


Figure 3-24 Measured Curvature Envelop along the Plastic Hinge of Specimen A1

The lateral load history for Specimen A2 is presented in Figure 3-25. The first visible flexural crack in the column occurred at approximately 280 mm (11 in.) from the column base. The corresponding lateral load was 143 kN (32 Kips). At a lateral load of 232 kN (52 Kips), several flexural cracks appeared along the bottom half of the column. The pattern of these cracks was consistent with the hoop set spacing. The effective average yield displacement was determined experimentally as 20 mm (0.79 in.). The measured lateral load-displacement response of Specimen A2 is presented in Figure 3-26.

Spalling of the cover concrete started to show at the bottom of the compression side when the column was pushed to  $\mu_{\Delta} = +2$  for the first cycle. Despite the fact that spalling of the cover concrete was spreading on both sides of the column bottom with increasing drift, the hysteretic response was very stable and the stiffness degradation between the same ductility cycles was negligible up to  $\mu_{\Delta} = +4$ . The lateral load peaked at 396 kN (89 Kips) when the displacement ductility of +5 was attained for the first time. At  $\mu_{\Delta} = -5$ , first excursion, the longitudinal bars on the compression side started to buckle between the second and the third tie sets. During the next two cycles at displacement ductility of 5, the lateral steel end hooks were opening at the second and the third tie sets. This was accompanied by significant stiffness degradation and strength decay. At  $\mu_{\Delta} = +6$ , the longitudinal compression bars buckled completely and the lateral load dropped to 223 kN (50 Kips), signifying failure of the specimen. This load corresponded to 56 percent of the measured peak load and 71 percent of the effective lateral yield load (nominal load). Figures 3-27 through 3-30 show Specimen A2 during the development of the test.

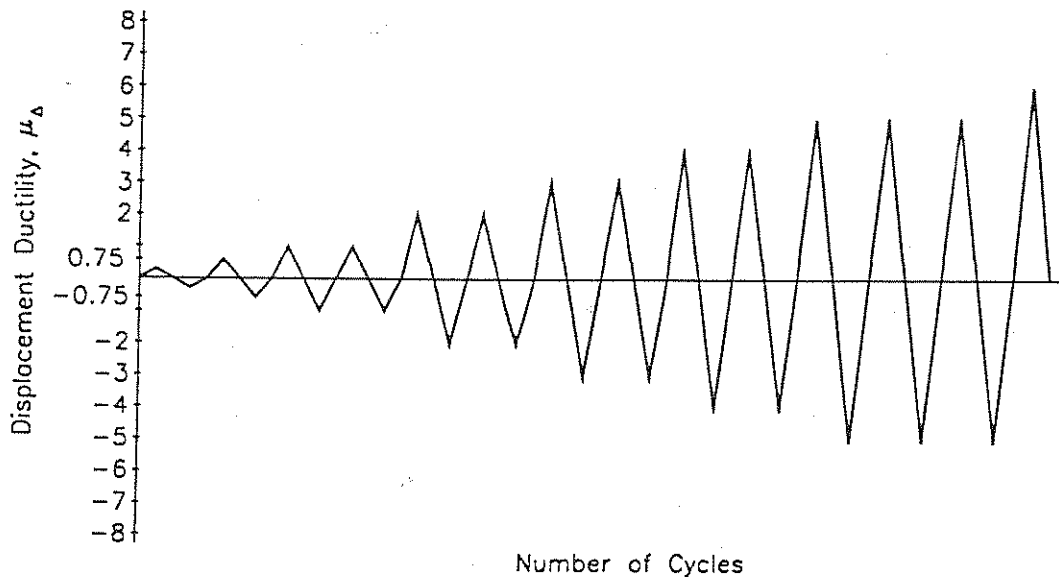


Figure 3-25 Lateral Load History for Specimen A2

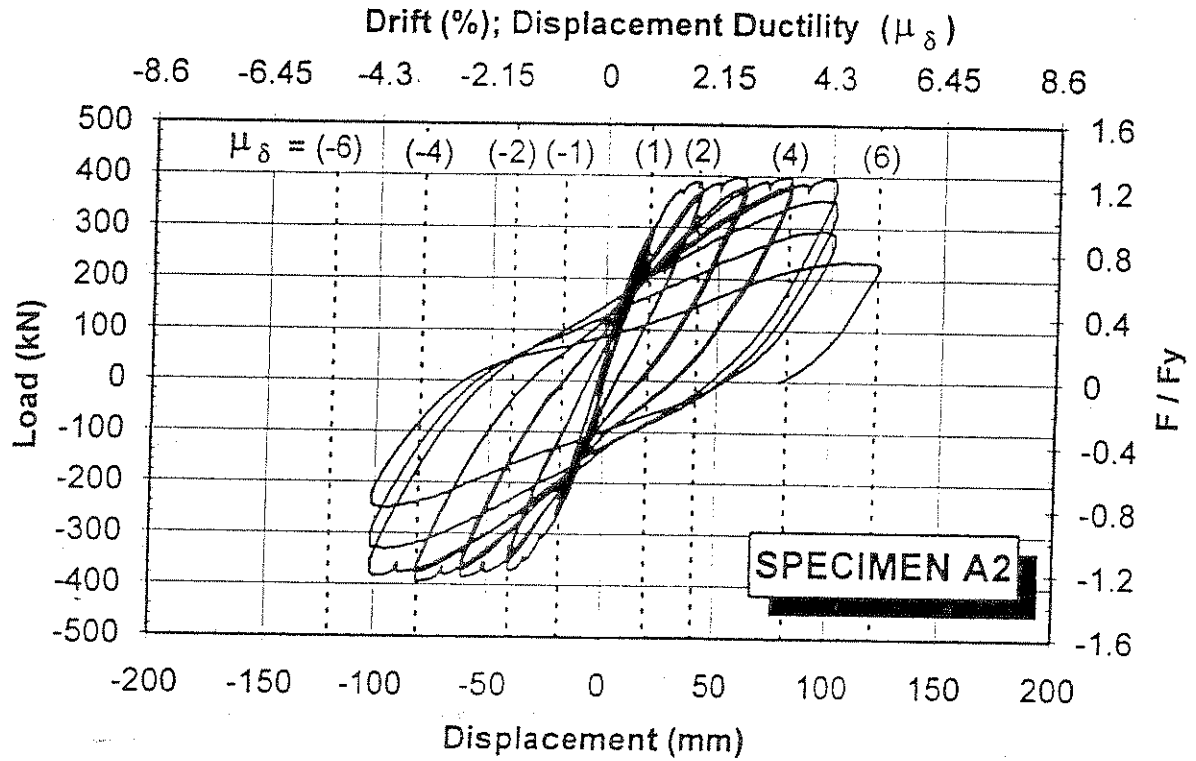


Figure 3-26 Measured Lateral Load-Deflection Hysteresis Loops for Specimen A2

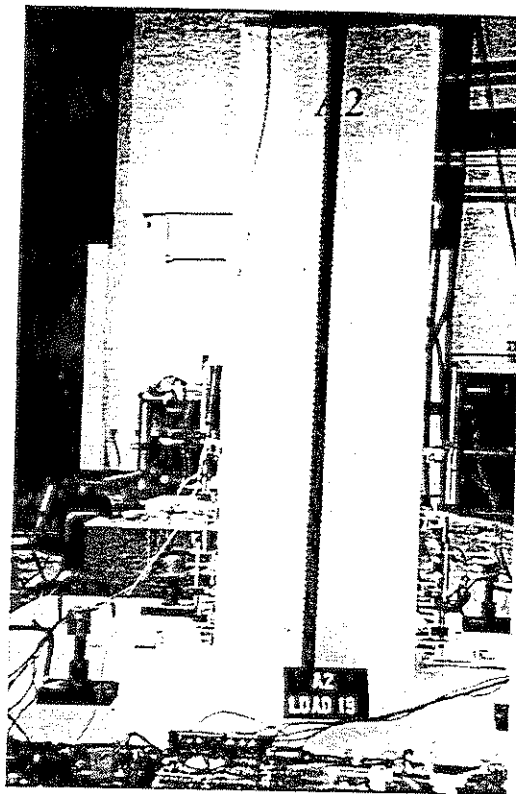


Figure 3-27 Specimen A2 at  $\mu_\Delta = +1$  (2nd Excursion)

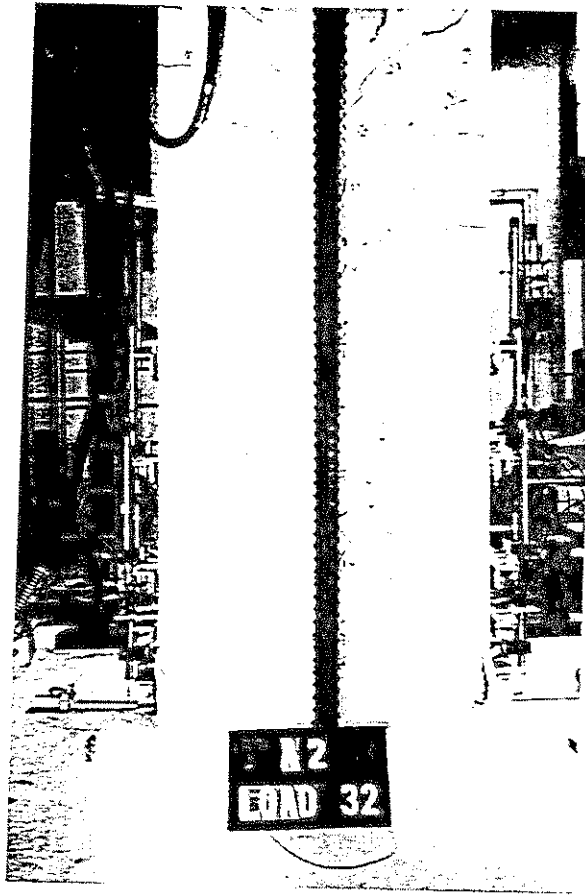


Figure 3-28 Specimen A2 at  $\mu_{\Delta} = -2$  (2nd Excursion)

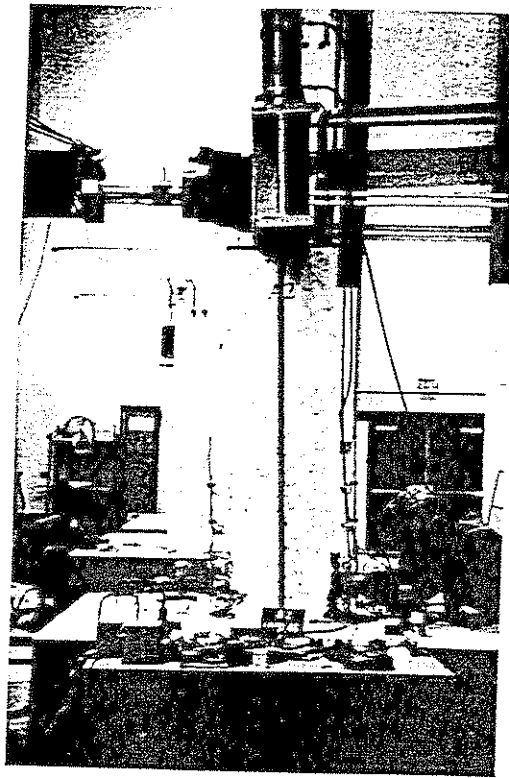


Figure 3-29 Specimen A2 at  $\mu_{\Delta} = -4$  (1st Excursion)

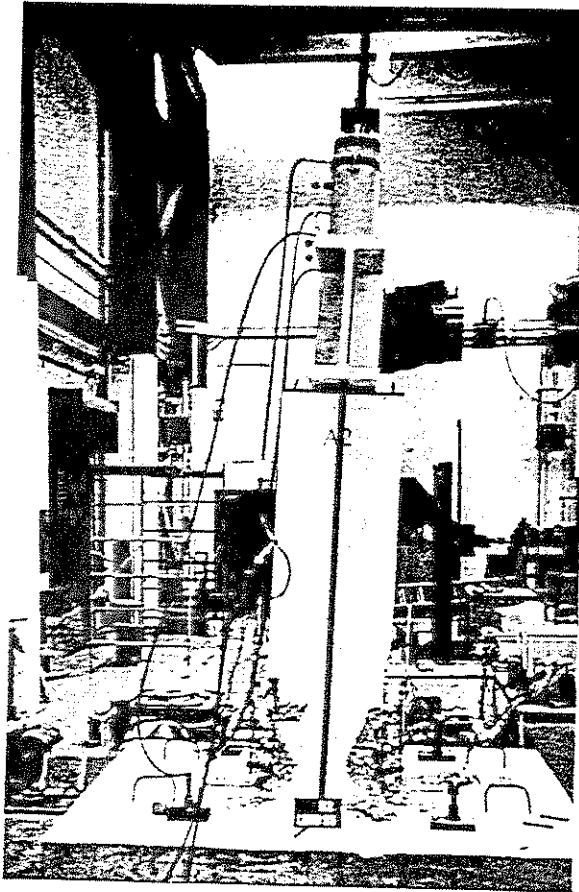


Figure 3-30 Plastic Hinge in Specimen A2 at the End of the Test

Measured strains in one longitudinal bar and two lateral bars are shown in Figure 3-31 and Figures 3-32 and 3-33, respectively (Gages No. 1, 18 and 19 in Figures 3-9 and 3-10). As with Specimen A1, yielding of the outer layer longitudinal bars in Specimen A2 was reached before the point of effective section yield. On the other hand, yielding of the lateral steel coincided with the specimen failure.

Figure 3-34 exhibits the plastic hinge measured curvature envelop for Specimen A2. The corresponding measured plastic hinge length was 570 mm (22.5 in.).

#### 3.7.4 Specimen B1

Specimen B1 was initially subjected to an axial load of 601 kN (135 Kips) or  $0.09 f_c' A_g$ . At high drift levels, the axial load peaked at 637 kN (143 Kips). The calculated effective yield moment and the corresponding lateral load were 645 kN-m (5710 Kip-in) and 276 kN (62 Kips), respectively.

Figure 3-35 shows the lateral loading history of Specimen B1. No effort was made to observe the initial flexural cracks because it was believed that the column concrete was pre-cracked during specimen setup. Since the axial load of Specimen B1 was similar to that of Specimen A1, it was decided to assume that both specimens had the same effective yield displacement of 23 mm (0.92 in.). The load-displacement hysteresis for Specimen B1 is shown in Figure 3-36.

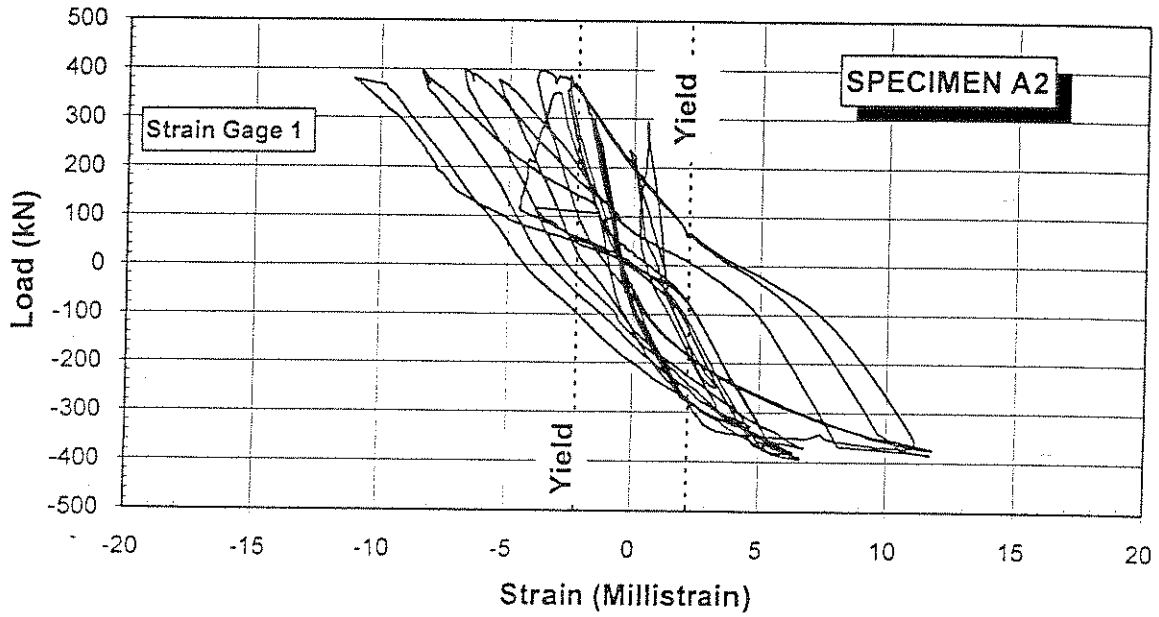


Figure 3-31 Measured Lateral Load-Strain Hysteresis in Specimen A2 Longitudinal Bar

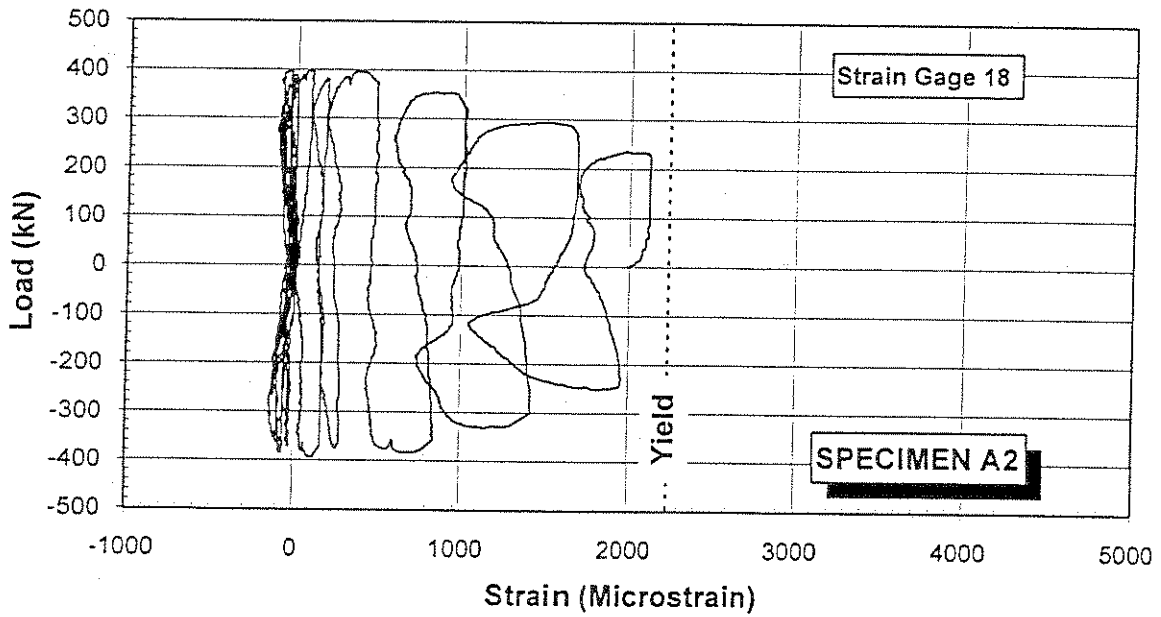


Figure 3-32 Measured Lateral Load-Strain in Specimen A2 Lateral Steel at SG 18

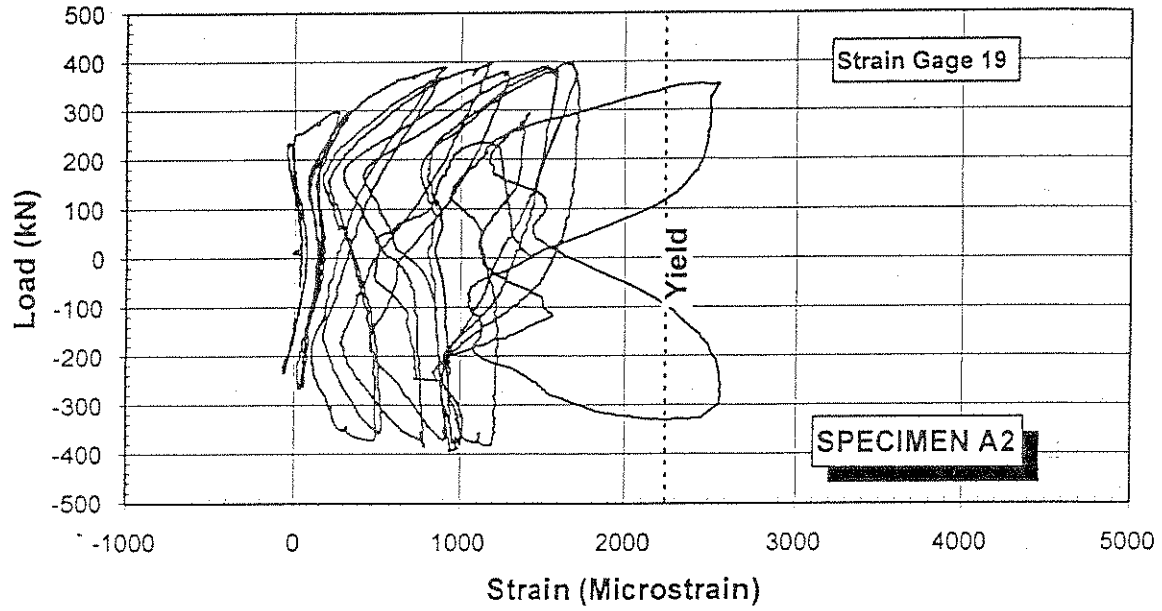


Figure 3-33 Measured Lateral Load-Strain in Specimen A2 Lateral Steel at SG 19

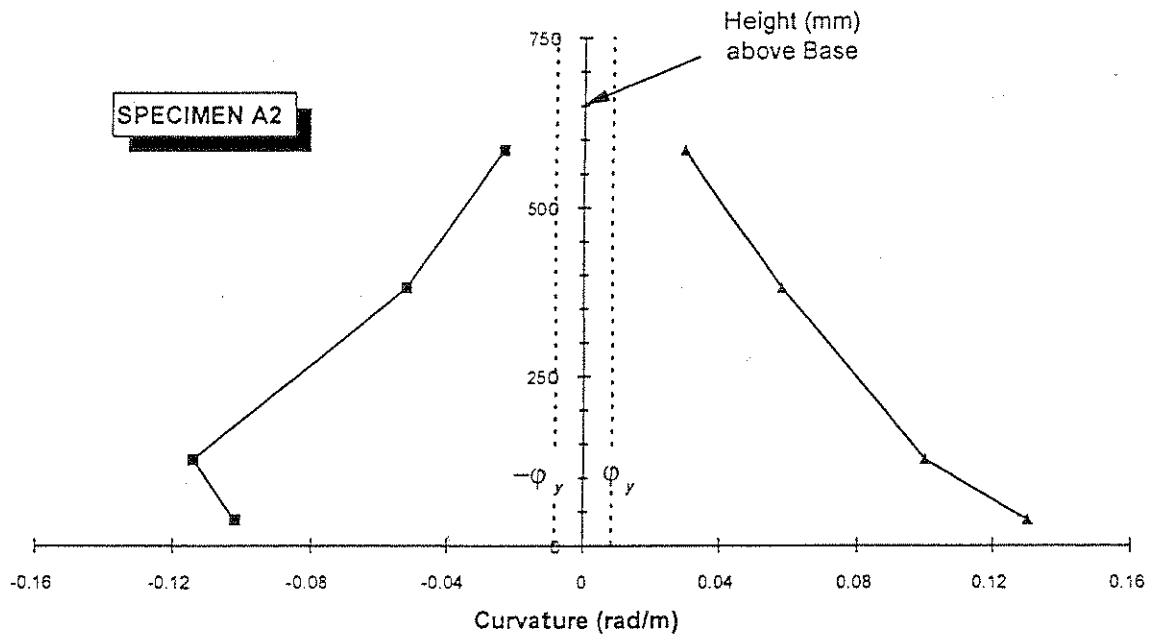


Figure 3-34 Measured Curvature Envelop along the Plastic Hinge of Specimen A2

At displacement ductility  $\mu_{\Delta} = +2$ , first loop, the cover concrete at the bottom of the column started to spall. As the test progressed and the column was pushed to higher drifts, the cover concrete spalling spread upward along the potential plastic hinge length. The hysteresis loops were stable up to a displacement ductility of 6 although signs of minor stiffness degradation were showing during second loops. During the second cycle of  $\mu_{\Delta} = +6$ , the 90° hook of the second tie set on the compression side started to open. At displacement ductility of 7, the core concrete deteriorated rapidly and the end hooks of the second and the third tie sets opened. This was accompanied by buckling of the longitudinal bars and strength decay. As the specimen was pushed to the target displacement ductility of 8, the second bar of the first steel layer on the compression side fractured due to low-cycle fatigue. The test was terminated when the lateral load dropped to 209 kN (47 Kips) at a ram displacement of 186 mm (7.33 in.). The peak recorded lateral load was 379 kN (85 Kips) and it occurred at  $\mu_{\Delta} = +6$ , first loop. The load at failure was 55 percent of the measured peak load and 75 percent of the nominal lateral load. Figures 3-27 through 3-40 show Specimen B1 during different stages of the test.

The longitudinal bar load-strain behavior in Specimen B1 was similar to those of Specimen A1 and Specimen A2. The outer two layers longitudinal bars yielded early in the test as is shown in Figure 3-41 (Gage No. 1 in Figure 3-9). The yielding in the transverse steel occurred on the onset of specimen failure. Figures 3-42 and 3-43 present the lateral load versus tie strain at two locations in the specimen (Gages No. 20 and 22, respectively, in Figure 3-10).

The measured curvature envelop along the potential plastic hinge length is shown in Figure 3-44. Since the top segment of the right-hand-side envelop was not realistic (Figure 3-44), it was decided that this segment could be more appropriately represented by the extension of the second envelop segment from the top. The corresponding measured plastic hinge length would be 415 mm (16.9 in.).

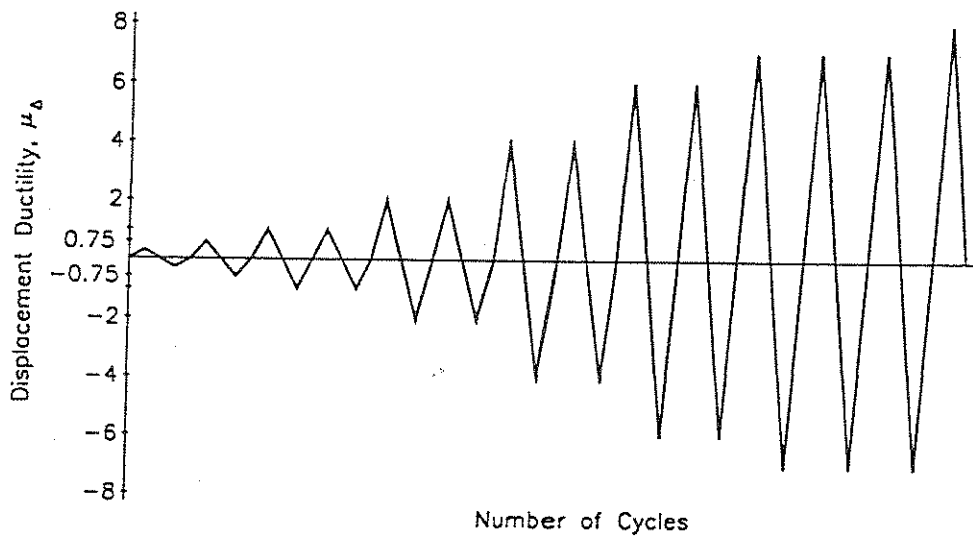


Figure 3-35 Lateral Load History for Specimen B1

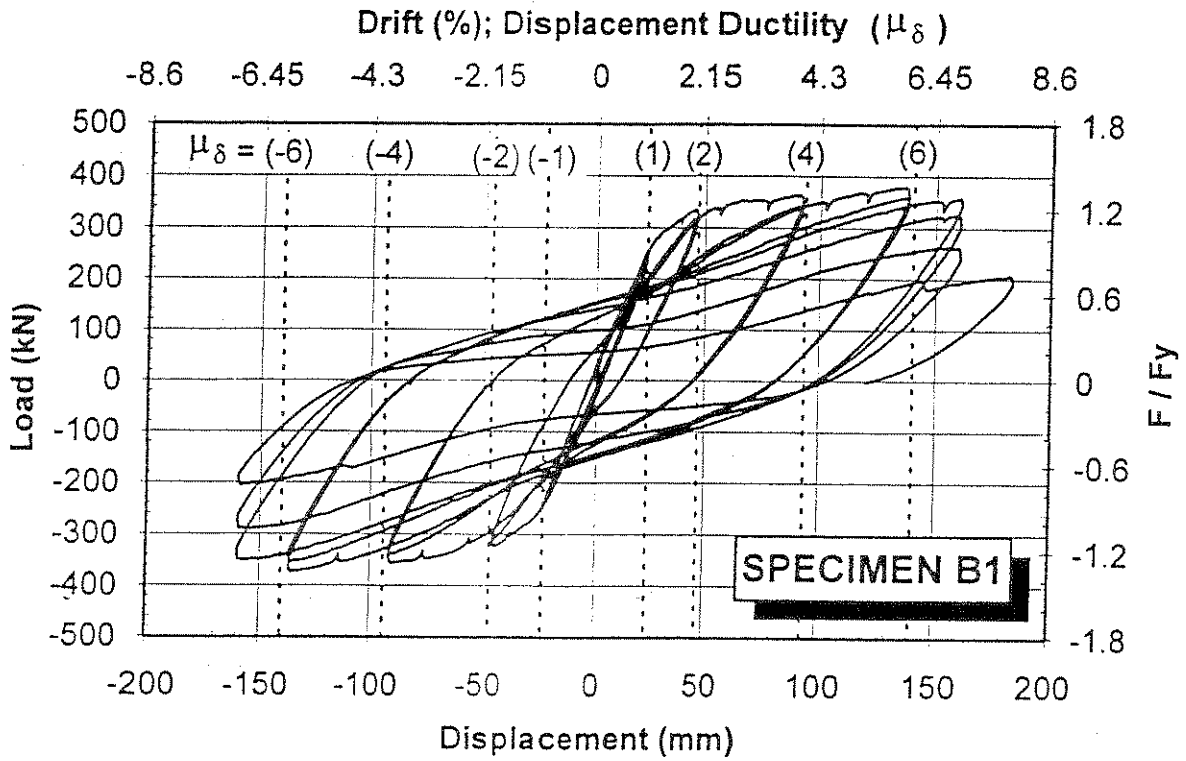


Figure 3-36 Measured Lateral Load-Deflection Hysteresis Loops for Specimen B1

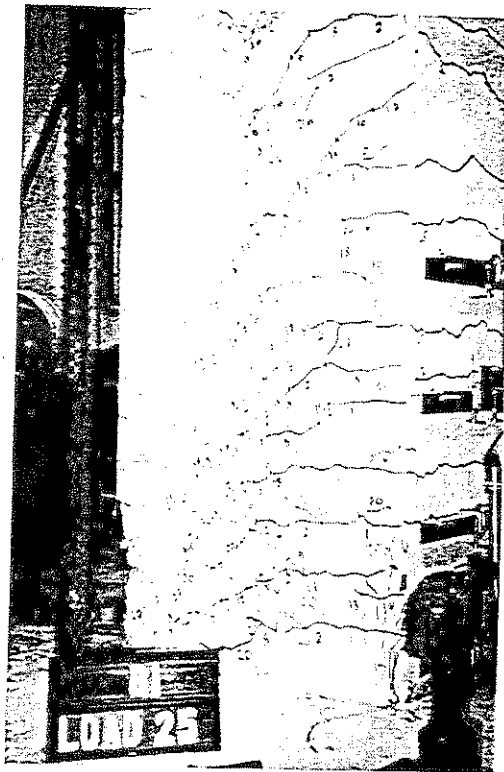


Figure 3-37 Specimen B1 at  $\mu_\Delta = -4$  (1st Excursion)

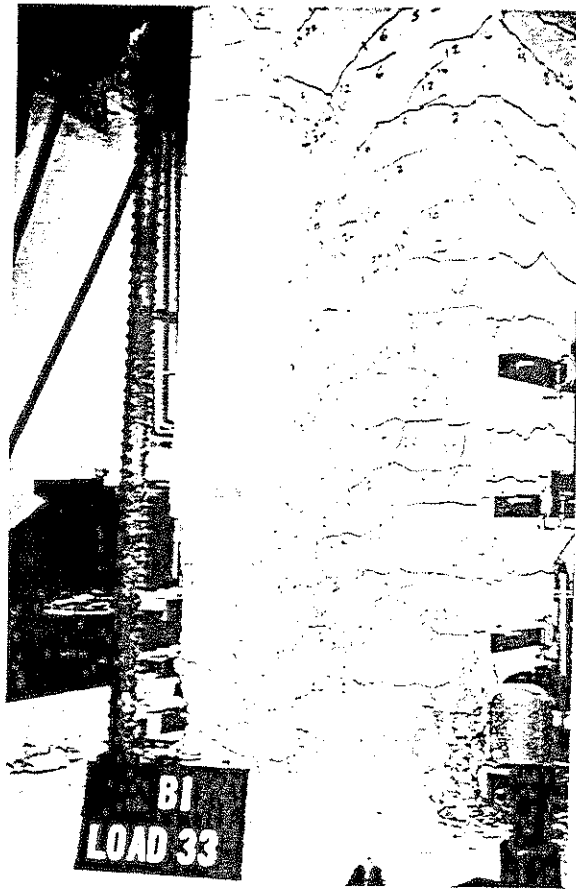


Figure 3-38 Specimen B1 at  $\mu_{\Delta} = -6$  (1st Excursion)

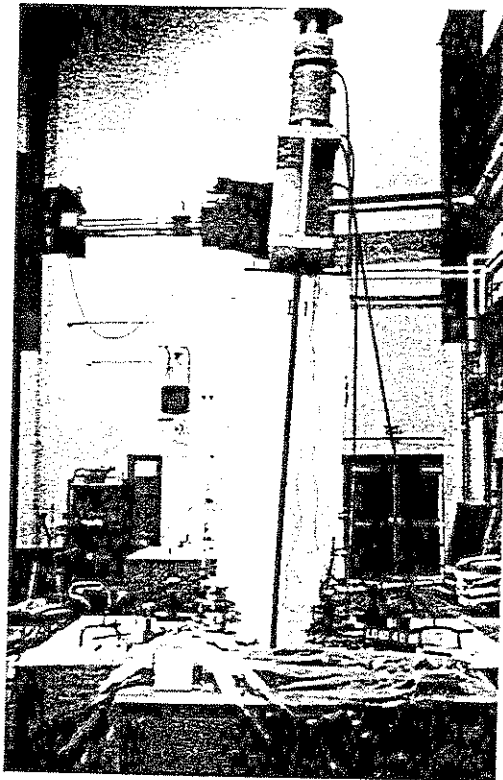


Figure 3-39 Specimen B1 at  $\mu_{\Delta} = +8$

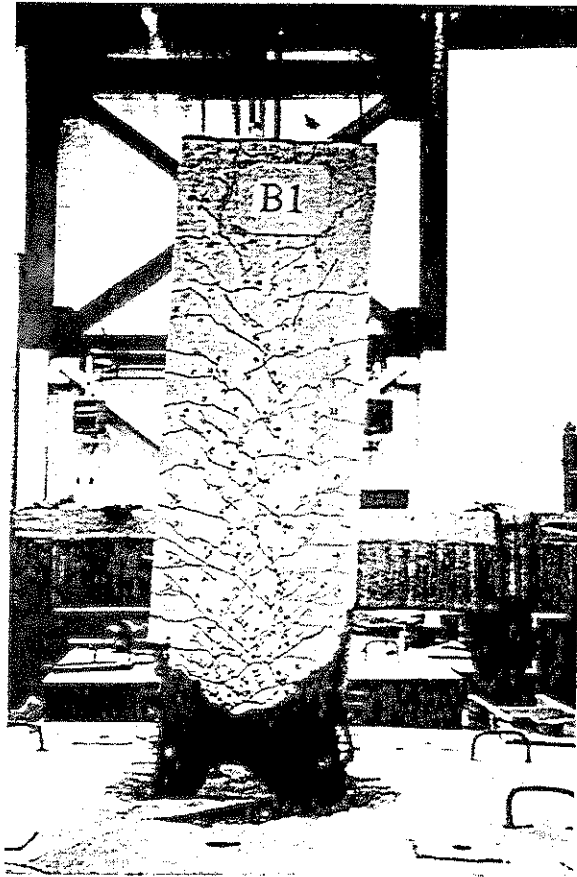


Figure 3-40 Plastic Hinge in Specimen B1 at the End of the Test

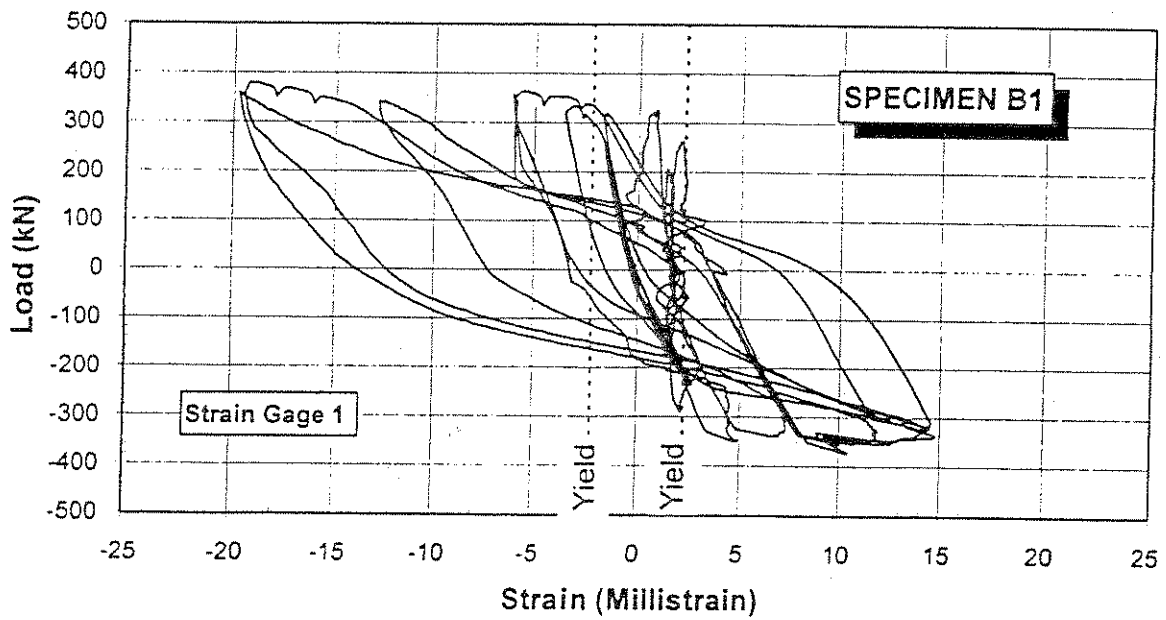


Figure 3-41 Measured Lateral Load-Strain Hysteresis in Specimen B1 Longitudinal Bar

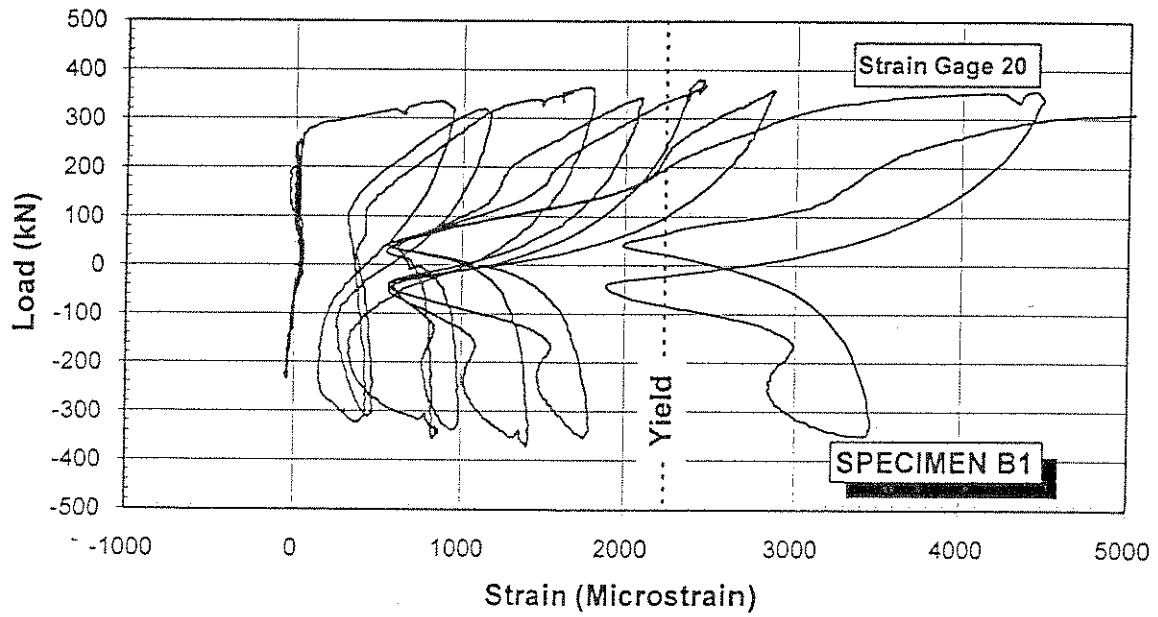


Figure 3-42 Measured Lateral Load-Strain in Specimen B1 Lateral Steel at SG 20

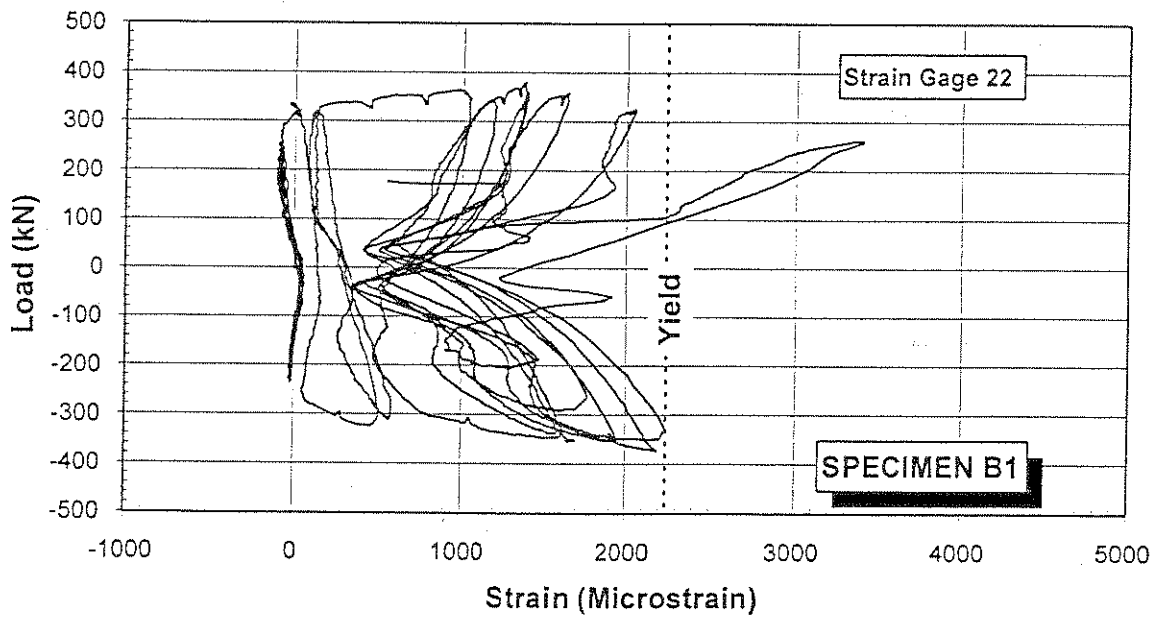


Figure 3-43 Measured Lateral Load-Strain in Specimen B1 Lateral Steel at SG 22

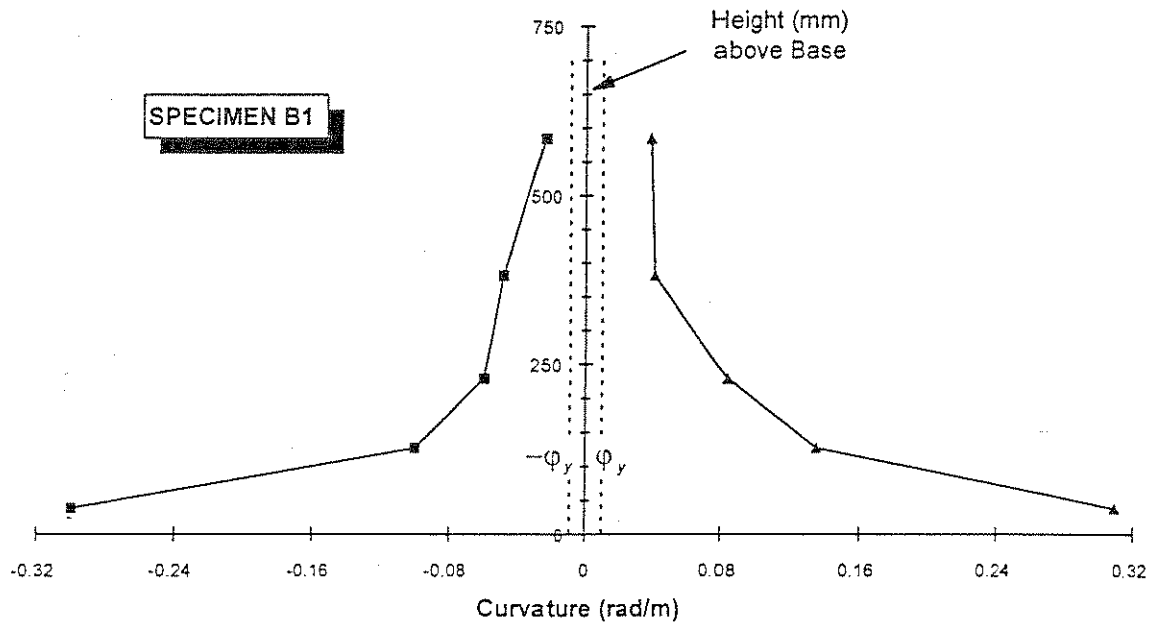


Figure 3-44 Measured Curvature Envelop along the Plastic Hinge of Specimen B1

### 3.7.5 Specimen B2

Specimen B2 was subjected to an initial axial load of 1514 kN (340 Kips) corresponding to an axial load index of 0.23. At low amplitude displacements, the minimum measured axial load was 1497 kN (336 Kips). A maximum axial load of 1603 kN (360 Kips) was recorded during high amplitude displacements. Based on an axial load of 1532 kN (344 Kips), the calculated effective yield moment and the corresponding lateral load were 742 kN-m (6570 Kip-in) and 318 kN (71.3 Kips), respectively.

The lateral load history for Specimen B2 is shown in Figure 3-45. Similar to the other specimens, flexural cracks along the column height started to develop before the section effective yield was reached. The measured effective yield displacement was 21 mm (0.81 in.). The sudden jump to a high displacement in the fifth loading cycle was due to a malfunction in the hydraulic system which caused the actuator to increase the lateral displacement from 30 mm (1.16 in.) to more than 76 mm (3 in.) in about five seconds. The lateral loads corresponding to those displacements were 356 kN (75.4 Kips) and 408 kN (91.5 Kips), respectively. The induced high lateral load initiated the spall of cover concrete at the compression side. The hysteretic load-displacement response for Specimen B2 is shown in Figure 3-46.

Specimen B2 exhibited very stable hysteresis loops up to a displacement ductility of 6. At this point,

the lateral load peaked at 417 kN (93.7 Kips). During the second excursion of  $\mu_{\Delta} = +6$ , the 90° hook of the third tie set started to open on the compression side of the specimen. The core concrete was deteriorating at a faster rate during the third cycle of  $\mu_{\Delta} = 6$  and the longitudinal bars started to buckle. The test was terminated after the specimen was pushed to a lateral displacement of 150 mm (5.95 in.) and the corresponding lateral load dropped to 258 kN (58.0 Kips). The failure load was 62 percent of the measured peak load or 81 percent of the effective lateral yield load. Figures 3-47 through 3-50 show Specimen B2 at different stages of the test.

Figure 3-51 and Figures 3-52 and 3-53 present the measured lateral load-strain relationships at one longitudinal bar and two transverse bars, respectively (Gages No. 1, 19 and 22, respectively, in Figures 3-9 and 3-10). The measured plastic hinge length at the end of the test was 560 mm (22 in.). The measured curvature envelop and plastic hinge length at the bottom of the column are reflected in Figure 3-54.

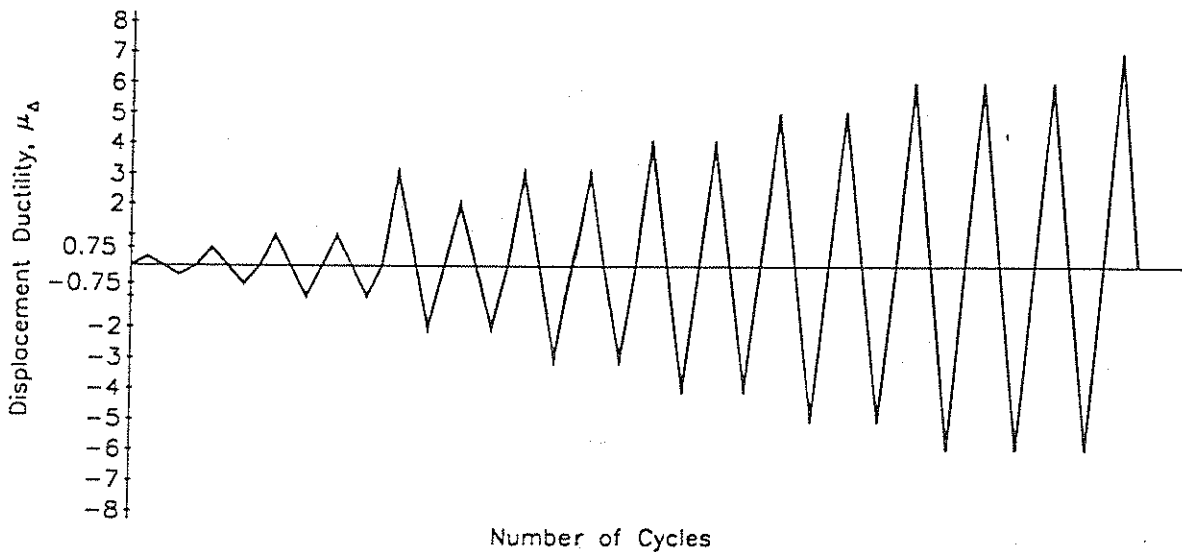


Figure 3-45 Lateral Load History for Specimen B2

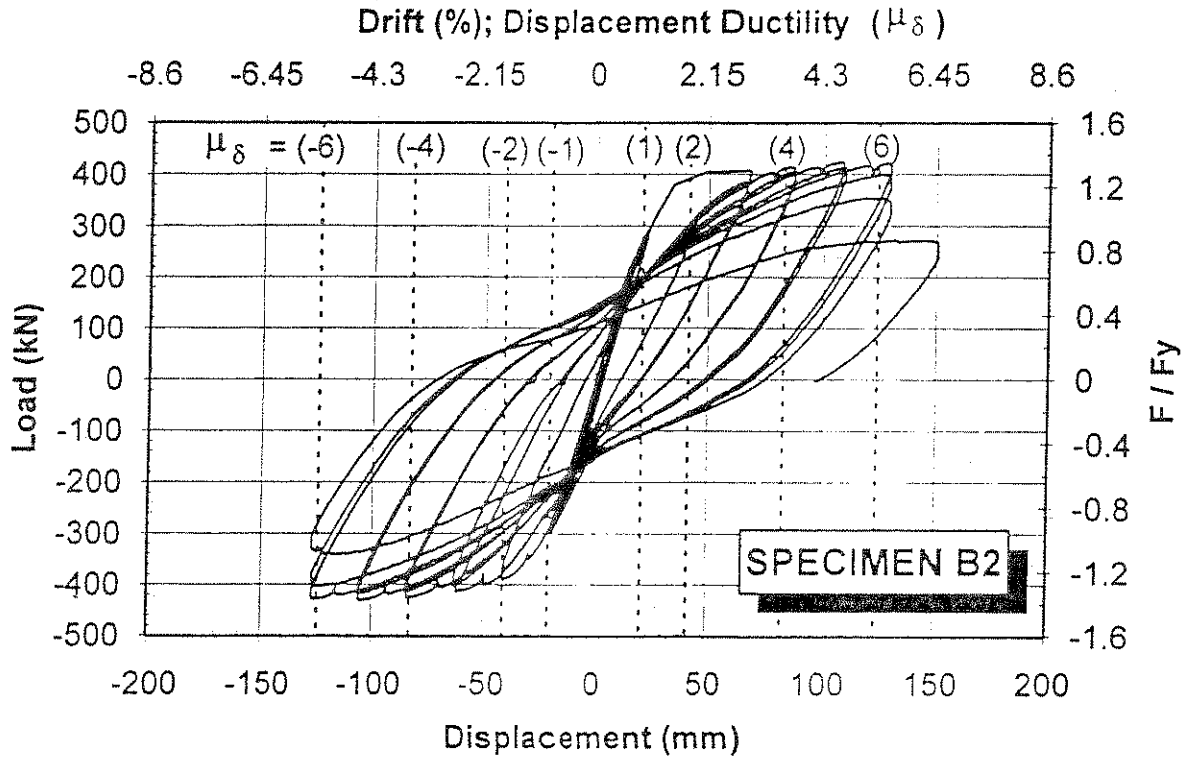


Figure 3-46 Measured Lateral Load-Deflection Hysteresis Loops for Specimen B2

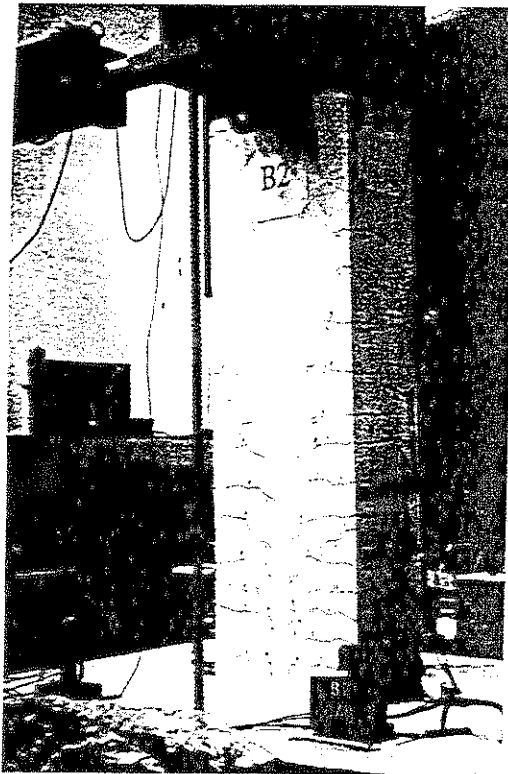


Figure 3-47 Specimen B2 at  $\mu_\delta = -1$  (1st Excursion)

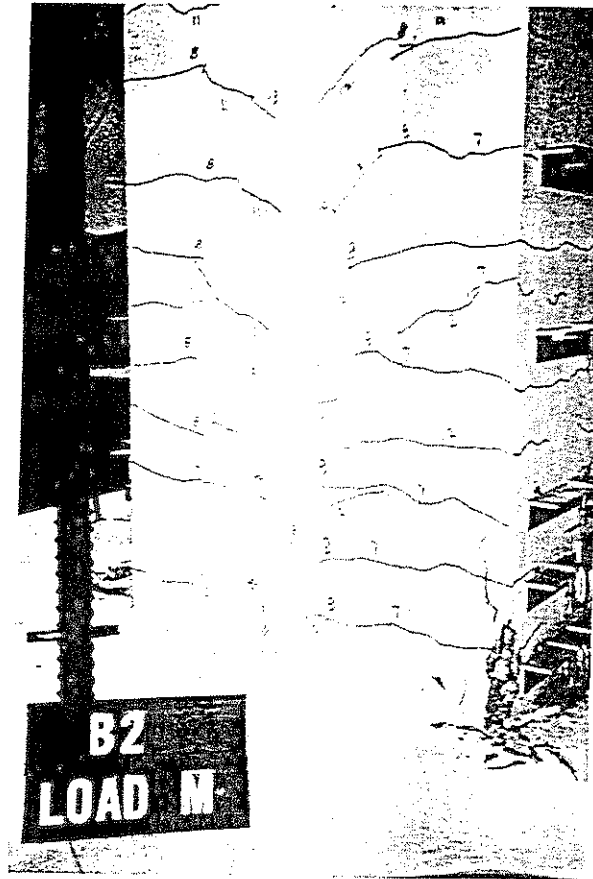


Figure 3-48 Specimen B2 at  $\mu_d = +3$  (1st Excursion)

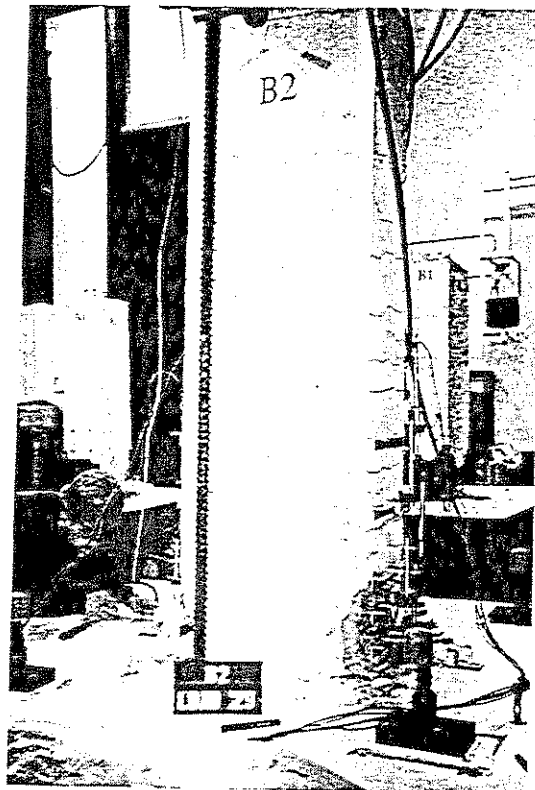


Figure 3-49 Specimen B2 at  $\mu_d = +4$  (1st Excursion)

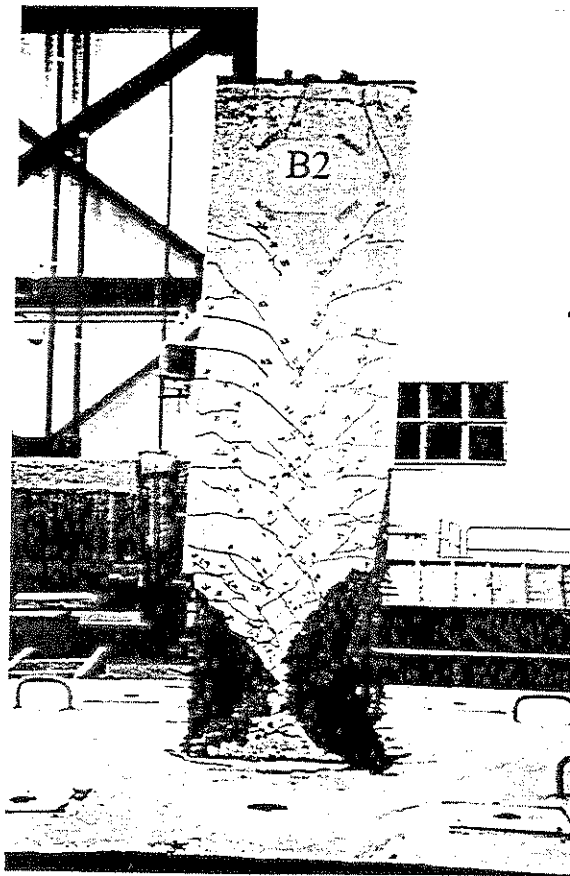


Figure 3-50 Plastic Hinge in Specimen B2 at the End of the Test

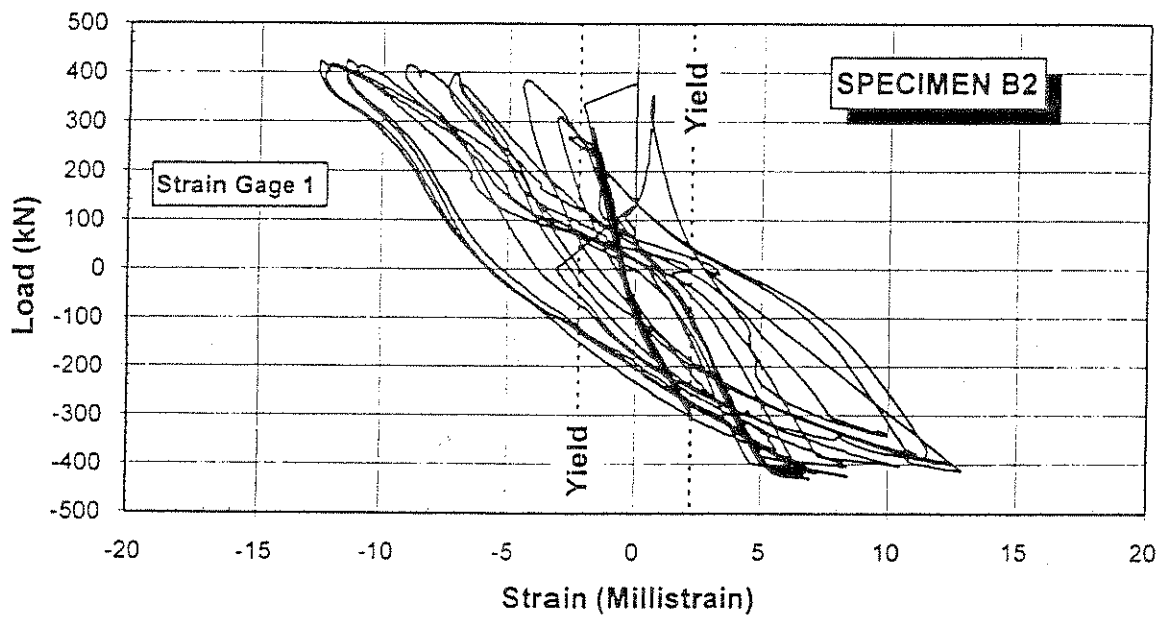


Figure 3-51 Measured Lateral Load-Strain Hysteresis in Specimen B2 Longitudinal Bar

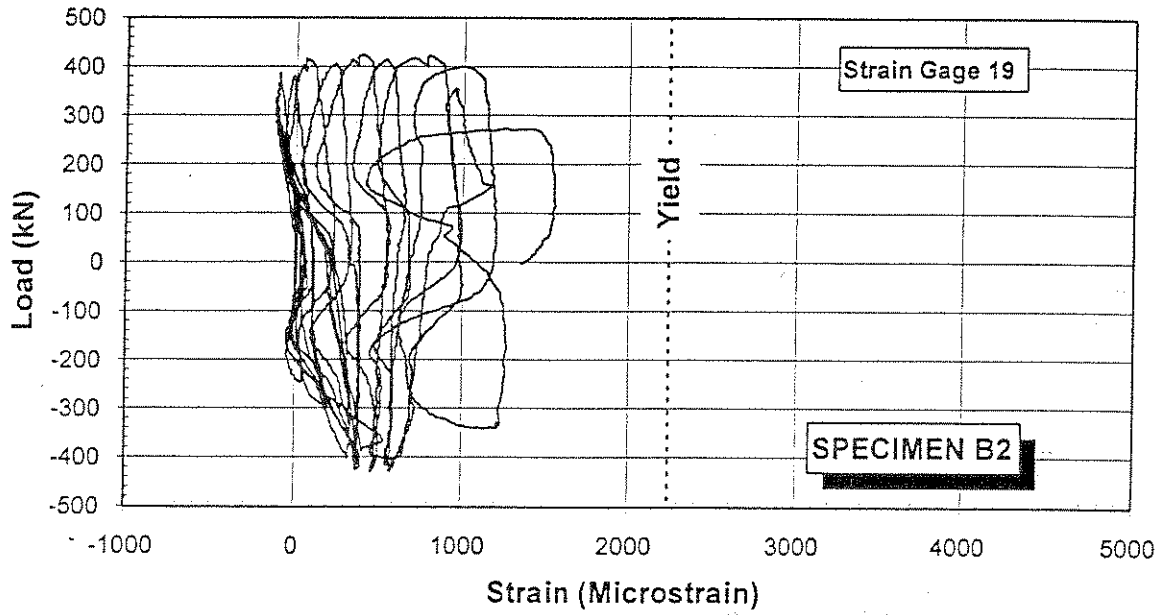


Figure 3-52 Measured Lateral Load-Strain in Specimen B2 Lateral Steel at SG 19

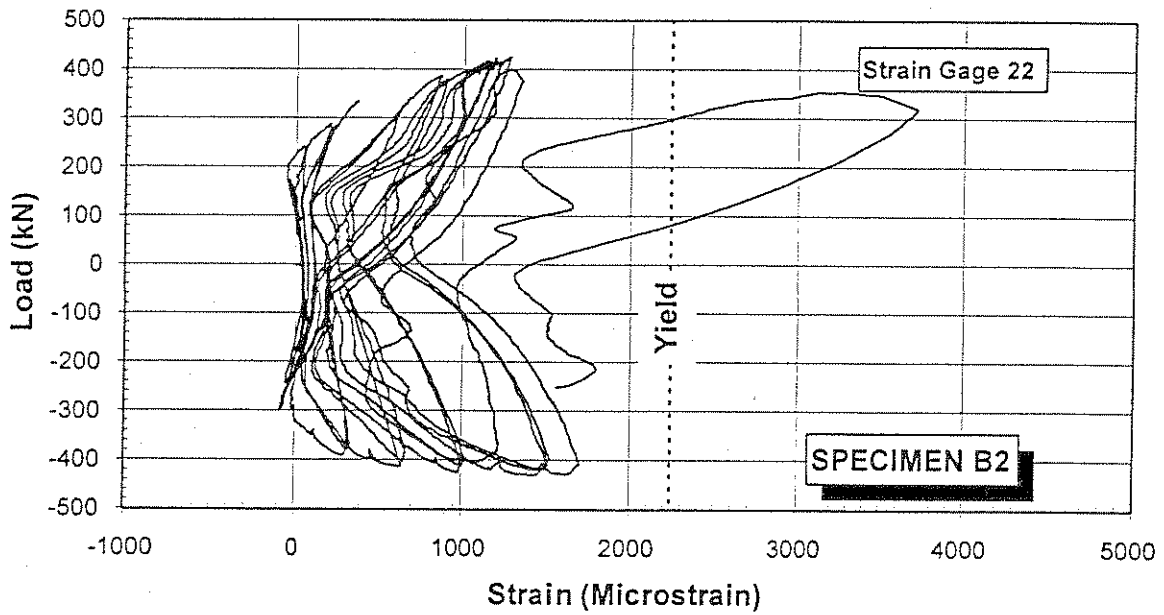


Figure 3-53 Measured Lateral Load-Strain in Specimen B2 lateral Steel at SG 22

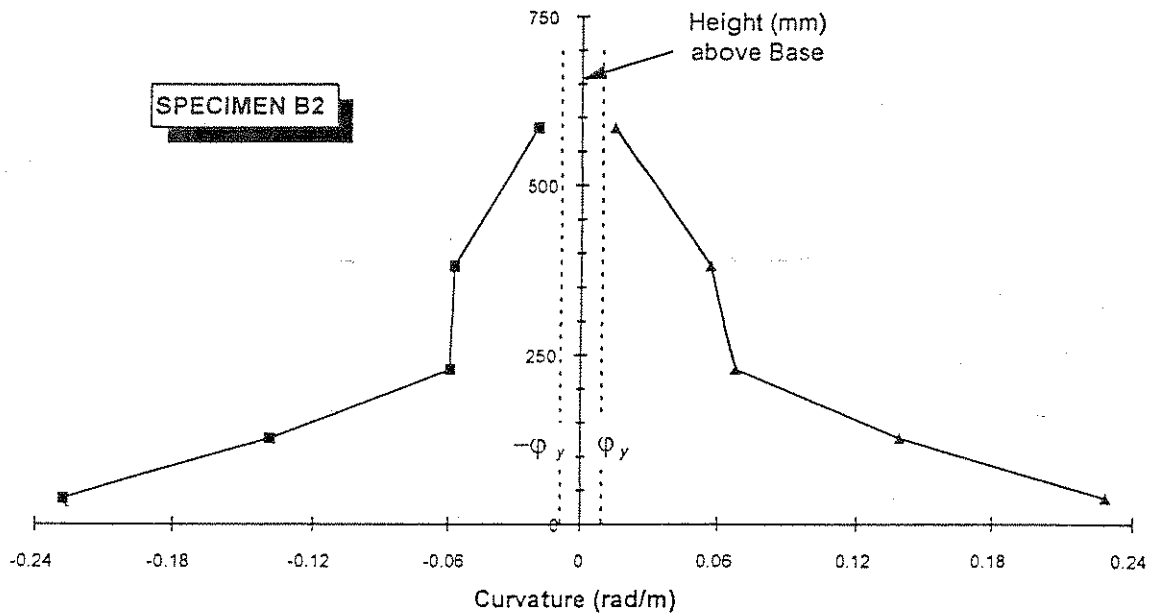


Figure 3-54 Measured Curvature Envelop along the Plastic Hinge of Specimen B2

### 3.8 Summary and Observations

A summary of the measured lateral loads, curvature at yield, and plastic hinge lengths is presented in Table 3-6.

Table 3-6 Measured Lateral Loads, Yield Curvatures, and Plastic Hinge Lengths

Specimen	Yield Curvature $\phi_y$ rad/m (rad/in)	Lateral Force, kN (Kips)		Plastic Hinge Length, mm (in)	
		@ Yield	Peak	Based on Measured Loads	Based on Measured Curvatures
A1	$8.19 \times 10^{-3}$ ( $0.208 \times 10^{-3}$ )	275 (61.8)	361 (81.0)	554 (21.8)	645 (25.4)
A2	$8.46 \times 10^{-3}$ ( $0.215 \times 10^{-3}$ )	314 (70.4)	396 (89.0)	488 (19.2)	747 (29.4)
B1	$9.45 \times 10^{-3}$ ( $0.240 \times 10^{-3}$ )	276 (62.0)	379 (85.0)	632 (24.9)	767 (30.2)
B2	$9.45 \times 10^{-3}$ ( $0.240 \times 10^{-3}$ )	318 (71.3)	417 (93.7)	526 (20.7)	612 (24.1)

Review and comparison of the test data allowed for several observations to be made. Following are some remarks about the experimental results.

1. The lateral deflection response of concrete members such as those tested in this study consists mainly of three components: flexural, shear, and bond slip (15). When deflection is mainly due to flexure, the hysteresis loops are normally wide and "fat" with little pinching effect at the beginning of the reloading stage. On the other hand, when a major portion of the response is due to high shear and/or bond slip deflections, the hysteresis loops are characterized by strong pinching effect. Examination of the measured lateral load-deflection hysteresis loops of the specimens tested in this study indicate that the deflection response was mainly flexural. The prominent pinching at higher ductility levels can be attributed to the closing of flexural cracks prior to which the applied load is met with little resistance until the cracks are closed.
2. The effect of axial load on ductility can be observed by comparing the measured ductilities of specimens with the same transverse steel amount. Specimens A1 and B1 attained slightly higher ductilities than specimens A2 and B2, respectively. Although the specimens with lower axial load (approximately  $0.1 f_c' A_g$ ) reached higher ductilities than their respective counterparts with higher axial loads (approximately  $0.25 f_c' A_g$ ), the difference in ductilities was not substantial. This is probably due to the fact that at relatively low axial load ranges the axial load effect on ductility is minimal.
3. Even though the lateral steel ratio was approximately 40 percent of that required by codes in Specimens A1 and A2, the specimens were able to carry the vertical load up to displacement ductility of 5 and a drift ratio in excess of 4 percent.
4. Even with reduced amounts of lateral steel below those required by the codes for seismic provision, specimens with higher amounts of transverse steel (B1 and B2) attained higher ductilities than their respective counterparts with lower amounts of lateral steel (A1 and A2). This observation holds true provided that shear failure and premature longitudinal bar buckling are prevented by proper design and detailing.
5. The absence of the "P- $\Delta$  effect" in the tests was due to the fact that the Dywidag™ bars applying the axial load assumed a curvature similar to the column curvature as the specimen was pushed to higher drift levels. Thus, the axial load remained nearly concentric throughout the test.
6. The number of specimens tested in this study was too limited to draw conclusive remarks relating the plastic hinge length to the lateral steel amount and the axial load level. However, it was observed that there was no specific trend associating the plastic hinge length to either the confining steel amount or the axial load level.

## SECTION 4 ANALYTICAL STUDY

### 4.1 Introduction

In Section 3, it was experimentally shown that rectangular reinforced concrete bridge columns with approximately 50 percent less lateral steel than the minimum required by AASHTO were able to attain moderate displacement ductilities ranging between 4 and 7. In this section, the analytical models used to predict the response of such columns are discussed.

The analysis was based on existing models and procedures that have been widely used to predict the response of reinforced concrete columns to lateral loading. To calculate column deflections, models pertaining to concrete stress-strain relationship, bond slip and shear deformations, and plastic hinge length were first selected. The calculated response beyond the yield point was highly sensitive to the estimated plastic hinge length and, to a lesser extent, to the stress-strain concrete model. This section describes the theoretical derivations and results. The analytical results are also presented and compared to the test results.

### 4.2 Theoretical Analysis

#### 4.2.1 Lateral Deflection

For a cantilever column subjected to a lateral load at the free end, the total lateral deflection can be attributed to deformations due to flexure, bond slip (yield penetration) between the bar anchored in the footing and the surrounding concrete, and shear. Additional lateral deflection due to rocking of the footing may also occur. The cantilever column may represent a fixed-pinned column and may also represent the segment of a fixed-fixed column between the section of maximum bending moment and the point of contraflexure. When footing rotation is prevented, the total lateral tip deflection of the cantilever column,  $\Delta_t$ , may be expressed as (15):

$$\Delta_t = \Delta_f + \Delta_s + \Delta_{sh} \quad (4-1)$$

where

$$\begin{aligned} \Delta_f &= \text{deflection due to flexure} \\ \Delta_s &= \text{deflection due to bond slip} \\ \Delta_{sh} &= \text{deflection due to shear} \end{aligned}$$

When the lateral deformation of the column is mainly due to flexure, it is possible for the column to form a plastic hinge at the critical section. For a column with uniform cross section, the plastic hinge forms at the fixed end. As is shown in Figure 4-1, the flexural deflection can be found as:

$$\Delta_f = \Delta_y + \Delta_p \quad (4-2)$$

where

- $\Delta_y$  = lateral deflection at effective flexural yield of the critical section  
 $\Delta_p$  = additional deflection due to rigid body rotation at the plastic hinge

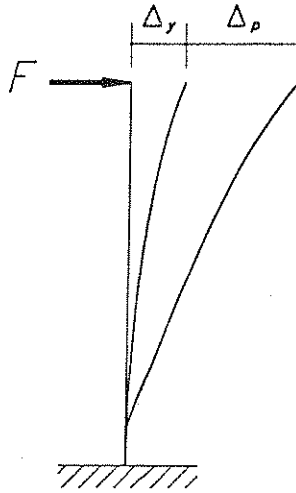


Figure 4-1 Flexural Deflection of a Cantilever Column

Figure 4-2 shows the bending moment diagram and the corresponding curvature of the cantilever column when the fixed end reaches the yield moment,  $M_y$ .  $M_{cr}$  and  $\varphi_{cr}$  are the cracking moment and the corresponding curvature, respectively. The lateral tip deflection at yield,  $\Delta_y$ , can then be found by applying the moment area theorem as follows

$$\Delta_y = \int_0^l \varphi x dx \quad (4-3)$$

which is the static moment of the area under the curvature diagram about the free end of the column.

When a plastic hinge is formed at the fixed end of the cantilever column, the additional lateral tip deflection,  $\Delta_p$ , due to rigid body rotation associated with plastic hinging can be found from geometry. Figure 4-3 presents an idealized curvature profile of the cantilever column after the plastic hinge has developed. In this idealization, the actual plastic hinge length is replaced by an equivalent plastic hinge length that would result in the same plastic displacement at the free end. Assuming that the total plastic rotation is concentrated at the middle of the equivalent plastic hinge,  $\Delta_p$  can be found as (15)

$$\Delta_p = (\varphi_u - \varphi_y) l_p \left( l - \frac{l_p}{2} \right) \quad (4-4)$$

where

- $\phi_u$  = ultimate curvature of the column cross section
- $\phi_y$  = yield curvature
- $l_p$  = equivalent plastic hinge length
- $l$  = total length of the cantilever column

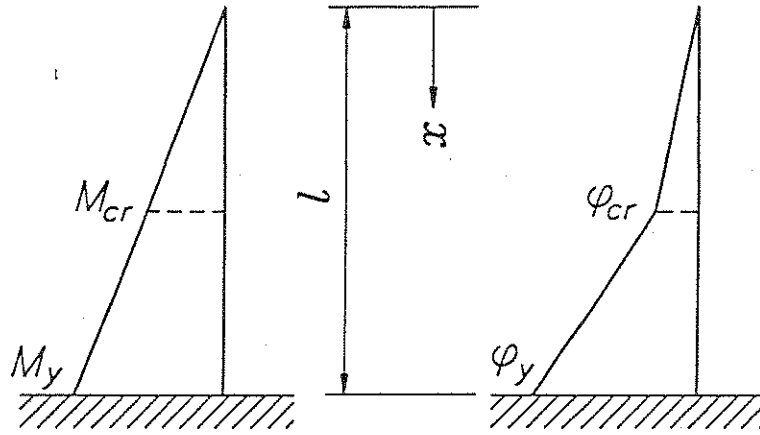


Figure 4-2 Bending Moment and Curvature at Yield of Fixed End

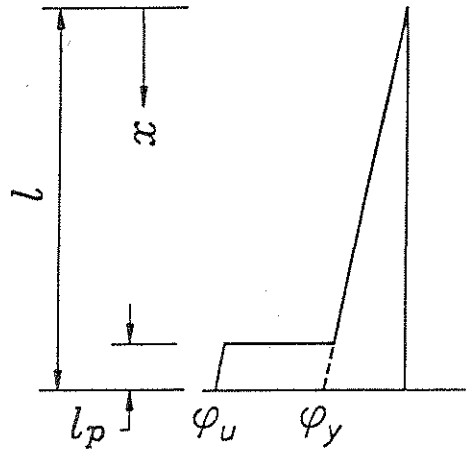


Figure 4-3 Idealized Curvature at the Equivalent Plastic Hinge

To account for the additional deflection due to yield penetration into the footing, the bond slip rotation at the fixed end is first estimated. It has been shown that the bond slip rotation,  $\theta'$ , can be found as (see Appendix A for derivation)

$$\theta' = \frac{1}{8} \frac{d_b}{E_s u} \frac{f_y^2}{d - d'} \left( \frac{M}{M_y} \right)^2 \quad (4-5)$$

where

- $d_b$  = bar diameter
- $E_s$  = modulus of elasticity of steel reinforcement
- $f_y$  = yield stress of steel
- $M_y$  = yield moment
- $M$  = applied moment
- $d$  = depth of tension bars
- $d'$  = depth of compression bars from the extreme compression fiber
- $u$  = bond strength of main bars

For SI No. 35 (#11) or smaller deformed bars, the basic bond strength of tension bars can be found as (10)

$$u = \frac{20 \sqrt{f'_c}}{d_b} \leq 5.5 \text{ (MPa)} \quad (4-6)$$

$$u = \frac{9.5 \sqrt{f'_c}}{d_b} \leq 800 \text{ (psi)} \quad (4-7)$$

At yield, the bond slip rotation,  $\theta'$ , can be found from Equation 4-5 where the applied moment is set equal to the effective yield moment of the column. The corresponding lateral tip deflection of the column can then be found by multiplying the bond slip rotation by the cantilever length. Bond slip rotation beyond yield can be implicit in Equation 4-4 by using an appropriate  $l_p$ . Thus, the bond slip deflection term,  $\Delta_s$ , in Equation 4-1 can be reduced to

$$\Delta_s = \theta' \cdot l \quad (4-8)$$

Since the column specimens in this study were subjected to relatively low axial loads, the lateral deflection due to shear may be estimated by utilizing shear deflection formulas used for reinforced concrete beams. Although such approach would slightly overestimate the shear deflection, yet the calculated shear deflections would be indicative of the magnitude order of the actual shear deflections. For a beam with 45° diagonal cracks, Park and Paulay (14) derive the beam shear stiffness,  $K_{v,45}$ , as

$$K_{v,45} = \frac{\rho_v}{1 + 4n\rho_v} E_s b_w d \quad (4-9)$$

where

- $K_{v,45}$  = shear deflection in one unit length due to one unit shear load
- $E_s$  = elastic modulus of shear reinforcement
- $b_w$  = section width perpendicular to applied shear
- $d$  = effective section depth parallel to applied shear
- $n$  =  $E_s/E_c$  (modular ratio)
- $E_c$  = elastic modulus of concrete

- $\rho_v$  =  $A_v/sb_w$  (shear reinforcement ratio)
- $A_v$  = area of shear reinforcement
- $s$  = spacing of shear reinforcement sets along the member longitudinal axis

Knowing the member shear stiffness, applied shear, and member length, it would be possible to calculate the tip shear deflection of a reinforced concrete cantilever.

#### 4.2.2 Moment-Curvature Analysis

The theoretical moment-curvature relationships of the test specimens were calculated based on plane section analysis which assumes that plane sections before bending remain plane after bending (linear strain gradient). To facilitate the analysis, the constitutive relationships of steel and concrete were first idealized, then the moment-curvature analysis was performed using the computer program IA1.UNR (26). The program is written in FORTRAN-77 and it calculates the moment-curvature of rectangular reinforced concrete sections. In addition to the axial load and the outermost concrete strain limit for which the analysis is required, the input data include the geometrical dimensions of the section, the areas and locations of the main reinforcement layers, and the constitutive relationships of steel and concrete.

The constitutive relationship for steel was idealized using a tri-linear curve. The first segment represented the stress-strain behavior of steel up to the yield point, followed by a yield plateau up to the beginning of strain hardening, and finally, a strain hardening segment up to the fracture of steel. The longitudinal steel idealized stress-strain curve used in the analysis is shown in Figure 4-4.

Since the computer program IA1.UNR can use only one concrete constitutive relationship, the section of each test specimen was analyzed twice. In the first analysis, the concrete was assumed to be unconfined up to the section effective yield point. Full section properties were used in this analysis. To calculate the curvature and the corresponding moment at ultimate, the section was analyzed again presuming that the cover concrete had spalled and that the core concrete had assumed a confined concrete stress-strain behavior. Thus, two concrete models were needed to represent the constitutive relationships of unconfined and confined concrete sections.

The Kent and Park concrete model (9) was selected to represent the behavior of unconfined concrete. This model is the basis of the modified Kent and Park model for confined concrete which was presented in Section 2.2.1 of this report. To define the unconfined model, a  $K$  factor of unity is used in Equations 2-1, 2-3 and 2-4. Figure 4-5 shows the theoretical unconfined concrete stress-strain relationships for the specimens in Group I and Group II.

Two different models were used to represent the behavior of confined concrete. The first model was the modified Kent and Park (9) and the other was the model by Mander et al (11) as modified by Paulay and Priestley (15). The two models were presented in Section 2.2 of this report. The theoretical stress-strain relationships of both models are shown in Figure 4-6 and Figure 4-7 for the specimens in Group I and Group II, respectively.

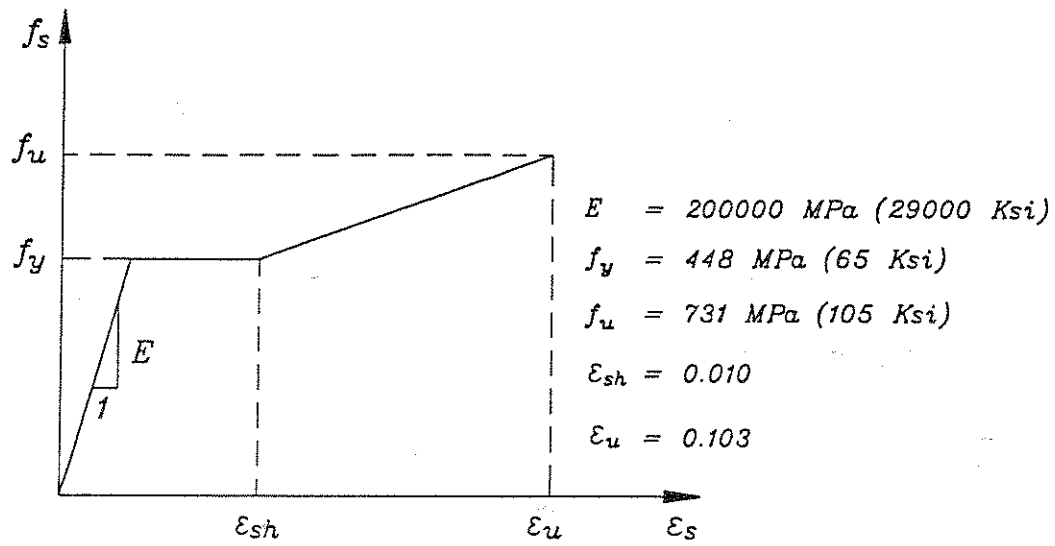


Figure 4-4 Idealized Stress-Strain Curve of Main Steel

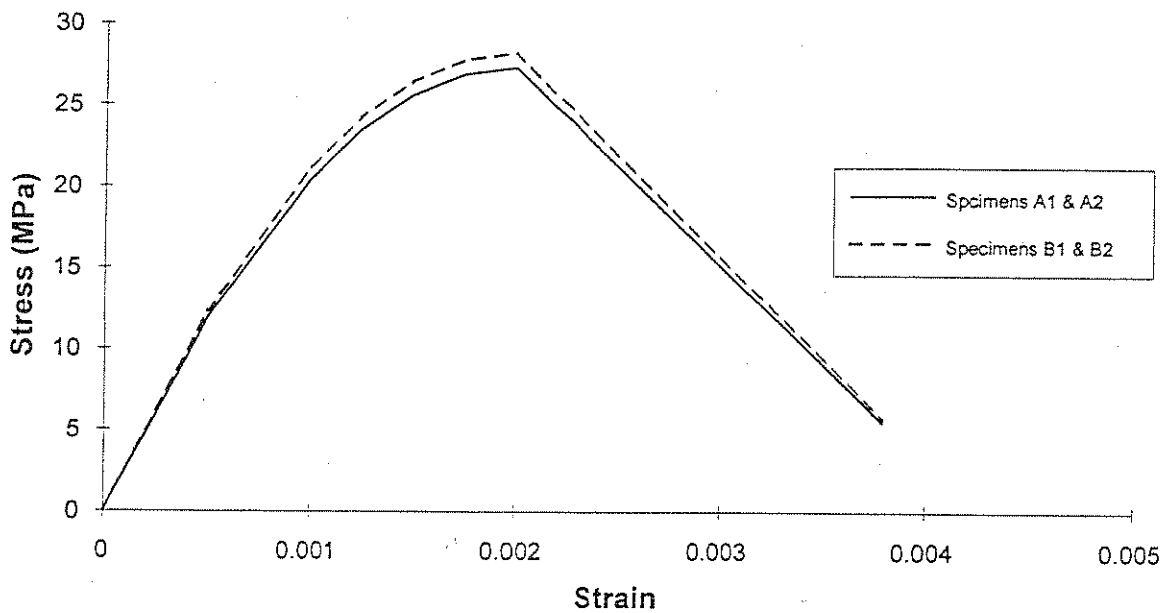


Figure 4-5 Unconfined Concrete Models

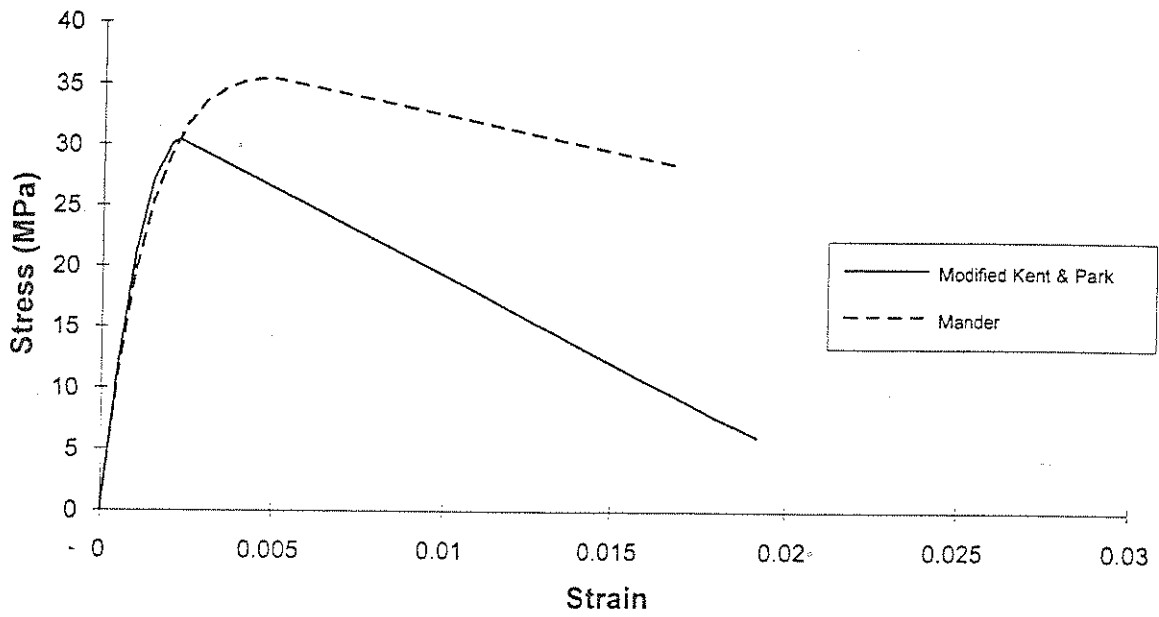


Figure 4-6 Confined Concrete Models for Specimens A1 and A2

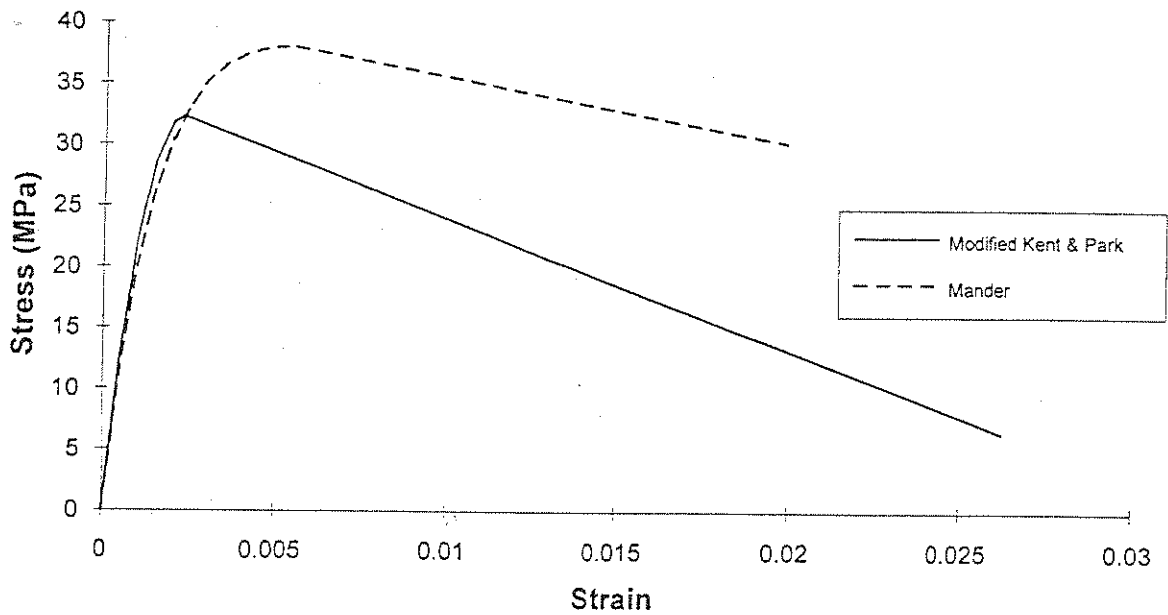


Figure 4-7 Confined Concrete Models for Specimens B1 and B2

Based on the measured material properties and the applied axial loads, the curvatures at section cracking, yield, and ultimate were calculated for the four test specimens. The calculated results are presented in Table 4-1.

Table 4-1 Calculated Curvature

Specimen	Curvature rad/m (rad/in)			
	Kent & Park		Modified Kent & Park	Mander et al.*
	$\phi_c$	$\phi_y$	$\phi_u$	$\phi_u$
A1	$0.787 \times 10^{-3}$ ( $0.020 \times 10^{-3}$ )	$7.91 \times 10^{-3}$ ( $0.201 \times 10^{-3}$ )	$92.5 \times 10^{-3}$ ( $2.35 \times 10^{-3}$ )	$97.2 \times 10^{-3}$ ( $2.47 \times 10^{-3}$ )
A2	$1.300 \times 10^{-3}$ ( $0.033 \times 10^{-3}$ )	$8.19 \times 10^{-3}$ ( $0.208 \times 10^{-3}$ )	$66.1 \times 10^{-3}$ ( $1.68 \times 10^{-3}$ )	$72.8 \times 10^{-3}$ ( $1.85 \times 10^{-3}$ )
B1	$0.787 \times 10^{-3}$ ( $0.020 \times 10^{-3}$ )	$7.87 \times 10^{-3}$ ( $0.200 \times 10^{-3}$ )	$128.4 \times 10^{-3}$ ( $3.26 \times 10^{-3}$ )	$116.5 \times 10^{-3}$ ( $2.96 \times 10^{-3}$ )
B2	$1.300 \times 10^{-3}$ ( $0.033 \times 10^{-3}$ )	$8.11 \times 10^{-3}$ ( $0.206 \times 10^{-3}$ )	$92.9 \times 10^{-3}$ ( $2.36 \times 10^{-3}$ )	$89.4 \times 10^{-3}$ ( $2.27 \times 10^{-3}$ )

\* As modified by Paulay and Priestley

### 4.2.3 Plastic Hinge Length

To calculate the plastic deflection,  $\Delta_p$  using Equation 4-4, it is essential to properly evaluate the equivalent plastic hinge length,  $l_p$ . Based on previous studies by other researchers, two empirical methods were selected and used in this study to calculate the equivalent plastic hinge length.

Baker (4) investigated plastic hinging of reinforced concrete members and presented two different expressions for the evaluation of the plastic hinge length of unconfined and confined members. For members with unconfined concrete, the equivalent plastic hinge length is given by

$$l_p = k_1 k_2 k_3 \left( \frac{z}{d} \right)^{1/4} d \quad (4-10)$$

where

- $k_1$  = 0.7 for mild steel and 0.9 for cold-worked steel
- $k_2$  =  $1 + 0.5P_u/P_0$
- $P_u$  = axial compressive load
- $P_0$  = axial compressive strength of member
- $k_3$  = 0.6 for  $f'_c = 35.2$  MPa (5100 psi)
- = 0.9 for  $f'_c = 11.7$  MPa (1700 psi)
- $z$  = distance of critical section to point of contraflexure

$d$  = effective depth of member

For members confined with transverse steel, Baker proposed a modified version of Equation 4-10 to calculate the equivalent plastic hinge length as follows

$$l_p = 0.8 k_1 k_3 \left( \frac{z}{d} \right) c \quad (4-11)$$

where

$c$  = neutral axis depth under the ultimate moment

It can be seen that Baker's equation for confined concrete implicitly includes the effects of axial load (through  $c$ ) and confinement on the equivalent plastic hinge length.

Paulay and Priestley (15), on the other hand, proposed an empirical expression to calculate the equivalent plastic hinge length of reinforced concrete members which is independent of the axial load and the amount of confining steel. This expression is given by

$$l_p = 0.08l + 0.022 d_b f_y \quad (MPa) \quad (4-12)$$

$$l_p = 0.08l + 0.15 d_b f_y \quad (Ksi) \quad (4-13)$$

where

$l$  = length of member between critical section and point of contraflexure

$d_b$  = longitudinal bar diameter

$f_y$  = yield stress of longitudinal bars

Based on Equations 4-11 and 4-12, the equivalent plastic hinge length of each test specimen was calculated twice using measured material properties. The calculated equivalent plastic hinge lengths are presented in Table 4-2.

#### 4.2.4 Calculated Deflections

Based on the analytical procedures presented in section 4.2.1, the lateral deflections were calculated at yield and ultimate points. In this section, the calculated displacements according to different models are presented and compared. Measured material properties were used.

At yield, the calculated lateral deflections due to flexure ( $\Delta_f$ ) and bond slip ( $\Delta_s$ ) were 13.2 mm (0.52 in.) and 2.0 mm (0.08 in.), respectively, for all four specimens. The calculated values were identical in all specimens due to the fact that at low axial loads, the modest change in the applied axial load from  $0.1 f'_c A_g$  to  $0.25 f'_c A_g$  resulted in negligible difference in the calculated displacements. Moreover, the small variation in the concrete compressive strengths did not cause any significant difference in the calculated displacements.

**Table 4-2 Calculated Equivalent Plastic Hinge Lengths**

Specimen	$l_p$ , mm (in)	
	Paulay & Priestley	Baker
A1	375 (14.7)	410 (16.2)
A2	375 (14.7)	550 (21.7)
B1	375 (14.7)	400 (15.8)
B2	375 (14.7)	530 (20.9)

The calculated plastic displacement ( $\Delta_p$ ), in contrast, was strongly sensitive to the models selected for the equivalent plastic hinge length and the stress-strain relationship of confined concrete. For each equivalent plastic hinge length given in Table 4-2, the plastic displacement was calculated twice corresponding to the two confined concrete models considered in this study. The calculated plastic displacements are presented in Table 4-3.

**Table 4-3 Calculated Ultimate Plastic Displacement,  $\Delta_p$**

Specimen	Calculated* Plastic Displacement, $\Delta_p$ mm (in.)			
	Modified Kent & Park Concrete Model		Mander et al. Concrete Model**	
	$l_p$ by Priestley	$l_p$ by Baker	$l_p$ by Priestley	$l_p$ by Baker
A1	67.8 (2.67)	74.2 (2.92)	71.6 (2.82)	78.3 (3.08)
A2	46.5 (1.83)	65.8 (2.59)	51.8 (2.04)	73.4 (2.89)
B1	95.5 (3.80)	103.3 (4.07)	87.1 (3.43)	93.2 (3.67)
B2	67.8 (2.67)	93.3 (3.67)	65.0 (2.56)	89.4 (3.52)

\* Based on measured material properties and applied axial loads

\*\* As modified by Paulay and Priestley

Beam shear deflections were calculated based on the shear stiffness given by Equation 4-9. Because the steel cross beam depth should not be considered as part of the shear span, a concrete beam length of 2032 mm (80 in.) was considered in the shear deflection analysis. The calculated beam shear deflections are presented in Table 4-4.

The calculated total displacements and displacement ductilities were found by summing the calculated displacement components at yield and at ultimate. This process was repeated for all plastic hinge length and confined concrete model combinations. Table 4-5 presents the calculated

results according to the modified Kent and Park concrete model whereas Table 4-6 presents the calculated results corresponding to the Mander et al. concrete model.

Table 4-4 Calculated Beam Shear Deflections

Specimen	Beam Shear Deflection, $\Delta_{sh}$ mm (in.)	
	@ Yield	@ Ultimate
A1	4.8 (0.19)	6.4 (0.25)
A2	5.6 (0.22)	6.9 (0.27)
B1	3.8 (0.15)	5.3 (0.21)
B2	4.3 (0.17)	5.6 (0.22)

Table 4-5 Calculated Displacements\* and Ductilities-Modified Kent and Park Model

Specimen	$(\Delta)_y$ mm (in.)	$l_p$ by Priestley			$l_p$ by Baker		
		$(\Delta)_u$ mm (in.)	$\mu_A$	Drift Ratio %	$(\Delta)_u$ mm (in.)	$\mu_A$	Drift Ratio %
A1	20.0 (0.79)	87.8 (3.46)	4.4	3.8	94.2 (3.71)	4.7	4.0
A2	20.8 (0.82)	67.3 (2.65)	3.2	2.9	86.6 (3.41)	4.2	3.7
B1	19.0 (0.75)	114.5 (4.55)	6.1	4.9	122.3 (4.82)	6.4	5.2
B2	19.5 (0.77)	87.3 (3.44)	4.5	3.7	112.8 (4.44)	5.8	4.8

\* Including flexural, bond slip, and shear displacements

Table 4-6 Calculated Displacements\* and Ductilities-Mander et al. Model\*\*

Specimen	$(\Delta)_y$ mm (in.)	$l_p$ by Priestley			$l_p$ by Baker		
		$(\Delta)_u$ mm (in.)	$\mu_\Delta$	Drift Ratio %	$(\Delta)_u$ mm (in.)	$\mu_\Delta$	Drift Ratio %
A1	20.0 (0.79)	91.6 (3.61)	4.6	3.9	98.3 (3.87)	4.9	4.2
A2	20.8 (0.82)	72.6 (2.86)	3.5	3.1	94.2 (3.71)	4.5	4.0
B1	19.0 (0.75)	106.1 (4.18)	5.6	4.5	112.2 (4.42)	5.9	4.8
B2	19.5 (0.77)	84.5 (3.33)	4.3	3.6	108.9 (4.29)	5.6	4.7

\* Including flexural, bond slip, and shear displacements

\*\* As modified by Paulay and Priestley

### 4.3 Remarks and Observations

The use of different mathematical models in the analytical study allowed for the evaluation of those models and their applicability to predict the response of rectangular bridge columns to lateral loading.

The calculated ultimate displacements revealed that the flexural component of the lateral displacement is highly sensitive to the equivalent plastic hinge length. The expression given by Baker (Equation 4-11) to calculate the equivalent plastic hinge length yielded closer results to the measured values than the expression given by Paulay and Priestley (Equation 4-12).

The predicted displacements and ductilities were not very sensitive to the selected confined concrete model. When the calculated plastic hinge length as given by Baker's equation was considered, the predicted response was very close to the measured response as can be seen in Tables 4-5 and 4-6. The concrete model by Mander et al. (as modified by Paulay and Priestley) resulted in better response predictions for Specimens A1 and A2 than the Modified Kent and Park model. For Specimens B1 and B2, the calculated response according to the Modified Kent and Park model was in better agreement with the measured response than that according to the modified Mander's model.

The theoretical analysis appears to slightly underestimate the actual response. Comparisons between the calculated and measured displacements at yield and ultimate are presented in Tables 4-7 and 4-8, respectively. The calculated ultimate displacements were always less than their respective measured displacements. This could be partly because the theoretical models applied in this study are inherently conservative (lower bound) especially in predicting the ultimate confined concrete strain. The measured displacements could also be artificially higher due to some additional

displacements induced by the loading mechanism. Under lateral loads, the top cross steel beam might have slightly rotated or slid until it became tightly snug against the anchor bolts at the top of the column.

Table 4-7 Measured and Calculated Displacements at Yield

Specimen	Measured $(\Delta_y)_m$ mm (in.)	Calculated $(\Delta_y)_c$ mm (in.)	$(\Delta_y)_c / (\Delta_y)_m$
A1	23 (0.92)	20 (0.79)	0.86
A2	20 (0.79)	20.8 (0.82)	1.04
B1	23 (0.92)	19.0 (0.75)	0.82
B2	21 (0.82)	19.5 (0.77)	0.94

Table 4-8 Comparison of Measured and Calculated Displacements at Ultimate

Specimen	Measured $(\Delta_u)_m$ mm (in.)	Calculated/Measured Displacement at Ultimate			
		$I_p$ by Baker		$I_p$ by Priestley	
		Modified Kent & Park Concrete Model	Mander et al. Concrete Model	Modified Kent & Park Concrete Model	Mander et al. Concrete Model
		$(\Delta_u)_c / (\Delta_u)_m$	$(\Delta_u)_c / (\Delta_u)_m$	$(\Delta_u)_c / (\Delta_u)_m$	$(\Delta_u)_c / (\Delta_u)_m$
A1	122 (4.82)	0.77	0.80	0.72	0.75
A2	102 (4.02)	0.85	0.92	0.66	0.71
B1	161 (6.33)	0.76	0.70	0.72	0.66
B2	130 (5.10)	0.87	0.84	0.67	0.65

In general, the existing analytical tools for monotonic loading analysis appear to result in reasonably accurate prediction of ductilities of rectangular bridge columns with moderate confinement. Moreover, Equation 1-4 (by Paulay and Priestley) predicts the response well at an axial load index of 0.25 as is shown in Figure 1-2, but it greatly overestimates the ductility at lower axial loads. Since bridge columns are normally subjected to low axial loads while building columns are usually under high axial loads, it is believed that Equation 1-4 is more suitable for building columns and for bridge columns with relatively high axial loads.

## SECTION 5 SUMMARY AND CONCLUSIONS

### 5.1 Summary

The study presented in this report is part of a project to develop detailing guidelines for reinforced concrete bridge columns and walls in areas of moderate seismicity. This study examined the ductility and behavior of rectangular reinforced concrete bridge columns with moderate confinement. The research comprised experimental and analytical investigation of the response of such columns when subjected to lateral loading.

#### 5.1.1 Experimental Study

For the experimental part of the study, four half-scaled rectangular bridge columns were built and tested. The geometrical dimensions and the amount of longitudinal reinforcement were kept the same for all specimens. The cross section of each column was 380 mm (15 in.) by 610 mm (24 in.) with longitudinal reinforcement volumetric ratio,  $\rho_l$ , of 2.2 percent. The columns were built as cantilever columns with a total height between the horizontal loading point and the top of the footing of 2335 mm (92 in.). Each specimen was tested under constant axial load while subjected to lateral load reversals with increasing drift levels. The loading was quasi-static and it was uniaxial in the column strong direction.

Two parameters were varied: the transverse steel reinforcement amount and the axial load level. Based on the amount of lateral steel, the specimens were divided into two groups. The transverse reinforcement ratios,  $A_s/(s \cdot h)$ , in the long direction for Group I (Specimens A1 and A2) and Group II (Specimens B1 and B2) were 0.0033 and 0.0043, respectively. These ratios corresponded to 42 percent and 54 percent of the minimum lateral reinforcement required by AASHTO for seismic detailing. The tie sets vertical spacing was kept less than six longitudinal bar diameters. Other confinement details pertaining to hook extension and longitudinal bar engagement were maintained according to AASHTO requirements. The nominal shear capacity of the specimens was calculated and was found to exceed the shear demand under the test conditions. The applied axial loads were approximately  $0.1f_c'A_g$  for Specimens A1 and B1 and  $0.25f_c'A_g$  for Specimens A2 and B2.

The specimens were tested to failure. Failure was considered to have occurred when the lateral load carrying capacity was reduced by at least 15 percent of the maximum measured lateral load. Although flexural-shear cracks developed along the column height, all specimens were able to attain moderate ductilities without failing in shear. The measured displacement ductilities of Specimens A1, A2, B1 and B2 were 5.2, 5.1, 6.9 and 6.2, respectively. The corresponding drift ratios were 5.2 percent, 4.4 percent, 6.9 percent and 5.5 percent. Plastic hinges were developed in all four specimens at the bottom of the columns. The measured plastic hinge lengths were 645 mm (25.4 in.), 747 mm (29.4 in.), 767 mm (30.2 in.) and 612 mm (24.1 in.) for Specimens A1, A2, B1 and B2, respectively.

### 5.1.2 Analytical Study

The calculated response of the test specimens to lateral loading was based on plane section analysis. To calculate column deflections, models pertaining to concrete stress-strain relationship, bond slip and shear deformations, and plastic hinge length were selected.

The Kent and Park model (9) was employed to represent the constitutive relationship of unconfined concrete. For confined concrete, two widely used models were selected for this study. One model was the modified Kent and Park (9), and the other was by Mander et al. (11).

The plastic hinge length was calculated according to two different empirical expressions. The first expression, given by Baker (4), implicitly included the effects of axial load level and the amount of confining steel on the plastic hinge length. The other model was presented by Paulay and Priestley (15) and was independent of the degree of confinement and the applied axial load.

Bond slip rotation was calculated using an expression that was derived from basic relationships relating to geometry, compatibility, and bond strength between the main bars and the concrete in the footing.

Since the test specimens were subjected to relatively low axial loads, shear deformations were approximated by utilizing a method used for calculating the shear deflection of reinforced concrete beams. The method, described in Park and Paulay (15), required that a unit shear stiffness term be calculated first. Based on the unit shear stiffness, column length, and applied shear force, the shear deflection at the top of the column specimen was calculated.

The moment-curvature analysis was performed using the computer program IA1.UNR. The program was written in FORTRAN-77 and it calculates the moment-curvature of rectangular reinforced concrete sections.

The calculated equivalent plastic hinge length varied widely between the two equivalent plastic hinge length expressions employed in this study. According to the expression by Paulay and Priestley (15), the calculated equivalent plastic hinge length was 375 mm (14.7 in.) for all four column specimens. On the other hand, Baker's equation (4) resulted in equivalent plastic hinge lengths of 410 mm (16.2 in.), 550 mm (21.7 in.), 400 mm (15.8 in.), and 530 mm (20.9 in.) for Specimens A1, A2, B1, and B2, respectively.

The analysis result revealed that the yield displacements were slightly dependent on the concrete model used in the analysis. However, the calculated ultimate displacements were very sensitive to the calculated ultimate concrete strain and the equivalent plastic hinge length. The displacements at the top of the columns were calculated for all combinations of concrete models and plastic hinge lengths. The results were summarized in Tables 4-5 and 4-6.

## 5.2 Conclusions

Based on the experimental observations, test data analysis, and theoretical study performed in this research, the following conclusions can be drawn.

1. At relatively low axial loads ( $0.1 f_c' A_g$  to  $0.25 f_c' A_g$ ) such as those encountered in bridges, rectangular reinforced concrete columns with confinement steel at approximately 50 per cent the minimum amount required by AASHTO for seismic provision may exhibit moderate displacement ductilities ranging between 4 and 7. This would be true provided that shear failure and premature bar buckling are prevented by proper detailing of transverse steel.
2. For rectangular bridge columns with relatively low axial loads and moderate confinement such as those employed in this study, it is possible to predict with reasonable accuracy the response of the columns to lateral cyclic loading. However, proper evaluation of the plastic hinge length would greatly enhance the accuracy of the predicted ultimate displacements.
3. Within the range of parameters included in this study, the plastic hinge length would be more accurately predicted using Baker's equation (4). The expression given by Paulay and Priestley (14) yields plastic hinge lengths that are much lower than the measured lengths, thus underestimating the ultimate displacements and ductilities.
4. The inclusion of shear deformations in this study resulted in more accurate prediction of displacements and ductilities. However, shear displacements in columns are relatively small and may be neglected for practical purposes.
5. Even at low axial loads and moderate confinement, some observations made in this study conform with the results of previous studies done by other researchers on columns with significantly higher axial loads and confinement levels. For the same degree of confinement, the ductility capacity of reinforced concrete columns decreases as the applied axial load increases. On the other hand, for the same axial load, the ductility capacity of reinforced concrete columns is enhanced with higher level of confinement. Moreover, failure in ductile columns is normally initiated by opening of the hoop bends in the plastic hinge region, followed by buckling of main bars.
6. The equation given by Paulay and Priestley (Equation 1-4) relating the amount of confinement steel to the ductility capacity may be applicable to columns with high axial loads. Such cases would arise in building columns or in some bridges. At low axial loads, Equation 1-4 results in substantial error and, therefore, should be used with caution when applied to bridge columns.

## 5.3 Recommendations

Current design philosophy in earthquake engineering is based on the "Demand-Capacity" concept.

Recent developments in earthquake ground motion estimation (8) has made it possible to produce Uniform Hazard Spectra (UHS) maps for all regions of the United States. In the UHS maps, the spectral values for different structural periods are based on the same probability of exceedance for a specified time window. These maps can be used to estimate the seismic "demand" on bridge structures in different parts of the nation.

In locations where the demand is moderate, it would be practical to design bridge columns to attain moderate ductility levels. In this study, it was shown that for rectangular columns with moderate amount of confinement steel, it was possible to achieve moderate ductilities without compromising the axial load carrying capacity of the columns. Thus good seismic performance of rectangular columns with moderate amount of transverse reinforcement may be expected in areas of low to moderate seismicity. However, post-earthquake serviceability can not be guaranteed since the strength of such columns is limited by lateral steel hook opening which is difficult to repair.

## SECTION 6 REFERENCES

1. American Association of State Highway and Transportation Officials, "*Standard Specifications for Highway Bridges*," Fifteenth Edition, Washington, D.C., 1992.
2. American Concrete Institute Committee 318, "*Building Code Requirements for Reinforced Concrete and Commentary*," American Concrete Institute, Detroit, Michigan, 1992.
3. Azizinamini, A., W. Corley, and L. Johal, "*Effects of Transverse Reinforcement on Seismic Performance of Columns*," ACI Structural Journal, July-August, 1992, pp. 442-450.
4. Baker, A.L.L. and A.M.N. Amarakone, "*Inelastic Hyperstatic Frames Analysis*," Proceedings of the International Symposium on the Flexural Mechanics of Reinforced Concrete, ASCE-ACI, Miami, November, 1964, pp. 85-142.
5. California Department of Transportation, "*Bridge Design Specifications, 1983 AASHTO with Interims and Revisions by CALTRANS*," Sacramento, California.
6. Commission of the European Communities, "*Eurocode 8 -- Structures in Seismic Regions - Design, Part 2 - Bridges*," Draft Report, March, 1994.
7. Federal Highway Administration, "*Seismic Retrofitting Manual for Highway Bridges*," Publication No. FHWA-RD-94-052, May 1995, 6300 Georgetown Pike, McLean, Virginia 22101-2296.
8. Frankel, A., P. Thenhaus, D. Perkins, E.V. Leyendecker, "*Ground Motion Mapping--Past, Present and Future*," Proceedings of Seminar on New Developments in Earthquake Motion Estimation and Implications for Engineering Design Practice, ATC 35-1, 1994.
9. Kent, D.C. and R. Park, "*Flexural Members with Confined Concrete*," ASCE Journal of the Structural Division, Vol. 97, No. ST7, July, 1971, pp. 1969-1990.
10. Leet, K., "*Reinforced Concrete Design*," Second Edition, McGraw Hill, Inc., New York, 1991.
11. Mander, J.B., M.J.N. Priestley, and R. Park, "*Theoretical Stress-Strain Model for Confined Concrete Columns*," ASCE Journal of Structural Engineering, Vol. 114, No. 8, August, 1988, pp. 1804-1826.
12. Ozcebe, G. and M. Saatcioglu, "*Confinement of Concrete Columns for Seismic Loading*," ACI Structural Journal, July-August, 1987, pp. 308-315.
13. Park, R., M.J.N. Priestley, and W. Gill, "*Ductility of Square Confined Concrete Columns*,"

- ASCE Journal of Structural Division, Vol. 108, April, 1982, pp. 929-980.
14. Park, R. and T. Paulay, "*Reinforced Concrete Structures*," John Wiley & Sons, New York, 1975.
  15. Paulay, T. and M.J.N. Priestley, "*Seismic Design of Reinforced Concrete and Masonry Buildings*," John Wiley & Sons, Inc., New York, 1992.
  16. Priestley, M. J. N. and R. Park, "*Strength and Ductility of Concrete Bridge Columns under Seismic Loading*," ACI Structural Journal, January-February, 1987, pp. 61-76.
  17. Priestley, M. J. N., Verma, R., and Xiao, Y., "*Seismic Shear Strength of Reinforced Concrete Columns*," ASCE Journal of Structural Engineering, Vol. 120, No. 8 August, 1994, pp. 2310-2329.
  18. Saatcioglu, M. and R. Razvi, "*Strength and Ductility of Confined Concrete*," ASCE Journal of Structural Engineering, Vol. 118, No. 6, June, 1992, pp. 1590-1607.
  19. Sheikh, S. and S. Houry, "*Confined Concrete Columns with Stubs*," ACI Structural Journal, July-August, 1993, pp. 414-431.
  20. Sheikh, S.A. and S.M. Uzumeri, "*Analytical Model for Concrete Confinement in Tied Columns*," ASCE Journal of the Structural Division, Vol. 108, No. ST12, December, 1982, pp. 2703-2722.
  21. Soesianawati, M., R. Park, and N. Priestley, "*Flexural Ductility of Reinforced Concrete Columns with Low Axial Load and Limited Transverse Reinforcement*," Proceedings of the Pacific Conference on Earthquake Engineering, New Zealand, 5-7 August, 1987, Vol. 1, pp. 201-212.
  22. Standard Association of New Zealand, "*Code of Practice for Design of Concrete Structures, NSZ 3101 Part 1: 1982*," Wellington, New Zealand, 1982.
  23. Watson, S., Zahn, F. A., and Park, R., "*Confining Reinforcement for Concrete Columns*," ASCE Journal of Structural Engineering, Vol. 120, No. 6, June, 1994, pp. 1798-1823.
  24. Zahn, F., A., Park, R., Priestley, M. J. N., and Chapman, H., E., "*Development of Design Procedures for the Flexural Strength and Ductility of Reinforced Concrete Bridge Columns*," Bulletin of the New Zealand National Society for Earthquake Engineering, Vol. 19, No. 3, September, 1986, pp. 200-212.
  25. "*Bridge Memo to Designers Manual, Memo 20-4*," State of California, Department of Transportation, Office of the Structure Division, Sacramento, California.

26. *"IAI.UNR, User's Manual, Computer Program for Moment-Curvature Analysis of R/C Sections," 1989.*

## APPENDIX A BOND SLIP ROTATION

Consider the reinforced concrete member shown in Figure A-1. The tensile steel bar has a development length  $l_d$  and bar diameter  $d_b$ . When the member is subjected to a bending moment  $M$ , the bond slip of the embedded tensile bar in the adjacent member causes a rotation  $\theta'$ .

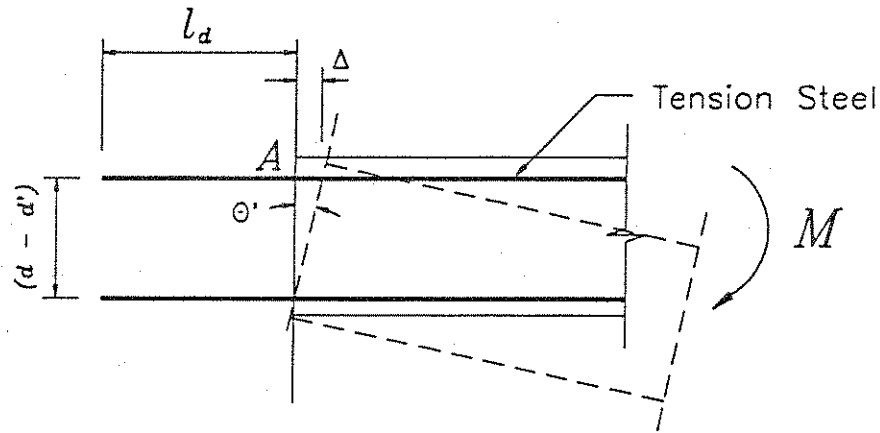


Figure A-1 Bond Slip Rotation

Assume that the bond stress,  $u$ , along the embedded bar development length is uniform and that the stress in the tension bar at point  $A$  is  $f_s$ . From equilibrium it follows that the tensile stress of the tension bar along  $l_d$  varies linearly from zero at the free end of the bar to  $f_s$  at the interface. Hence, the average stress in the embedded portion of the tension bar is  $f_s/2$ .

Consider the free body of the embedded length  $l_d$  of the tensile bar. From equilibrium of forces the following equality can be written

$$l_d (\pi d_b) u = A_s f_s \quad (\text{A-1})$$

Then, the development length,  $l_d$ , can be expressed as

$$l_d = \frac{A_s f_s}{\pi u d_b} \quad (\text{A-2})$$

The average strain along the development length may be written as

$$\epsilon_s = \frac{(f_s/2)}{E_s} \quad (\text{A-3})$$

where  $E_s$  is the modulus of elasticity of the steel bar.

The total bar extension,  $\Delta$ , at the interface can be found from  $\Delta = \epsilon_s l_d$ . Substituting from Equations

A-2 and A-3, the bar extension would be

$$\Delta = \frac{d_b f_s^2}{8 E_s u} \quad (\text{A-4})$$

Assuming that the beam will rotate about the centroid of the compression bar, the corresponding concrete element rotation,  $\theta'$ , is related to the bar extension as follows

$$\theta' = \frac{\Delta}{d - d'} \quad (\text{A-5})$$

where  $(d - d')$  is the distance between tension and compression bars.

Knowing that  $f_s/f_y \approx M/M_y$ , the tensile stress in the tension bar may be expressed as

$$f_s = f_y \frac{M}{M_y} \quad (\text{A-6})$$

Substituting Equations A-4 and A-6 into Equation A-5 the bond slip rotation is obtained as

$$\theta' = \frac{1}{8} \frac{d_b}{E_s u} \frac{f_y^2}{d - d'} \left( \frac{M}{M_y} \right)^2 \quad (\text{A-7})$$

## LIST OF CCEER PUBLICATIONS

Report No.	Publication
CCEER-84-1	Saiidi, M., and R. Lawver, "User's Manual for LZAK-C64, A Computer Program to Implement the Q-Model on Commodore 64," Civil Engineering Department, Report No. CCEER-84-1, University of Nevada, Reno, January 1984.
CCEER-84-1 Reprint	Douglas, B., Norris, G., Saiidi, M., Dodd, L., Richardson, J. and Reid, W., "Simple Bridge Models for Earthquakes and Test Data," Civil Engineering Department, Report No. CCEER-84-1 Reprint, University of Nevada, Reno, January 1984.
CCEER-84-2	Douglas, B. and T. Iwasaki, "Proceedings of the First USA-Japan Bridge Engineering Workshop," held at the Public Works Research Institute, Tsukuba, Japan, Civil Engineering Department, Report No. CCEER-84-2, University of Nevada, Reno, April 1984.
CCEER-84-3	Saiidi, M., J. Hart, and B. Douglas, "Inelastic Static and Dynamic Analysis of Short R/C Bridges Subjected to Lateral Loads," Civil Engineering Department, Report No. CCEER-84-3, University of Nevada, Reno, July 1984.
CCEER-84-4	Douglas, B., "A Proposed Plan for a National Bridge Engineering Laboratory," Civil Engineering Department, Report No. CCEER-84-4, University of Nevada, Reno, December 1984.
CCEER-85-1	Norris, G. and P. Abdollaholiae, "Laterally Loaded Pile Response: Studies with the Strain Wedge Model," Civil Engineering Department, Report No. CCEER-85-1, University of Nevada, Reno, April 1985.
CCEER-86-1	Ghusn, G. and M. Saiidi, "A Simple Hysteretic Element for Biaxial Bending of R/C in NEABS-86," Civil Engineering Department, Report No. CCEER-86-1, University of Nevada, Reno, July 1986.
CCEER-86-2	Saiidi, M., R. Lawver, and J. Hart, "User's Manual of ISADAB and SIBA, Computer Programs for Nonlinear Transverse Analysis of Highway Bridges Subjected to Static and Dynamic Lateral Loads," Civil Engineering Department, Report No. CCEER-86-2, University of Nevada, Reno, September 1986.
CCEER-87-1	Siddharthan, R., "Dynamic Effective Stress Response of Surface and Embedded Footings in Sand," Civil engineering Department, Report No. CCEER-86-2, University of Nevada, Reno, June 1987.
CCEER-87-2	Norris, G. and R. Sack, "Lateral and Rotational Stiffness of Pile Groups for Seismic Analysis of Highway Bridges," Civil Engineering Department, Report No. CCEER-87-2, University of Nevada, Reno, June 1987.
CCEER-88-1	Orie, J. and M. Saiidi, "A Preliminary Study of One-Way Reinforced Concrete Pier Hinges Subjected to Shear and Flexure," Civil Engineering Department, Report No. CCEER-88-1, University of Nevada, Reno, January 1988.
CCEER-88-2	Orie, D., M. Saiidi, and B. Douglas, "A Micro-CAD System for Seismic Design of Regular Highway Bridges," Civil Engineering Department, Report No. CCEER-88-2, University of Nevada, Reno, June 1988.
CCEER-88-3	Orie, D. and M. Saiidi, "User's Manual for Micro-SARB, a Microcomputer Program for Seismic Analysis of Regular Highway Bridges," Civil Engineering Department, Report No. CCEER-88-3, University of Nevada, Reno, October 1988.
CCEER-89-1	Douglas, B., M. Saiidi, R. Hayes, and G. Holcomb, "A Comprehensive Study of the

- Loads and Pressures Exerted on Wall Forms by the Placement of Concrete," Civil Engineering Department, Report No. CCEER-89-1, University of Nevada, Reno, February 1989.
- CCEER-89-2 Richardson, J. and B. Douglas, "Dynamic Response Analysis of the Dominion Road Bridge Test Data," Civil Engineering Department, Report No. CCEER-89-2, University of Nevada, Reno, March 1989.
- CCEER-89-2 Vrontinos, S., M. Saiidi, and B. Douglas, "A Simple Model to Predict the Ultimate Response of R/C Beams with Concrete Overlays," Civil Engineering Department, Report NO. CCEER-89-2, University of Nevada, Reno, June 1989.
- CCEER-89-3 Ebrahimpour, A. and P. Jagadish, "Statistical Modeling of Bridge Traffic Loads - A Case Study," Civil Engineering Department, Report No. CCEER-89-3, University of Nevada, Reno, December 1989.
- CCEER-89-4 Shields, J. and M. Saiidi, "Direct Field Measurement of Prestress Losses in Box Girder Bridges," Civil Engineering Department, Report No. CCEER-89-4, University of Nevada, Reno, December 1989.
- CCEER-90-1 Saiidi, M., E. Maragakis, G. Ghosn, Y. Jiang, and D. Schwartz, "Survey and Evaluation of Nevada's Transportation Infrastructure, Task 7.2 - Highway Bridges, Final Report," Civil Engineering Department, Report No. CCEER 90-1, University of Nevada, Reno, October 1990.
- CCEER-90-2 Abdel-Ghaffar, S., E. Maragakis, and M. Saiidi, "Analysis of the Response of Reinforced Concrete Structures During the Whittier Earthquake 1987," Civil Engineering Department, Report No. CCEER 90-2, University of Nevada, Reno, October 1990.
- CCEER-91-1 Saiidi, M., E. Hwang, E. Maragakis, and B. Douglas, "Dynamic Testing and the Analysis of the Flamingo Road Interchange," Civil Engineering Department, Report No. CCEER-91-1, University of Nevada, Reno, February 1991.
- CCEER-91-2 Norris, G., R. Siddharthan, Z. Zafir, S. Abdel-Ghaffar, and P. Gowda, "Soil-Foundation-Structure Behavior at the Oakland Outer Harbor Wharf," Civil Engineering Department, Report No. CCEER-91-2, University of Nevada, Reno, July 1991.
- CCEER-91-3 Norris, G., "Seismic Lateral and Rotational Pile Foundation Stiffnesses at Cypress," Civil Engineering Department, Report No. CCEER-91-3, University of Nevada, Reno, August 1991.
- CCEER-91-4 O'Connor, D. and M. Saiidi, "A Study of Protective Overlays for Highway Bridge Decks in Nevada, with Emphasis on Polyester-Styrene Polymer Concrete," Civil Engineering Department, Report No. CCEER-91-4, University of Nevada, Reno, October 1991.
- CCEER-91-5 O'Connor, D.N. and M. Saiidi, "Laboratory Studies of Polyester-Styrene Polymer Concrete Engineering Properties," Civil Engineering Department, Report No. CCEER-91-5, University of Nevada, Reno, November 1991.
- CCEER-92-1 Straw, D.L. and M. Saiidi, "Scale Model Testing of One-Way Reinforced Concrete Pier Hinges Subject to Combined Axial Force, Shear and Flexure," edited by D.N. O'Connor, Civil Engineering Department, Report No. CCEER-92-1, University of Nevada, Reno, March 1992.
- CCEER-92-2 Wehbe, N., M. Saiidi, and F. Gordaninejad, "Basic Behavior of Composite Sections Made of Concrete Slabs and Graphite Epoxy Beams," Civil Engineering Department, Report No. CCEER-92-2, University of Nevada, Reno, August 1992.
- CCEER-92-3 Saiidi, M. and E. Hutchens, "A Study of Prestress Changes in A Post-Tensioned Bridge

- During the First 30 Months," Civil Engineering Department, Report No. CCEER-92-3, University of Nevada, Reno, April 1992.
- CCEER-92-4 Saiidi, M., B. Douglas, S. Feng, E. Hwang, and E. Maragakis, "Effects of Axial Force on Frequency of Prestressed Concrete Bridges," Civil Engineering Department, Report No. CCEER-92-4, University of Nevada, Reno, August 1992.
- CCEER-92-5 Siddharthan, R., and Z. Zafir, "Response of Layered Deposits to Traveling Surface Pressure Waves," Civil Engineering Department, Report No. CCEER-92-5, University of Nevada, Reno, September 1992.
- CCEER-92-6 Norris, G., and Z. Zafir, "Liquefaction and Residual Strength of Loose Sands from Drained Triaxial Tests," Civil Engineering Department, Report No. CCEER-92-6, University of Nevada, Reno, September 1992.
- CCEER-92-7 Douglas, B., "Some Thoughts Regarding the Improvement of the University of Nevada, Reno's National Academic Standing," Civil Engineering Department, Report No. CCEER-92-7, University of Nevada, Reno, September 1992.
- CCEER-92-8 Saiidi, M., E. Maragakis, and S. Feng, "An Evaluation of the Current Caltrans Seismic Restrainer Design Method," Civil Engineering Department, Report No. CCEER-92-8, University of Nevada, Reno, October 1992.
- CCEER-92-9 O'Connor, D., M. Saiidi, and E. Maragakis, "Effect of Hinge Restrainers on the Response of the Madrone Drive Undercrossing During the Loma Prieta Earthquake," Civil Engineering Department, Report No. CCEER-92-9, University of Nevada, Reno, February 1993.
- CCEER-92-10 O'Connor, D., and M. Saiidi, "Laboratory Studies of Polyester Concrete: Compressive Strength at Elevated Temperatures and Following Temperature Cycling, Bond Strength to Portland Cement Concrete, and Modulus of Elasticity," Civil Engineering Department, Report No. CCEER-92-10, University of Nevada, Reno, February 1993.
- CCEER-92-11 Wehbe, N., M. Saiidi, and D. O'Connor, "Economic Impact of Passage of Spent Fuel Traffic on Two Bridges in Northeast Nevada," Civil Engineering Department, Report No. CCEER-92-11, University of Nevada, Reno, December 1992.
- CCEER-93-1 Jiang, Y., and M. Saiidi, "Behavior, Design, and Retrofit of Reinforced Concrete One-way Bridge Column Hinges," edited by D. O'Connor, Civil Engineering Department, Report No. CCEER-93-1, University of Nevada, Reno, March 1993.
- CCEER-93-2 Abdel-Ghaffar, S., E. Maragakis, and M. Saiidi, "Evaluation of the Response of the Aptos Creek Bridge During the 1989 Loma Prieta Earthquake," Civil Engineering Department, Report No. CCEER-93-2, University of Nevada, Reno, June 1993.
- CCEER-93-3 Sanders, D.H., B.M. Douglas, and T.L. Martin, "Seismic Retrofit Prioritization of Nevada Bridges," Civil Engineering Department, Report No. CCEER-93-3, University of Nevada, Reno, July 1993.
- CCEER-93-4 Abdel-Ghaffar, S., E. Maragakis, and M. Saiidi, "Performance of Hinge Restrainers in the Huntington Avenue Overhead During the 1989 Loma Prieta Earthquake," Civil Engineering Department, Report No. CCEER-93-4, University of Nevada, Reno, June 1993 (in final preparation).
- CCEER-93-5 Maragakis, E., M. Saiidi, S. Feng, and L. Flourney, "Effects of Hinge Restrainers on the Response of the San Gregorio Bridge During the Loma Prieta Earthquake," (in final preparation) Civil Engineering Department, Report No. CCEER-93-5, University of

Nevada, Reno.

- CCEER-93-6 Saiidi, M., E. Maragakis, S. Abdel-Ghaffar, S. Feng, and D. O'Connor, "Response of Bridge Hinge Restrainers During Earthquakes -Field Performance, Analysis, and Design," Civil Engineering Department, Report No. CCEER-93-6, University of Nevada, Reno, May 1993.
- CCEER-93-7 Wehbe, N., Saiidi, M., Maragakis, E., and Sanders, D., "Adequacy of Three Highway Structures in Southern Nevada for Spent Fuel Transportation, Civil Engineering Department, Report No. CCEER-93-7, University of Nevada, Reno, August 1993.
- CCEER-93-8 Roybal, J., Sanders, D.H., and Maragakis, E., "Vulnerability Assessment of Masonry in the Reno-Carson City Urban Corridor," Civil Engineering Department, Report No. CCEER-93-8, University of Nevada, Reno, May 1993.
- CCEER-93-9 Zafir, Z. and Siddharthan, R., "MOVLOAD: A Program to Determine the Behavior of Nonlinear Horizontally Layered Medium Under Moving Load," Civil Engineering Department, Report No. CCEER-93-9, University of Nevada, Reno, August 1993.
- CCEER-93-10 O'Connor, D.N., Saiidi, M., and Maragakis, E.A., "A Study of Bridge Column Seismic Damage Susceptibility at the Interstate 80/U.S. 395 Interchange in Reno, Nevada," Civil Engineering Department, Report No. CCEER-93-10, University of Nevada, Reno, October 1993.
- CCEER-94-1 Maragakis, E., B. Douglas, and E. Abdelwahed, "Preliminary Dynamic Analysis of a Railroad Bridge," Report CCEER-94-1, January 1994.
- CCEER-94-2 Douglas, B.M., Maragakis, E.A., and Feng, S., "Stiffness Evaluation of Pile Foundation of Cazenovia Creek Overpass," Civil Engineering Department, Report No. CCEER-94-2, University of Nevada, Reno, March 1994.
- CCEER-94-3 Douglas, B.M., Maragakis, E.A., and Feng, S., "Summary of Pretest Analysis of Cazenovia Creek Bridge," Civil Engineering Department, Report No. CCEER-94-3, University of Nevada, Reno, April 1994.
- CCEER-94-4 Norris, G.M. and Madhu, R., "Liquefaction and Residual Strength of Sands from Drained Triaxial Tests, Report 2," Civil Engineering Department, CCEER-94-4, University of Nevada, Reno, August 1994.
- CCEER-94-5 Saiidi, M., Hutchens, E., and Gardella, D., "Prestress Losses in a Post-Tensioned R/C Box Girder Bridge in Southern Nevada," Civil Engineering Department, CCEER-94-5, University of Nevada, Reno, August 1994.
- CCEER-95-1 Siddharthan, R., El-Gamal, M., and Maragakis, E.A., "Nonlinear Bridge Abutment, Verification, and Design Curves," Civil Engineering Department, CCEER-95-1, University of Nevada, Reno, January 1995.
- CCEER-95-2 Norris, G.M., Madhu, R., Valceschini, R., and Ashour, M., "Liquefaction and Residual Strength of Loose Sands from Drained Triaxial Tests," Report 2, Civil Engineering Department, Report No. CCEER-95-2, University of Nevada, Reno, February 1995.
- CCEER-95-3 Wehbe, N., Saiidi, M., Sanders, D., and Douglas, B., "Ductility of Rectangular Reinforced Concrete Bridge Columns with Moderate Confinement," Civil Engineering Department, Report No. CCEER-95-3, University of Nevada, Reno, July 1995.
- CCEER-95-4 Martin, T., Saiidi, M., and Sanders, D., "Seismic Retrofit of Column-Pier Cap Connections in Bridges in Northern Nevada," Civil Engineering Department, Report No. CCEER-95-4, University of Nevada, Reno, August 1995.

- CCEER-95-5 Darwish, I., Saiidi, M., and Sanders, D., "Experimental Study of Seismic Susceptibility Column-Footing Connections," Civil Engineering Department, Report No. CCEER-95-5, University of Nevada, Reno, September 1995.
- CCEER-95-6 Griffin, G., Saiidi, M., and Maragakis, E., "Nonlinear Seismic Response of Isolated Bridges and Effects of Pier Ductility Demand," Civil Engineering Department, Report No. CCEER-95-6, University of Nevada, Reno, November 1995.
- CCEER-95-7 Acharya, S., Saiidi, M., and Sanders, D., "Seismic Retrofit of Bridge Footings and Column-Footing Connections," Report for the Nevada Department of Transportation, Civil Engineering Department, Report No. CCEER-95-7, University of Nevada, Reno, November 1995.
- CCEER-95-8 Maragakis, E., Douglas, B., and Sandirasegaram, U., "Full-Scale Field Resonance Tests of a Railway Bridge," A Report to the Association of American Railroads, Civil Engineering Department, Report No. CCEER-95-8, University of Nevada, Reno, December 1995.
- CCEER-95-9 Douglas, B., Maragakis, E., and Feng, S., "System Identification Studies on Cazenovia Creek Overpass," Report for the National Center for Earthquake Engineering Research, Civil Engineering Department, Report No. CCEER-95-9, University of Nevada, Reno, October 1995.
- CCEER-96-1 El-Gamal, M.E. and Siddharthan, R.V., "Programs to Computer Translational Stiffness of Seat-Type Bridge Abutment," Civil Engineering Department, Report No. CCEER-96-1, University of Nevada, Reno, March 1996.
- CCEER-96-2 Labia, Y., Saiidi, M., and Douglas, B., "Evaluation and Repair of Full-Scale Prestressed Concrete Box Girders," A Report to the National Science Foundation, Research Grant CMS-9201908, Civil Engineering Department, Report No. CCEER-96-2, University of Nevada, Reno, May 1996.
- CCEER-96-3 Darwish, I., Saiidi, M., and Sanders, D., "Seismic Retrofit of R/C Oblong Tapered Bridge Columns with Inadequate Bar Anchorage in Columns and Footings," A Report to the Nevada Department of Transportation, Civil Engineering Department, Report No. CCEER-96-3, University of Nevada, Reno, May 1996.